論文 / 著書情報
Article / Book Information

題目(和文)	
Title(English)	Kondo effect due to (5f)n impurities : numerical renormalization group analysis
著者(和文)	古賀幹人
Author(English)	Koga Mikito
出典(和文)	学位:博士(理学), 学位授与機関:東京工業大学, 報告番号:甲第3109号, 授与年月日:1996年3月26日, 学位の種別:課程博士, 審査員:
Citation(English)	Degree:Doctor (Science), Conferring organization: Tokyo Institute of Technology, Report number:甲第3109号, Conferred date:1996/3/26, Degree Type:Course doctor, Examiner:
学位種別(和文)	博士論文
Type(English)	Doctoral Thesis

Thesis

Kondo Effect Due to $(5f)^n$ Impurities:

Numerical Renormalization Group Analysis

Mikito Koga

Tokyo Institute of Technology

December 1995

Acknowledgments

The author would like to thank Professor H. Shiba for guiding him throughout his master and doctor courses. Professor Shiba introduced to him the field of heavy fermion and Kondo problems and has been giving him helpful suggestions and discussing together throughout the course of the present work. And thanks are due to his critical reading of the manuscript.

The author thanks Professor O. Sakai and Dr. Y. Shimizu for helpful suggestions and stimulating discussions. He also thanks Mr. K. Satori for showing him the program for NRG method. He is grateful to all members in the group of the theoretical condensed matter physics in Tokyo Institute of Technology for helpful discussions.

This work is supported by Grant-in-Aid for Scientific Research from the Ministry of Education, Science and Culture. The numerical calculations have been performed on S-3800 at Tokyo University and SX-3 at Institute for Molecular Science, Okazaki National Institute.

Abstract

The Kondo effect is a quenching phenomenon of localized magnetic moment caused by Fermi statistics and many-body effects. The details of the quenching depend on the atomic structure of impurities and the interaction with the host. For plural $5f$-electrons, the spin-orbit and Hund couplings are large and more important compared with d-electrons. We show that in this case the Kondo effect due to even-number f-electrons is different from the case of odd-number f-electrons. In connection with the theory of multi-channel Kondo problem, we focus our discussion on the Kondo effect due to U-type impurities having plural $5f$-electrons, $(5f)^2$ and $(5f)^3$ in particular. Through this study, we first derive from the large Coulomb limit an effective exchange Hamiltonian for a realistic model and then apply the numerical renormalization group (NRG) method. Our main concern lies in the stability of the Fermi liquid and non-Fermi liquid.

First, we derive from a realistic Anderson model, via the Schrieffer-Wolff transformation, an effective exchange interaction in the absence of the crystal field. It is expressed in terms of irreducible tensor operators and is given by the same form for any number of localized f-electrons whose states are determined through the j-j coupling scheme. We assume that the spin-orbit coupling is larger than the Hund coupling. In the presence of crystal field, the tensorial expression becomes useful to derive an effective exchange interaction straightforwardly.

Secondly, considering a cubic crystal field, we examine differences between the Kondo effect due to a non-Kramers doublet for f^2 and that due to a Kramers doublet for f^3. All intermediate states are taken into account in deriving an effective exchange Hamiltonian. For f^2, additional exchange terms appear in addition to the two-channel Kondo model with a $1/2$ spin. It is also shown that this result holds for a

tetragonal or hexagonal crystal field. The NRG result shows that those additional terms are not relevant and the fixed point is of the same non-Fermi liquid type as given by Cox's model. For f^3, on the other hand, the Hund coupling reduces the number of relevant channel to one and the Fermi liquid is realized at the fixed point.

Finally, we asses the importance of excited states lying above the non-Kramers doublet ground state for f^2. For simplicity, the singlet excited state is assumed to represent those excited states. Whether the Fermi liquid or the non-Fermi liquid is stabilized depends mainly on three parameters: the exchange coupling within the lowest doublet, the exchange connecting with both doublet and singlet and the crystal field splitting. The case where the ground state for f^2 changes from the doublet to the singlet has been studied also. The quenching of the local moment at the Fermi liquid fixed point is influenced by both types of local singlet: One is the local f^2 singlet which is independent of conduction electrons; the other is the local singlet formed with the local moment and conduction electrons which are coupled strongly with each other due to the Kondo effect.

Contents

Chapter 1

Introduction

1.1 Heavy Fermion Systems

There are a class of materials which we call heavy fermion systems. They are Ce or U based compounds which have the property of Fermi liquid with a large mass enhancement at low temperatures [1–5]. At high temperatures, on the other hand, most of them show a logarithmic increase in the resistivity as the temperature decreases. It is reasonable to think it is due to Kondo effect, which is believed to be present in dilute alloys. Usually interatomic interactions (RKKY interaction) lead to magnetic order of some kind in these materials when the density of magnetic ions is high. Therefore it is surprising that each magnetic ion plays the role of local spin independently in heavy fermion systems. This picture is well supported by the experiment of the temperature dependence of magnetic resistivity in $Ce_xLa_{1-x}Cu_6$ [6]. The resistivity in the dilute limit shows a logarithmic increase as the temperature decreases before it finally reaches a constant value, which is so called unitarity limit. For the lattice case ($x \to 1$), it decreases proportionally to the square of temperature (T^2) like the Fermi liquid, although it increases in the same way for all values of x (except $x = 0$) in the high temperature region.

At present we do not have clear explanation about the formation of the heavy Fermi liquid state as mentioned above. We believe that the Kondo effect occurs on each Ce site independently and makes the conduction electrons coupled with the local f-electrons with the decrease of temperature. It is due to the mixing between both electrons. As a result, the f-electrons lose the property of local spin and every

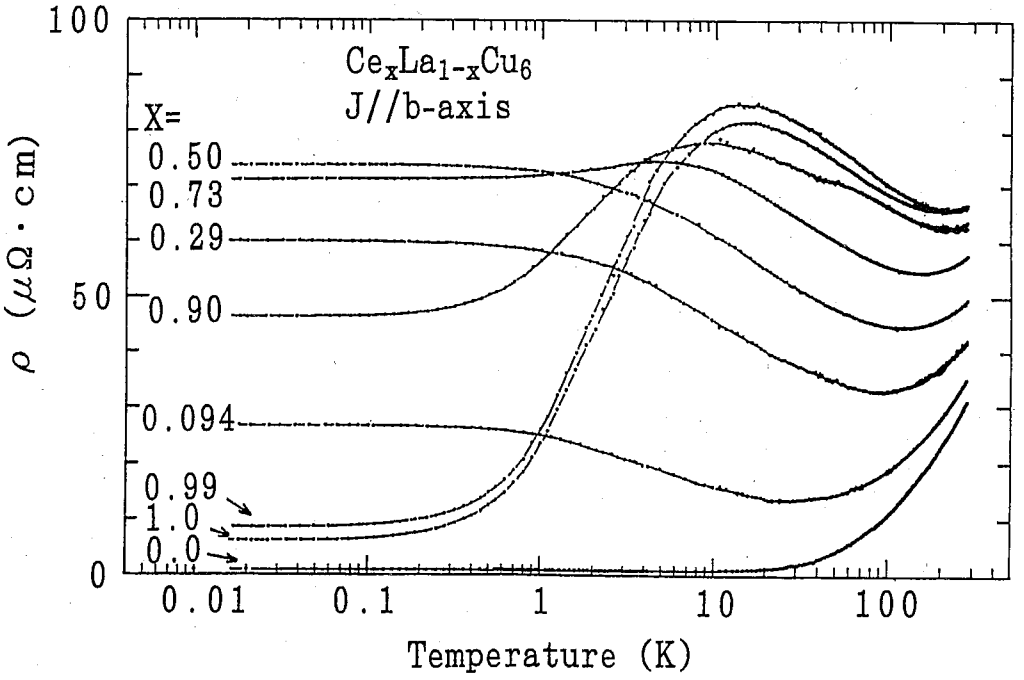

Figure 1.1: Temperature dependence of magnetic resistivity of $Ce_xLa_{1-x}Cu_6$ [6].

Ce site is occupied by a singlet cloud which consists of conduction electrons and an f-electron. The nearest neighbor singlet clouds have small overlap with each other since they are not completely localized on Ce sites. The overlap of the singlet clouds finally forms a narrow coherent band of heavy fermions. The Fermi liquid behavior shows up in the magnetic susceptibility χ and the specific heat coefficient γ which become constant values at low temperatures.

The same scenario as in Ce systems would be applicable to U systems if the same type of Kondo effect occurred in both kinds of materials. However there are some experimental reports showing evidence that the Kondo effect may cause unusual behavior in the dilute limit of U. In $U_xTh_{1-x}Ru_2Si_2$ [7, 8], the magnetic susceptibility of impurity site still increases with the decrease of temperature below $\sim$0.1K and the $5f$ specific heat C/T seems to diverge at $T \to 0$. The electrical resistivity ρ decreases logarithmically as temperature decreases. The similar result is obtained in the specific heat of $Y_{1-x}U_xPd_3$ [9].

Although it is not well understood whether the unusual behavior different from

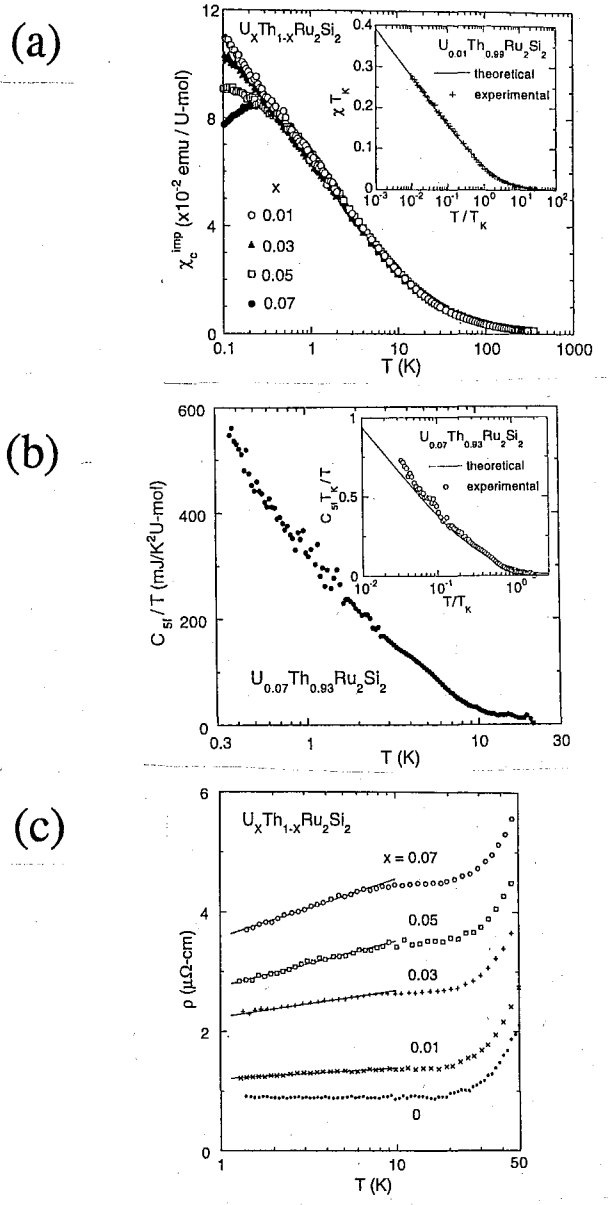

Figure 1.2: Experiment data of single Uranium-site properties of $U_{0.07}Th_{0.93}Ru_2Si_2$ ($x \leq 0.07$) [8]: (a) Magnetic susceptibility along the c-axis per U-mol, $\chi_c^{\rm imp}$ vs $\log T$, of $U_xTh_{1-x}Ru_2Si_2$ single crystals: $x = 0, 0.01, 0.03, 0.05$ and 0.07. The inset shows a comparison between the $\chi_c^{\rm imp}$ data for $x = 0.01$, scaled by using $\mu = 1.7\mu_B$ and $T_K = 11.1K$, and the numerical calculations based on the $S = 1/2$ two-channel Kondo model [22] (solid line); (b) Temperature dependence of the $5f$-electronic specific heat C_{5f}/T vs $\log T$ for $U_{0.07}Th_{0.93}Ru_2Si_2$. The inset shows a comparison between the C_{5f}/T data, scaled by using $T_K = 11.1K$, and the numerical calculations based on the $S = 1/2$ two-channel Kondo model [22] (solid line). (c) Temperature dependence of the low temperature electrical resistivity along the a-axis, ρ vs $\log T$, for $U_xTh_{1-x}Ru_2Si_2$ (x=0, 0.01, 0.03, 0.05, 0.07). The solid lines indicate an empirical formula $\rho_0 + A\log T$, where ρ_0 and A are determined by the best fitting of the data for each concentration below 7 K.

the Fermi liquid is caused by a single magnetic ion, it is possible that it is closely connected with the difference between Ce and U: The latter has plural local electrons on $5f$ orbit and the Hund coupling as well as the spin-orbit coupling is very large. In addition to this, it is interesting to examine the Kondo effect due to the orbital moment of $4f$ and $5f$ impurities which is different from $3d$ impurities. For $3d$ case, the orbital magnetic effect is not important because of the relatively large mixing between the conduction band and the impurity orbital. On the other hand, it is important for U impurities; various types of Kondo effect are expected to appear, depending sensitively on the atomic structure.

1.2 Theoretical Background

The Kondo problem has become as one of basic problems in condensed matter physics since Kondo's seminal work in 1964 [10]. The antiferromagnetic *s-d* exchange model on which Kondo's theory is based can be derived from the Anderson model [11] in the limit of small mixing. Following Kondo's work, many researchers tried hard to understand the physics for the whole temperature region. In 1975 this difficult problem was solved by Wilson's numerical renormalization group (NRG) method. This epoch-making theory uses numerical calculations in an ingenious way [12]. The theoretical effort ended at the beginning of 1980's with the exact Bethe Ansatz solution for the Anderson model [13] and the *s-d* exchange model [14–16]. In these studies the atomic structure of the impurity is simplified in that the models have no orbital degeneracy and no local correlation other than direct Coulomb interaction.

Together with these efforts, some researchers extended to more complex situations. The orbital degeneracy was taken into account for Ce dilute alloys by Coqblin and Schrieffer [17]. For *d*-electrons, Okada and Yosida derived an effective spin and orbit exchange interaction, introducing the intraatomic exchange interaction (Hund coupling) to the extended Anderson model and discussing the Kondo effect due to orbitally degenerate impurities with plural *d*-electrons [18]. In 1980 a more thorough study on the realistic Kondo effect was first made by Noziéres and Blandin [19]. Their work has led to the multi-channel Kondo problem as an important issue of theoretical studies [20–22].

Now let us show the historical review of the theory of Kondo effect as mentioned above, beginning from Kondo's work as the first breakthrough of the Kondo problem [4, 24].

1.2.1 *s-d* Exchange Model and Anderson Model

It was known since 1930's that the resistivity shows a minimum at low temperatures in dilute alloys such as Cu containing $3d$ impurity atoms with magnetic moment like Mn and Fe. In pure metals it decreases monotonically as the temperature decreases as a result of scattering of conduction electrons by phonons and finally reaches a constant value, which is a residual resistivity. However, Cu-Mn dilute alloys show a minimum at about 10K, and the resistivity increases with the decrease of temperature. This effect due to the local magnetic moment is called the Kondo effect, which can be explained by using the antiferromagnetic *s-d* model:

$$H = H_{\mathrm{k}} + H_{sd}, \tag{1.1}$$

$$H_{\mathrm{k}} = \sum_{ks} \varepsilon_k a^{\dagger}_{ks} a_{ks}, \tag{1.2}$$

$$H_{sd} = -\frac{J}{2N} \sum_{kk'ss'} a^{\dagger}_{k's'} a_{ks} (\boldsymbol{s})_{s's} \cdot \boldsymbol{S}. \tag{1.3}$$

Here H_{k} and H_{sd} represent the kinetic energy of conduction electrons and the exchange interaction, respectively. $a^{\dagger}_{ks}$ and a_{ks} are, respectively, the creation and annihilation operators of a conduction electron with momentum k and spin s. $\boldsymbol{s}$ is the spin operator of conduction electrons defined by the Pauli matrix $\boldsymbol{\sigma}$ as $\boldsymbol{s} = \boldsymbol{\sigma}/2$. $\boldsymbol{S}$ is the spin operator of the local magnetic moment. The transition matrix (T matrix) up to the second-order perturbation of the *s-d* Hamiltonian contains a $\log T$ (T: temperature) term. It comes from the terms containing the Fermi distribution function, which remain as a result of the noncommutability of the spin operator. This means that the scattering of conduction electrons is influenced by many other conduction electrons. Therefore the phenomenon of resistance minimum is understood as a many-particle effect. For a negative coupling constant J (i.e. antiferromagnetic) the resistivity increases logarithmically with the decrease of temperature. The existence of the minimum can be explained by adding the resistivity due to phonons.

The antiferromagnetic s-d model can be derived from the Anderson model in the limit of small mixing via Schrieffer-Wolff transformation [25] (see Appendix A). The Anderson model is given as

$$H = H_{\rm k} + H_0 + H_{\rm mix}, \tag{1.4}$$

$$H_{\rm k} = \sum_{ks} \varepsilon_k a_{ks}^\dagger a_{ks}, \tag{1.5}$$

$$H_0 = \varepsilon_0 \sum_s a_{0s}^\dagger a_{0s} + U n_{0\uparrow} n_{0\downarrow}, \tag{1.6}$$

$$H_{\rm mix} = V_0 \sum_{ks} (a_{ks}^\dagger a_{0s} + {\rm h.c.}), \tag{1.7}$$

where $H_{\rm k}$ represents the energy of conduction electrons. The first and second terms in H_0 represent the energy of localized orbital of the impurity and the direct Coulomb interaction between localized electrons, respectively, where $a_{0s}^\dagger$ is the creation operator of a localized electron; n_{0s} is the number operator $n_{0s} = a_{0s}^\dagger a_{0s}$. For simplicity, only spin degeneracy is taken into account here, although the localized orbital is five-fold degenerate in the case of $3d$ electrons. Finally $H_{\rm mix}$ represents the mixing between the conduction band and the impurity orbital.

The impurity orbital is filled by one electron, if $|\varepsilon_0|$ and U are much larger than $\Delta = \pi\rho|V_0|^2$ (ρ is the density of states at the Fermi energy for conduction electrons). It means a formation of a local moment. On the other hand, if $|\varepsilon_0|$ and U are similar to Δ in magnitude, the charge fluctuation is too large to keep the state of local moment stable. Thus the s-d model belongs to the strong coupling Anderson model; the latter model is more fundamental and general. Although it is more direct and general to examine the Anderson model, the exchange model like the s-d model gives us a picture of quenching the local moment in the strong coupling region. Namely, conduction electrons couple with a local spin strongly to form a local singlet state. It is due to the increase of the antiferromagnetic exchange coupling with the decrease of temperature. It leads to a complete compensation of local spin, so that the system shows Fermi liquid behavior; for example, the magnetic susceptibility at impurity site shows Pauli paramagnetic behavior at low temperatures below Kondo temperature $T_{\rm K}$, while it follows Curie-Weiss law at high temperatures. The specific heat is linear in temperature at low temperatures. The NRG method first gave a consistent picture valid for the whole temperature region [12, 26].

1.2.2 Kondo Effect in Real Metals

In the simple Anderson model the orbital is restricted to one; the intraatomic interaction other than the direct Coulomb interaction is neglected. For $4f$ ions like Ce, the orbital degeneracy has to be included in the Anderson model (1.4). Ce^{3+} ion is well described by f^1 configuration, in which the spin-orbit coupling leads to the total angular momentum $j = 5/2$ in the ground state. Taking into account this fact, Coqblin and Schrieffer derived the orbital exchange interaction from the Anderson model to explain the Kondo effect in Ce dilute alloys [17]. It is given by the following exchange Hamiltonian:

$$H_{\mathrm{C.S}} = -\frac{J}{2N} \sum_{kk'MM'} a^{\dagger}_{k'M'} a_{kM} f^{\dagger}_{M} f_{M'}, \tag{1.8}$$

where $a^{\dagger}_{kM}$ and $f^{\dagger}_{M}$ are the creation operators for conduction and local electrons with orbital channel M which represents $j_z = 5/2, 3/2, \cdots, -5/2$, respectively. k represents the wave number. J turns out to be negative. With use of this exchange Hamiltonian, the Kondo temperature is given by

$$T_{\mathrm{K}} \sim D_0 \exp\Big[-\frac{N}{(2j+1)|J|\rho}\Big]. \tag{1.9}$$

Here D_0 and ρ represent the half width of conduction band and the density of state at Fermi energy, respectively. The factor $2j + 1$ is the number of orbital channels. This result shows clearly that orbital degeneracy enhances the Kondo temperature.

In a simple way, Okada and Yosida discussed the one-d electron case in the absence of the spin-orbit interaction [18]. They obtained the spin and orbit exchange interaction as

$$H_{\mathrm{O.Y}} = -\frac{J}{2N} \sum_{\substack{kk' \\ mm'ss'}} a^{\dagger}_{k'm's'} a_{kms} d^{\dagger}_{ms} d_{m's'}. \tag{1.10}$$

Here m represents the z component of the angular momentum $l = 2$, i.e. $m = 2, 1, \cdots, -2$. s is the spin ($s = \uparrow, \downarrow$). J is also negative. The Kondo temperature is given by

$$T_{\mathrm{K}} \sim D_0 \exp\Big[-\frac{N}{(2l+1)|J|\rho}\Big], \tag{1.11}$$

where the factor $(2l + 1)$ is the number of orbital channel. On the other hand, the Hund coupling is important for plural localized electrons. For a special case of a

half-filled shell and a strong Hund coupling as in Mn, Okada and Yosida showed that the Kondo temperature is given by

$$T_{\rm K} \sim D_0 \exp\Big[-\frac{(2l+1)N}{|J|\rho}\Big]. \tag{1.12}$$

The strong Hund coupling restricts the electron transfer among the impurity orbital channels, thereby reducing the Kondo temperature.

Looking at the problem from a more general view point, Noziéres and Blandin first pointed out the Kondo effect depends sensitively on the number of scattering channels of conduction electrons ($N_{\rm ch}$) and the magnitude of the impurity spin (S) [19]. Their discussion is restricted to the orbital singlet case where the orbital means the scattering channel. $N_{\rm ch}$ depends on the crystal field and S is determined by the first Hund's rule. In the absence of crystal field, d-orbitals ($l = 2$) are $2l + 1$ ($= 5$)-fold degenerate. For a cubic crystal field, the degenerate orbital splits into two-fold degenerate E channels and three-fold degenerate T channels. We define the couplings related to the scattering channels as Γ_E for the former and Γ_T for the latter. Far $\Gamma_T \gg \Gamma_E$, the E channels are irrelevant; in practice we have $N_{\rm ch} = 3$. If the anisotropy is absent ($\Gamma_T = \Gamma_E$), we obtain $N_{\rm ch} = 5$. On the other hand, S is given by the half value of the d-electron number (less than five) in the stable configuration.

Generalizing the above discussion, let us consider the Kondo problem with arbitrary values for $N_{\rm ch}$ and S. Noziéres and Blandin discussed the isotropic multichannel Kondo model, for which the exchange Hamiltonian is written as

$$H_{\rm m.ch} = \Gamma \sum_{\substack{kk' \\ mm'ss'}} a^\dagger_{k'm's'} a_{kms} (\boldsymbol{s})_{s's} \cdot \boldsymbol{S}. \tag{1.13}$$

The complete compensation of the impurity moment is achieved only for $N_{\rm ch} = 2S$. This corresponds to the case of Mn impurities in Cu in the absence of crystal field. The scaling approach shows us how the exchange interaction is renormalized at low temperatures. For the $N_{\rm ch} = 2S$ case, the strong coupling fixed point is stable. The ground state is obtained by forming a singlet combination of one impurity electron and one conduction electron in each orbital channel. It means that the local spin is completely quenched. For $2S > N_{\rm ch}$, however, the trapped electrons cannot quench

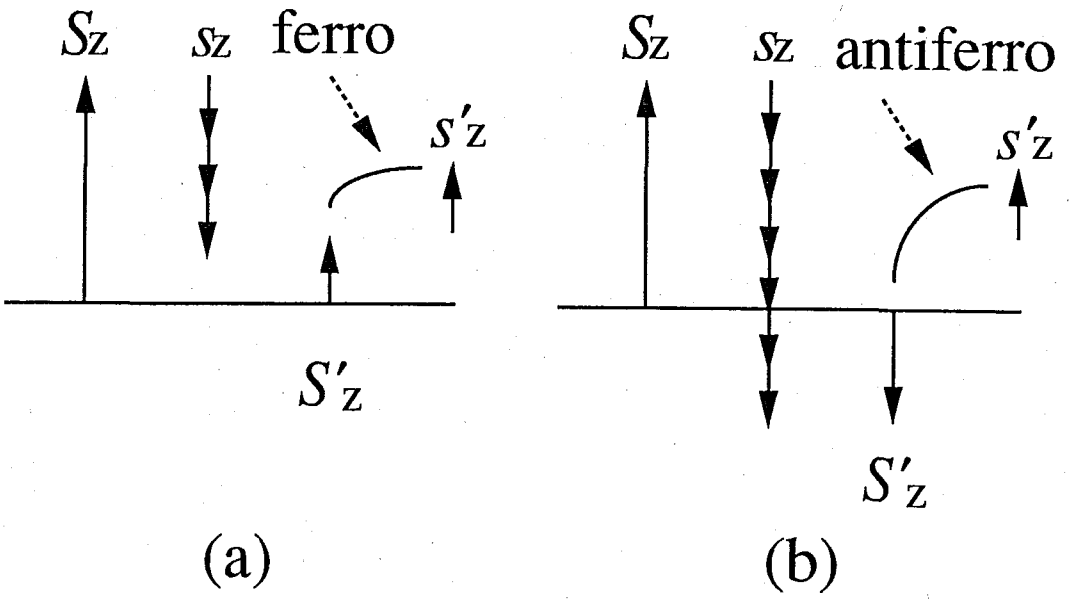

Figure 1.3: The strong coupling arrangement of spins for the impurity and n trapped electrons (a) when $N_{\rm ch} < 2S$, (b) when $N_{\rm ch} > 2S$.

the spin S completely. In this case an effective interaction is present between the dressed spin with the magnitude $S' = S - N_{\rm ch}/2$ and the conduction electrons around it. The interaction is ferromagnetic, since conduction electrons with its spin parallel to the impurity spin have lower energy. It is concluded that the strong coupling fixed point is stable. This situation is illustrated in Figs. 1.3 (a) and 1.4 (a). For $2S < N_{\rm ch}$, the z component of the dressed spin S'_z is opposite to that of the pure spin S_z. As mentioned above, the electrons with spin parallel to the impurity spin couple with the local spin, but the effective coupling Γ' is now antiferromagnetic. It is concluded that the strong coupling fixed point is unstable this time. There must necessarily exist at least one fixed point at a finite Γ. This situation is illustrated in Figs. 1.3 (b) and 1.4 (b). This consideration demonstrates that the scaling trajectories depend on the parameters $N_{\rm ch}$ and S drastically.

Here we briefly touch on the effect of crystal field splitting. In the above discussion, the localized moment is restricted to a simple structure described by the spin

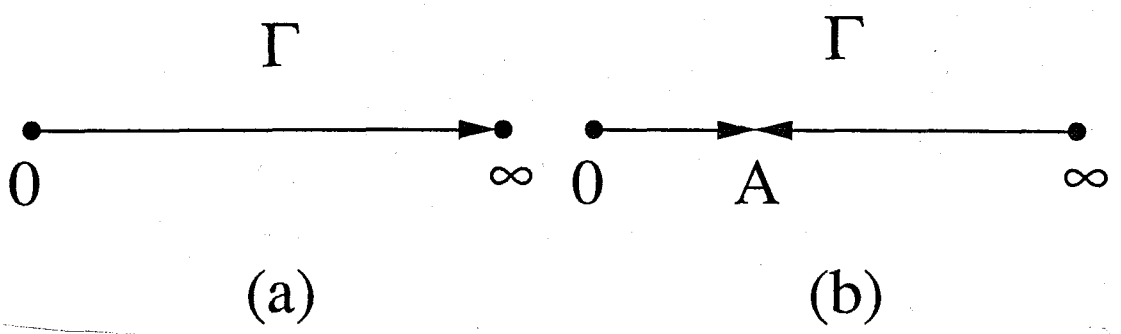

Figure 1.4: The scaling trajectories along the Γ axis, (a) when $N_{\rm ch} < 2S$, (b) when $N_{\rm ch} > 2S$: an extra fixed point A with finite Γ must exist somewhere.

operator. This treatment can be justified if the impurity ground state is well separated from the excited states due to a strong crystal field. For a weak crystal field, however, the contribution from the excited states cannot be ignored. This problem was studied by Yamada *et al* [27, 28], who applied the scaling approach to a model appropriate to Ce and Yb with f^1 configuration. The scaling theory shows that $T_{\rm K}$ depends on the splitting as

$$T_{\rm K} = \left(\frac{D_0}{\Delta_1}\right)^{N_1/N_0} \left(\frac{D_0}{\Delta_2}\right)^{N_2/N_0} \cdots \left(\frac{D_0}{\Delta_m}\right)^{N_m/N_0} T_{\rm K}^0, \tag{1.14}$$

where $T_{\rm K}^0$ is the Kondo temperature for the case without the excited levels. Δ_i and N_i are the level splitting between i and 0 levels and the degeneracy of i level, respectively. $i = 0$ corresponds to the ground level. For example, Ce system forms the lowest state of spin-orbit splittings, $j = 5/2$ for Ce^{3+}. It splits into Γ_7 doublet and Γ_8 quartet under a cubic crystal field. If we assume that Γ_7 doublet is lower than Γ_8 quartet, $T_{\rm K}$ is given as a function of Δ. In the region $T_{\rm K} \ll \Delta \ll D_0$, the result in (1.14) leads to

$$T_{\rm K} = \left(\frac{D_0}{\Delta}\right)^2 D_0 e^{-N/\rho|J|} = \left(\frac{D_0}{\Delta}\right)^2 T_{\rm K}^0. \tag{1.15}$$

In this way, the contribution of crystal field splitting cannot be neglected as far as $\Delta \ll D_0$.

1.2.3 Cox's Model

In the above discussion the orbital plays the role of only scattering channel. In reality localized electrons form multiplets due to spin-orbit and Hund couplings. For a rare

earth or an actinide impurity, localized states are first expressed by the total angular momentum J before the crystal field splitting is taken into account. Then we must consider the angular momentum of orbital channel explicitly to derive the effective exchange interaction due to the magnetic moment J. In the presence of crystal field, the localized states specified by J split into several states, which are classified by the point group. Especially there are two types of doublets: Kramers doublet and non-Kramers doublet for odd and even number of localized electrons, respectively.

Cox presented a realistic two-channel model for non-Kramers doublet, having in mind the Kondo effect due to a single uranium impurity with f^2 configuration [23]. Cox discussed the quadrupolar Kondo effect, starting from the Anderson model under the following realistic conditions:

(1) For f^2 configuration, non-Kramers Γ_3 doublet is a ground state of the cubic crystal field-split $J = 4$ multiplet. The Γ_3 energy level is taken as ε_f.

(2) The $5f^1$ configuration lies above the Γ_3 level by an amount $|\varepsilon_f|$; all other configurations are neglected.

(3) The conduction electrons contributing to the mixing with the impurity orbital is restricted to $j = 5/2$ partial waves since the energy is lower for the mixing with $j = 5/2$ than for that with $j = 7/2$ due to the spin-orbit interaction.

(4) The crystal field is assumed to be so strong that only ground state is left for each configuration: non-Kramers Γ_3 doublet for f^2 and Kramers Γ_7 doublet for f^1. The point group symmetry selects Γ_8 partial waves in the exchange interaction due to the Γ_3 doublet.

The effective exchange Hamiltonian can be obtained by applying Schrieffer-Wolff transformation to the original model Hamiltonian. The exchange Hamiltonian can be written with the bases of cubic symmetry. It can be mapped to so called two-channel exchange Hamiltonian if the partial waves of conduction electrons are classified with pseudo-spin $(\uparrow, \downarrow)$ and channel index $(+, -)$: Γ_3 doublet is expressed with spin 1/2 operator corresponding to a quadrupolar moment, while Γ_8 partial waves with symmetries $\Gamma_8(+2)$, $\Gamma_8(+1)$, $\Gamma_8(-2)$ and $\Gamma_8(-1)$ (see Table 1.1) correspond to $(\uparrow, +)$,

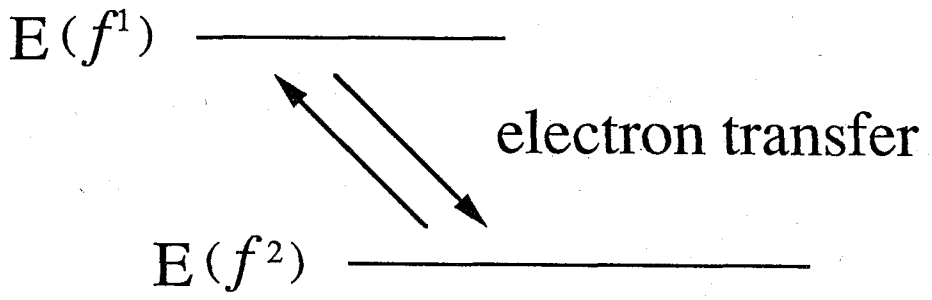

Figure 1.5: Energy level scheme for U^{4+} ion. Energy runs vertically. Only two configurations are kept, which is the restriction of the model.

$(\downarrow,+)$, $(\uparrow,-)$ and $(\downarrow,-)$, respectively. The two channels have the time reversal relationship with each other. As mentioned previously, the two-channel Kondo model leads to the non-Fermi liquid at low temperatures since $N_{\rm ch} > 2S$. The details will be discussed further in Chapter 4. In this connection the screening effect on the stability of the non-Fermi liquid has been examined by several authors [29–32].

State	$\langle J_z \rangle$	$\langle 3Jz^2 - J(J+1) \rangle$
$\|\Gamma_3+\rangle = \frac{\sqrt{42}}{12}(\|4\rangle + \|-4\rangle) - \frac{\sqrt{15}}{6}\|0\rangle$	0	+8
$\|\Gamma_3-\rangle = \sqrt{\frac{1}{2}}(\|2\rangle + \|-2\rangle)$	0	−8
$\|\Gamma_7\pm\rangle = \sqrt{\frac{1}{6}}\|\mp 5/2\rangle - \sqrt{\frac{5}{6}}\|\pm 3/2\rangle$	$\pm\frac{5}{6}$	0
$\|\Gamma_8 \pm 2\rangle = \sqrt{\frac{5}{6}}\|\pm 5/2\rangle + \sqrt{\frac{1}{6}}\|\mp 3/2\rangle$	$\pm\frac{11}{6}$	+8
$\|\Gamma_8 \pm 1\rangle = \|\pm 1/2\rangle$	$\pm\frac{1}{2}$	−8

Table 1.1: Cubic crystal field states.

1.2.4 Theoretical Approaches to Heavy Fermion Systems

Before examining an impurity model in realistic cases, we briefly touch on the theoretical approaches to lattice cases. The periodic Anderson Hamiltonian is believed to be the simplest model to describe the essence of heavy fermion systems. The periodic Anderson model has been examined by many researchers [33–36]. If the orbital degeneracy of f-electrons is neglected for simplicity, it is given by

$$\begin{aligned} H_{\rm PAM} &= -t \sum_{<i,j>} \sum_{s} a_{is}^{\dagger} a_{js} + \sum_{is} \varepsilon_f n_{is} \\ &\quad + V \sum_{is} (a_{is}^{\dagger} f_{is} + f_{is}^{\dagger} a_{is}) + U \sum_{i} n_{i\uparrow} n_{i\downarrow}. \end{aligned} \tag{1.16}$$

Here $a_{is}^{\dagger}$ and $f_{is}^{\dagger}$ represent the creation operators of the conduction electron and the localized f-electron with spin s on the i-th site, respectively. $n_{is} = f_{is}^{\dagger} f_{is}$ is the number operator for the f-electron. ε_f represents the energy measured from the center of the conduction band. The four terms of the above Hamiltonian (1.16) are the energy of conduction electrons, the energy of localized f-electrons, the mixing between conduction band and f-orbital, and the Coulomb interaction between the f electrons, respectively. The assumption $U > \Delta = \pi \rho V^2$ (ρ is the density of states at the Fermi energy) is reasonable since the localized f-orbital is good picture for our problem. If we put the case that the f-electron energy level is above the Fermi energy $\varepsilon_{\rm F}$ and the condition $\varepsilon_f - \varepsilon_{\rm F} \gg \Delta$ is satisfied, the Coulomb interaction is not so important since the number of f-electrons on a lattice site becomes much smaller than one. This situation corresponds to La based compounds. If the f-energy level is lowered and $\varepsilon_f - \varepsilon_{\rm F}$ reaches the order of Δ, we have the valence fluctuation between f^0 and f^1 configurations. In this situation, a new conduction band is formed by quasi-particles which arises as a result of mixing between conduction electrons and f-electrons. It makes the effective mass enhanced. When the f-level is lowered further, $\varepsilon_{\rm F} - \varepsilon_f$ and $\varepsilon_f + U - \varepsilon_{\rm F}$ become larger than Δ; the valence fluctuations are suppressed and the spin degree of freedom is more dominant. If it is allowed to represent the degree of freedom of the f-shell in terms of a local spin, this situation can be described by the Kondo lattice model:

$$H_{\rm KLM} = -t \sum_{<i,j>} \sum_{s} a_{is}^{\dagger} a_{js} + J \sum_{i} \sum_{ss'} \boldsymbol{S}_i \cdot (\boldsymbol{\sigma})_{s's} a_{is'}^{\dagger} a_{is}, \tag{1.17}$$

$$J = 2V^2\Big(\frac{1}{\varepsilon_{\rm F} - \varepsilon_f} + \frac{1}{\varepsilon_f + U - \varepsilon_{\rm F}}\Big) \tag{1.18}$$

Here the second term of the Hamiltonian expresses the exchange interaction due to the local spin on the i-th site. It can be derived from the periodic Anderson model (1.16) via Schrieffer-Wolff transformation by suppressing valence fluctuations.

In this model the exchange interaction between the conduction electrons and local f-electrons is responsible both for the Kondo effect and the magnetic ordering through RKKY interactions. The phase diagram of the ground state was studied with various theoretical approaches [37–40]. There are three basic parameters: (1) the total width of the conduction band $2D$, (2) the exchange parameter J and (3) the density of conduction electrons $n_{\rm c}$. In one-dimensional case, which is rather special, it has been almost completely understood for all region of the parameters: If J is large or $n_{\rm c}$ is small, a ferromagnetic metallic state is stabilized. It is believed that otherwise the most stable state becomes paramagnetic metallic state [41].

The low temperature Fermi liquid in heavy fermion systems is most conveniently studied by the perturbation theory for the Coulomb interaction. It leads to a large enhancement of the T-linear specific heat [36]. Recently the infinite dimensional case has been actively pursued by many researchers. In this case, the self energy can be exactly evaluated since it has no wave vector dependence, so that the model can be studied even for the strong coupling region by means of the quantum Monte Carlo [42] or the NRG method [43].

1.3 Outline of Thesis

In this thesis we study various effects related to the atomic structure in $5f$ impurities. We wish to answer the following general questions:

(1) How different is the Kondo effect due to $5f$ impurities from $3d$ impurities?

(2) Is the Kondo effect due to even-number f-electrons different from the case of odd-number f-electrons?

With these questions in mind, we wish to reconsider the multi-channel problem for a realistic situation. We examine the Kondo effect due to U-type impurities

having plural $5f$-electrons, $(5f)^2$ and $(5f)^3$ in particular. In the case of plural $5f$-electrons the spin-orbit and Hund couplings are large. In addition, the crystal field is important. Our main purpose is to study how the Fermi liquid or the non-Fermi liquid is stabilized or destabilized in these real systems. In contrast to Cox's work, we take into account crystal-field excited states above the ground state. We generalize Cox's analysis on two points. First, we examine the importance of excited states in f^1 configuration, which appear in the intermediate states of the exchange process. In this connection we compare $(5f)^2$ and $(5f)^3$ to see the difference between even-number and odd-number f-electrons. Second, we assess the importance of excited states lying above the non-Kramers doublet ground state for f^2 configuration. For both cases, to describe this complicated situation from the large Coulomb limit, we derive an effective exchange Hamiltonian, starting from the Anderson Hamiltonian suitable for plural $5f$-electrons. Then we study the Kondo effect by applying the NRG method [12].

In Chapter 2, we first discuss the atomic structure in f^n configuration. The largest intraatomic interaction is the direct Coulomb interaction between localized f-electrons. The formation of multiplet is due to the exchange couplings among them, which is generally related to both spin and orbital moments. To describe the multiplet in terms of quantum numbers such as the angular momentum, there are two approaches: Russell-Saunders coupling and j-j coupling schemes. Both schemes finally characterize the eigenstate with the total angular momentum J. Next the crystal field is introduced as a perturbation to the f-electron states with J. The cystal field Hamiltonian can be expressed with tensor operators formed with the total angular momentum operator $\boldsymbol{J}$. The eigenstates in the crystal field are classified by the point-group symmetry. This is explicitly applied to the $J = 4$ state for cubic, tetragonal and hexagonal crystal fields.

Second, we review the NRG method invented by Wilson. This is the most reliable method to treat a many-body effect all over temperature region. The principal idea of calculation is logarithmic descretization of a conduction band. The original Hamiltonian of the exchange model is transformed into a recursion relation of a hopping-type of Hamiltonian which is useful for numerical calculations. The energy levels are determined by diagonalizing the Hamiltonian. How they change as the

NRG step is increased will be demonstrated with the well-known one-channel Kondo model.

In Chapter 3, we derive, from an extended Anderson model with orbital degeneracy, an effective exchange interaction. The crystal field is not introduced at the first stage. The j-j coupling scheme is chosen to determine the local f-electron states. For simplicity, conduction electrons are restricted to partial waves with total angular momentum $j = 5/2$ which have the largest mixing with the local orbital. The effective exchange Hamiltonian is finally expressed in terms of tensor operators of $j = 5/2$ and J. The derivation was already presented in §2 in ref. 44; however it is described here in more detail.

In Chapter 4, an effective exchange Hamiltonian is derived for a Kramers doublet or non-Kramers doublet in the presence of crystal field. Kramers and non-Kramers doublets are obtained for odd and even number of f-electrons, respectively. For f^2 configuration, we obtain some additional terms, if we compare it with the two-channel exchange Hamiltonian in Cox's model. Whether these additional terms are relevant or not will be examined by the NRG method. Similarly, for f^3 configuration, we examine the effect of additional exchange terms which are related to the Hund coupling. The NRG results for both cases have been presented already in §4 in ref. 44, where a cubic crystal field has been chosen. Here tetragonal and hexagonal cases will be also examined.

In Chapter 5, the effect of local excited states is examined when the ground state for f^2 is a non-Kramers doublet. For simplicity the excited states are restricted to only one singlet. The effective exchange Hamiltonian contains exchange terms connecting the doublet with the singlet as well as only within doublet state. As a result, it brings about competition between the Fermi liquid and the non-Fermi liquid; it is also examined by the NRG method. This problem has been discussed in §3 in ref. 44. However the ground states at the fixed points is examined further in this chapter. Finally a generalized treatment is added to make sure the reliability of the conclusion based on the effective exchange Hamiltonian which is simplified by assuming a strong crystal field.

This thesis closes with conclusions in the last Chapter.

Chapter 2

Theoretical Preparation

2.1 Atomic Structure

We first review how to obtain the atomic structure by means of the Clebsch-Gordan method [45, 46] and the crystal field theory [47, 48]. They are useful to determine a localized electron state.

2.1.1 Multiplet of Localized State

Let us consider the following Hamiltonian in atomic units

$$H_{\rm atom} = -\sum_i \nabla_i^2 - \sum_i \frac{2Z}{r_i} + \sum_{i,j} \frac{2}{r_{i,j}} + \sum_i \xi_i(\boldsymbol{l}_i \cdot \boldsymbol{s}_i). \tag{2.1}$$

Here the first and the second terms are kinetic energy and potential energy due to the nucleus. Z is the atomic number. The eigenstates of the first and second terms are characterized by the combination of four quantum numbers, namely, principal n, azimuthal l, magnetic m and spin s. The third term represents the Coulomb interaction; its direct part depends only on the number of local electrons and the exchange part leads to spin multiplicity. As shown in more detailed discussion by Nozières and Blandin [19], there should be $(l+1)$ independent parameters to describe the Coulomb interaction for the l-shell. However orbital terms are expected to be much smaller compared with both direct and spin terms. The fourth term represents the spin-orbit interaction. It increases faster with the atomic number than the other effects, so that for heavy atoms it outweighs the other effects. For simplicity, the two limiting cases are usually considered; one is Russell-Saunders coupling, the other

j-j coupling. In the former the spin-orbit interaction is small compared with the electrostatic splitting of the levels. In this approximation, $\boldsymbol{J}^2$, J_z, $\boldsymbol{L}^2$ and $\boldsymbol{S}^2$ are diagonalized at the same time, where

$$\boldsymbol{J} = \boldsymbol{L} + \boldsymbol{S}, \quad \boldsymbol{L} = \sum_i \boldsymbol{l}_i, \quad \boldsymbol{S} = \sum_i \boldsymbol{s}_i. \tag{2.2}$$

Then the spin-orbit interaction can be expressed as $\lambda \boldsymbol{L} \cdot \boldsymbol{S}$. On the other hand, in the latter case, the electrostatic terms should be taken into account after the spin-orbit interaction is considered. At any rate, the derivation of the effective exchange interaction is more complicated in these cases, since orbital multiplicity must be considered as well as spin. For f-electrons, the crystal field is smaller in magnitude than the spin-orbit and Hund couplings. In this case, first, the Clebsch-Gordan method is applied to determine the multiplet which has the total angular momentum J as the quantum number, and secondly, a crystal field is introduced as a perturbation to the eigenstate of J.

Now let us discuss the f^2 configuration in the absence of crystal field by means of Russell-Saunders and j-j coupling schemes. In the Russell-Saunders coupling scheme, the degenerate states consisting of independent electrons split into the spin and orbital multiplets due to the intraatomic exchange interactions. They are expressed with $-\boldsymbol{S}_f^2$ and $-\boldsymbol{L}_f^2$, respectively, where $\boldsymbol{S}_f$ and $\boldsymbol{L}_f$ represent, respectively, the total spin and angular momenta. As a result, the eigenstates are classified into the multiplets which are characterized by the quantum numbers S and L at the same time. The ground state has the maximum magnitude of both quantum numbers, namely, $S = 1$ and $L = 5$ for f^2. Secondly, the spin-orbit interaction expressed with $\lambda \boldsymbol{L}_f \cdot \boldsymbol{S}_f$ splits the states further according to the total angular momentum $J = L + S, L + S - 1, \cdots L - S$, since

$$2\boldsymbol{L}_f \cdot \boldsymbol{S}_f = (\boldsymbol{L}_f + \boldsymbol{S}_f)^2 - \boldsymbol{L}_f^2 - \boldsymbol{S}_f^2. \tag{2.3}$$

The splitting is of the order of spin-orbit coupling λ. For f^2, the ground state corresponds to $J = 4$, since λ is positive.

On the other hand, for the j-j coupling scheme, we first form the eigenfunctions of the total angular momentum j for each electron, which has $s = 1/2$ and $l = 3$ for the f-electron. The spin-orbit coupling splits the eigenstates into two: $j = l + s = 7/2$

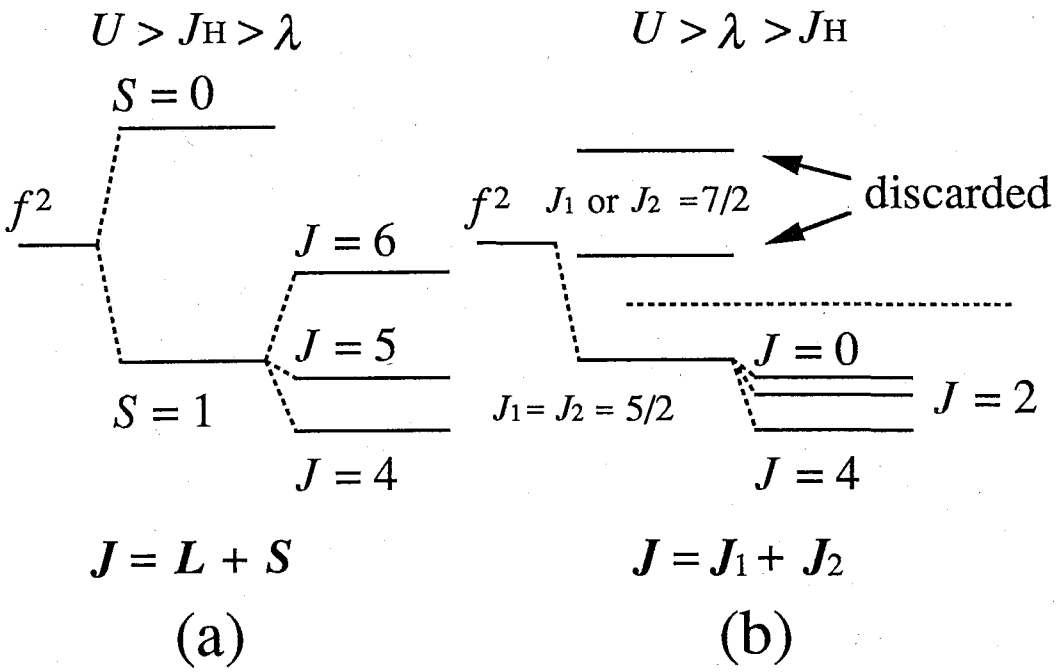

Figure 2.1: Energy level schemes:(a) Russell-Saunders and (b) j-j coupling.

and $j = l - s = 5/2$. Since the coupling constant is positive, first, the latter state is obtained as the ground state. Secondly, we form the multiplets according to the Hund coupling; they turns out to be the eigenstates of the total angular momentum J due to the effective intraatomic exchange interaction $-\boldsymbol{J}_f^2$. For f^2, the ground state corresponds to $J = 2j - 1 = 4$. The excited states are separated from the ground state by the order of the Hund coupling. Notice that the ground state has the same magnetic moment J in both coupling schemes.

2.1.2 Crystal Field Theory

Next we take into account the crystal field, which splits further the multiplets. There are two sources in the crystal field effect: the electrostatic potential from the surrounding ions and the mixing with them. Let us take the first effect and consider the potential energy due to point charges which are arranged with the cubic symmetry. Six point charges of $-Ze$ are located at the point $\pm a$ located on the x, y and z axes.

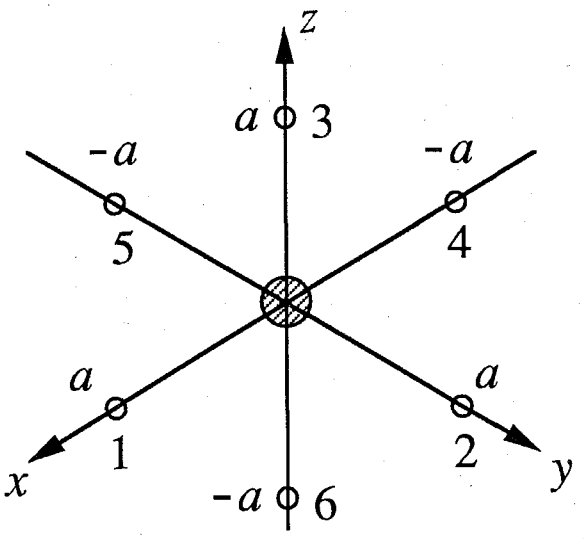

Figure 2.2: The system surrounded by six point-charges with cubic symmetry.

Then the Hamiltonian for the electron at $\boldsymbol{r}$ is given by

$$H_{\rm cub} = \sum_{i=1}^{6} \frac{Ze^2}{|\boldsymbol{R}_i - \boldsymbol{r}|} \tag{2.4}$$

where $\boldsymbol{R}_i$ $(i = 1, \cdots, 6)$ represents the position of the i-th point charge. By following ref. 47, it is easy to rewrite the Hamiltonian (2.4) with spherical harmonics as

$$\begin{aligned} H_{\rm cub} &= \frac{7Ze^2}{2a^5} r^4 \Big\{ C_0^{(4)}(\theta,\varphi) + \sqrt{\frac{5}{14}} [C_4^{(4)}(\theta,\varphi) + C_{-4}^{(4)}(\theta,\varphi)] \Big\} \\ &\quad + \frac{3Ze^2}{4a^7} r^6 \Big\{ C_0^{(6)}(\theta,\varphi) - \sqrt{\frac{7}{2}} [C_4^{(6)}(\theta,\varphi) + C_{-4}^{(6)}(\theta,\varphi)] \Big\} + \cdots \end{aligned} \tag{2.5}$$

where

$$C_m^{(l)}(\theta,\varphi) = \sqrt{\frac{4\pi}{2l+1}} Y_l^m(\theta,\varphi). \tag{2.6}$$

Here the common energy shift is ignored. The point charge model is not reliable quantitatively, but the symmetry of the crystal field is properly included.

To calculate the matrix elements of $H_{\rm cub}$, equivalent operators based on angular momentum operators are the most convenient. This method derives from the relationship between any vector operator $\boldsymbol{T}$ and the angular momentum operator $\boldsymbol{J}$ as

$$\langle \alpha JM | T_\lambda | \alpha' JM' \rangle \propto \langle JM | J_\lambda | JM' \rangle \quad (\lambda = x, y, z), \tag{2.7}$$

where $|\alpha JM\rangle$ is an eigenstate of J and its z component M $(= J, J-1, \cdots, -J)$. α represents a quantum number other than the angular momentum. This relation is also applicable to tensors; For example, we have

$$\langle \alpha JM | \sum x_i y_i | \alpha' JM' \rangle \propto \langle JM | \frac{1}{2}(J_x J_y + J_y J_x) | JM' \rangle. \tag{2.8}$$

The tensor operators defined as

$$(-1)^p \sqrt{\frac{(2p-1)(2p-3)\cdots 3\cdot 1}{2p(2p-2)\cdots 2}} J_+^p = J_p^{(p)} \tag{2.9}$$

and

$$[J_-, J_q^{(p)}] = \sqrt{(p+q)(p-q+1)} J_{q-1}^{(p)} \quad (q < p). \tag{2.10}$$

By using $J_q^{(p)}$, $H_{\rm cub}$ can be expressed with Stevens operators [49, 50] as

$$H_{\rm cub} = B_4 O_4 + B_6 O_6, \tag{2.11}$$

where

$$O_4 = O_4^0 + 5 \cdot O_4^4, \quad O_6 = O_6^0 - 21 \cdot O_6^4, \tag{2.12}$$

and

$$O_4^0 = 35 J_z^4 - [30J(J+1) - 25] J_z^2 - 6J(J+1) + 3J^2(J+1)^2, \tag{2.13}$$

$$O_4^4 = \frac{1}{2}(J_+^4 + J_-^4), \tag{2.14}$$

$$O_6^4 = 231 J_z^6 - 105[3J(J+1) - 7] J_z^4 + [105J^2(j+1)^2 - 525J(J+1) + 294] J_z^2 - 5J^3(J+1)^3 + 40J^2(J+1)^2 - 60J(J+1), \tag{2.15}$$

$$O_6^4 = \frac{1}{4}[11J_z^2 - J(J+1) - 38](J_+^4 + J_-^4) + \frac{1}{4}(J_+^4 + J_-^4)[11J_z^2 - J(J+1) - 38], \tag{2.16}$$

where $H_{\rm cub}$ is expanded up to the sixth order, and B_4 and B_6 represent crystal field parameters. For f^2, the $J = 4$ multiplet is split into the eigenstates according to the point group representations for O_h: a Γ_1 singlet, a Γ_3 doublet, a Γ_4 triplet and a Γ_5 triplet. The order of energy levels depends on the crystal field parameters.

The energy levels have been discussed in detail in ref. 51. Here we discuss f^1 and f^2 states in connection with Cox's model. For our purpose it is convenient to rewrite the crystal field parameters as

$$B_4 = Wx/F(4), \quad B_6 = W(1 - |x|)/F(6). \tag{2.17}$$

State	Energy (in W unit)
$\|\Gamma_1\rangle = \frac{\sqrt{30}}{12}(\|4\rangle + \|-4\rangle) + \frac{\sqrt{21}}{6}\|0\rangle$	$28x - 80(1-\|x\|)$
$\|\Gamma_3+\rangle = \frac{\sqrt{42}}{12}(\|4\rangle + \|-4\rangle) - \frac{\sqrt{15}}{6}\|0\rangle$ $\|\Gamma_3-\rangle = \sqrt{\frac{1}{2}}(\|2\rangle + \|-2\rangle)$	$4x + 64(1-\|x\|)$
$\|\Gamma_4\pm\rangle = \sqrt{\frac{1}{8}}\|\mp 3\rangle + \sqrt{\frac{7}{8}}\|\pm 1\rangle$ $\|\Gamma_4 0\rangle = \sqrt{\frac{1}{2}}(\|4\rangle - \|-4\rangle)$	$14x + 4(1-\|x\|)$
$\|\Gamma_5\pm\rangle = \sqrt{\frac{7}{8}}\|\pm 3\rangle - \sqrt{\frac{1}{8}}\|\mp 1\rangle$ $\|\Gamma_5 0\rangle = \sqrt{\frac{1}{2}}(\|2\rangle - \|-2\rangle)$	$-26x - 20(1-\|x\|)$

Table 2.1: Eigenstates and eigenvalues for $J = 4$ under a cubic crystal field.

Then

$$H_{\rm cub} = W\Big[x\Big(\frac{O_4}{F(4)}\Big) + (1-|x|)\Big(\frac{O_6}{F(6)}\Big)\Big] \quad (-1 < x < 1), \tag{2.18}$$

and it is better to choose

$$F(4) = 60, \quad F(6) = 1260, \tag{2.19}$$

for $J = 4$. The eigenstates and the energy levels are listed in Table 2.1. The x dependence of the energy levels are shown in Fig. 2.3. On the other hand, for f^1, we obtain a Γ_7 doublet and a Γ_8 quartet which are given in Table 2.2. The localized electron system in Cox's model is realistic when W is negative and large; then $-3/8 < x < 0$ holds. The Γ_3 doublet can become the ground state over $-3/4 < x < 10/19$. For the $x > 0$ region, the energy level of Γ_8 quartet lies lower

State	Energy (in W unit)
$\|\Gamma_7\pm\rangle = \sqrt{\frac{1}{6}}\|\mp 5/2\rangle - \sqrt{\frac{5}{6}}\|\pm 3/2\rangle$	$-4x$
$\|\Gamma_8 \pm 2\rangle = \sqrt{\frac{5}{6}}\|\pm 5/2\rangle + \sqrt{\frac{1}{6}}\|\mp 3/2\rangle$	$2x$
$\|\Gamma_8 \pm 1\rangle = \|\pm 1/2\rangle$	$2x$

Table 2.2: Eigenstates and eigenvalues for $J = 5/2$ under a cubic crystal field.

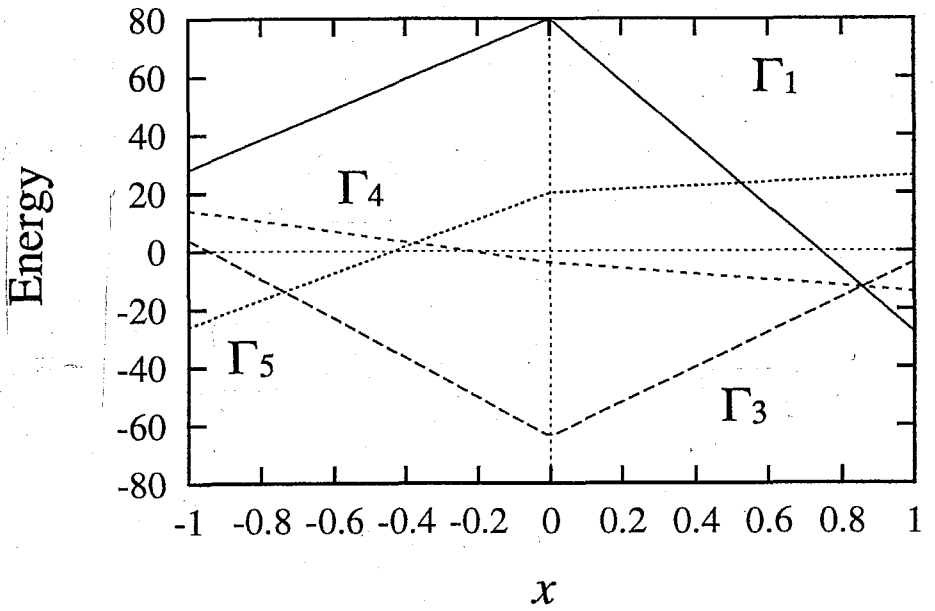

Figure 2.3: The x dependence of energy levels given in Table 2.1. The unit of energy is $-W$ ($W < 0$).

than that of Γ_7 doublet. Both energy levels has been exchanged in Cox's model. We note that the Γ_8 quartet as well as Γ_7 doublet has to be taken into account in order to make realistic the exchange interaction due to the Γ_3 doublet all over x. Such a general treatment will be carried out in Section 4.1.

Similarly, we obtain a non-Kramers doublet for tetragonal and hexagonal crystal fields. The crystal field Hamiltonian can be written in terms of Stevens operators as for the cubic case. For the tetragonal case, it is given by

$$H_{\text{tet}} = B_2^0 O_2^0 + B_4^0 O_4^0 + B_4^4 O_4^4 + B_6^0 O_6^0 + B_6^4 B_6^4 \tag{2.20}$$

where O_2^0 appears due to the uniaxial anisotropy:

$$O_2^0 = 3J_z^2 - J(J+1). \tag{2.21}$$

In this case, we have two Γ_1 singlets, Γ_2, Γ_3 and Γ_4 singlets and two Γ_5 doublets as a result of the splitting of $J = 4$ multiplet. The wave functions and the energy levels are summarized in Table 2.3. For $J = 5/2$ states, we have Γ_6, Γ_7 and Γ_8 doublets. For the hexagonal case, the crystal field Hamiltonian is given by

$$H_{\text{hex}} = B_2^0 O_2^0 + B_4^0 O_4^0 + B_6^0 O_6^0 + B_6^6 B_6^6, \tag{2.22}$$

where O_6^6 is due to the six-fold symmetry:

$$O_6^6 = \frac{1}{2}(J_+^6 + J_-^6). \tag{2.23}$$

In this case, we have Γ_1, Γ_3 and Γ_4 singlets, a Γ_5 doublet and two Γ_6 doublets from $J = 4$ multiplet. They are summarized in Table 2.4. For $J = 5/2$, we obtain Γ_7, Γ_8 and Γ_9 doublets.

Here we wish to make some general comments on the crystal field splitting. It depends on whether J is integer or a half odd integer. The former and the latter correspond to the case of even and odd number of electrons, respectively. For integer case, the multiplet splits finally into singlet, if the symmetry of the crystal field is low. It is possible to obtain doublet states for a high symmetric crystal field. Those doublets become identical after 2π rotation around the z axis. They are called non-Kramers doublets. For a half odd integer, on the other hand, it is impossible to lift

State	Energy
$\|\Gamma_{t1}^{(1)}\rangle = \varepsilon(\|4\rangle + \|-4\rangle) + \gamma\|0\rangle$	$4B_2 + 16B_4 - 2\sqrt{(12B_2 - B_4)^2 + 35B_4'^2}$
$\|\Gamma_{t1}^{(2)}\rangle = \frac{\gamma}{\sqrt{2}}(\|4\rangle + \|-4\rangle) - \sqrt{2}\varepsilon\|0\rangle$	$4B_2 + 16B_4 + 2\sqrt{(12B_2 - B_4)^2 + 35B_4'^2}$
$\|\Gamma_{t2}\rangle = \sqrt{\frac{1}{2}}(\|4\rangle - \|-4\rangle)$	$28B_2 + 14B_4$
$\|\Gamma_{t3}\rangle = \sqrt{\frac{1}{2}}(\|2\rangle + \|-2\rangle)$	$-8B_2 - 11B_4 + 15B_4'$
$\|\Gamma_{t4}\rangle = \sqrt{\frac{1}{2}}(\|2\rangle - \|-2\rangle)$	$-8B_2 - 11B_4 - 15B_4'$
$\|\Gamma_{t5}^{(1)}\pm\rangle = \alpha\|\mp 3\rangle + \beta\|\pm 1\rangle$	$-5B_2 - 6B_4 - \sqrt{9(4B_2 - 5B_4)^2 + 175B_4'^2}$
$\|\Gamma_{t5}^{(2)}\pm\rangle = \beta\|\mp 3\rangle - \alpha\|\pm 1\rangle$	$-5B_2 - 6B_4 + \sqrt{9(4B_2 - 5B_4)^2 + 175B_4'^2}$

Table 2.3: Eigenstates and eigenvalues for $J = 4$ under a tetragonal crystal field. Here the crystal field parameters are rewritten: $B_2 = B_2^0$, $B_4 = 60B_4^0$ and $B_4' = 12B_4^4$. For simplicity, B_6^0 and B_6^4 are taken as zero. $\alpha^2+\beta^2 = 1$ and $\gamma^2+2\varepsilon^2 = 1$ are satisfied.

State	Energy
$\|\Gamma_{h1}\rangle = \|0\rangle$	$-20B_2 + 36B_4 - 20B_6$
$\|\Gamma_{h3}\rangle = \sqrt{\frac{1}{2}}(\|3\rangle + \|-3\rangle)$	$7B_2 - 42B_4 - 17B_6 + 7B_6'$
$\|\Gamma_{h4}\rangle = \sqrt{\frac{1}{2}}(\|3\rangle - \|-3\rangle)$	$7B_2 - 42B_4 - 17B_6 - 7B_6'$
$\|\Gamma_{h5}\pm\rangle = \|\pm 1\rangle$	$-17B_2 + 18B_4 + B_6$
$\|\Gamma_{h6}^{(1)}\pm\rangle = \alpha\|\pm 4\rangle + \beta\|\mp 2\rangle$	$10B_2 + 3B_4 + 13B_6 - C(B_6')$
$\|\Gamma_{h6}^{(2)}\pm\rangle = \beta\|\pm 4\rangle - \alpha\|\mp 2\rangle$	$10B_2 + 3B_4 + 13B_6 + C(B_6')$

$$C(B_6') = \sqrt{(18B_2 + 25B_4 - 9B_6)^2 + 28B_6'^2}$$

Table 2.4: Eigenstates and eigenvalues for $J = 4$ under a hexagonal crystal field. The crystal field parameters are rewritten: $B_2 = B_2^0$, $B_4 = 30B_4^0$, $B_6 = 1260B_6^0$ and $B_6' = 360B_6^6$. $\alpha^2 + \beta^2 = 1$ is satisfied.

the degeneracy of Kramers doublets without breaking time reversal symmetry. The Kramers doublet acquires the phase π by the 2π rotation. In the character table, the irreducible representations are classified into two parts, depending on the time reversal symmetry. Identity and 2π rotation operations are denoted by E and R, respectively. The number in the E column corresponds to the degeneracy of the eigenstate. The sign of the character in the R column is positive in the upper part and negative in the lower part. It means that the Kramers doublet belongs to the lower part which is called a double point group. It is characterized by the reversal of sign of the wave function under R. The non-Kramers doublet, on the other hand, belongs to the upper part.

The effect of the crystal field is not negligible for heavy fermion materials. The typical U-based compounds include representatives of them are UBe_{13} with a cubic crystal, URu_2Si_2 with a tetragonal crystal and UPt_3 with a hexagonal crystal.

2.2 Numerical Renormalization Group Method

2.2.1 Model Hamiltonian

The Hamiltonian, to which we will apply the numerical renormalization group (NRG) method [12], consists of two parts; the kinetic energy of conduction electrons with spin and scattering channel and the effective exchange interaction. It is given by

$$H = \sum_{km} \varepsilon_k a^\dagger_{km} a_{km} + H_{\rm ex} \tag{2.24}$$

where $H_{\rm ex}$ is, for example, a multi-channel exchange Hamiltonian with a local spin S as

$$H_{\rm ex} = -J \sum_{\substack{kk' \\ ss'\mu}} a^\dagger_{k's'\mu} a_{ks\mu} (\boldsymbol{\sigma})_{s's} \cdot \boldsymbol{S}. \tag{2.25}$$

where s $(=\uparrow,\downarrow)$ and μ $(=1,2,\cdots)$ represent spin and channel, respectively.

Next we discuss how to transform the Hamiltonian to a form appropriate to the NRG calculation. In the NRG method, we first discretize the conduction band logarithmically. Each energy region is approximated by one state. In this procedure we first define the local orbital for the conduction electrons, which is coupled with the local moment through $H_{\rm ex}$. Next we construct new conduction orbitals connected

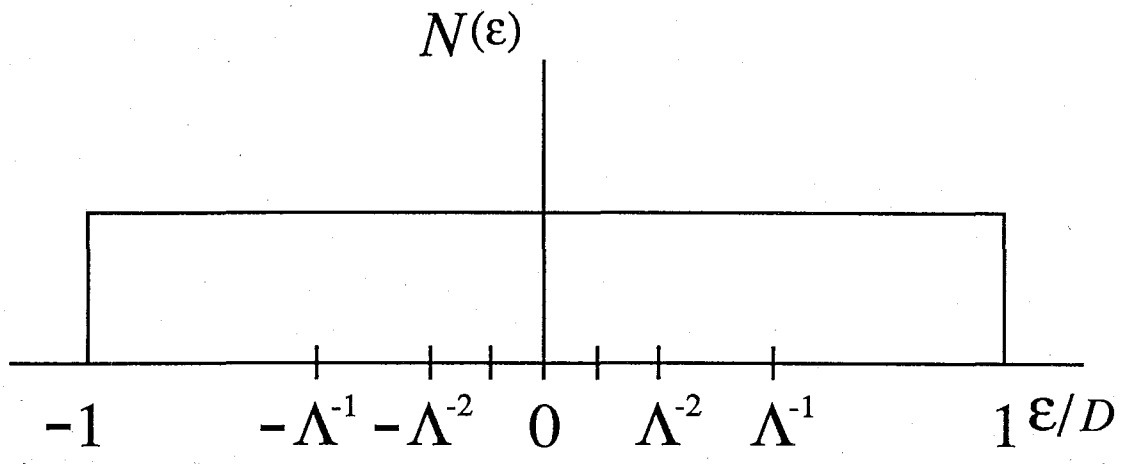

Figure 2.4: The logarithmic discretization of density of states for conduction electrons. The Fermi energy level is taken as the origin. The half width of band with D is logarithmically discretized with Λ.

with the old ones in order. These orbitals form a new basis of the conduction electrons. The logarithmic discretization is applied, for example, to the conduction band in Fig. 2.4. In the other words, we simplify the k dependence of the kinetic energy of conduction electrons as

$$\varepsilon_k = \frac{\hbar^2 k_{\rm F}^2}{2m^*} + \frac{\hbar^2 k_{\rm F}}{m^*} k, \tag{2.26}$$

and apply the logarithmic discretization to the k space. Here $\hbar$, $k_{\rm F}$ and m^* represent the Planck constant over 2π, the wave number at the Fermi sea and the effective mass of the conduction electron, respectively. The discretization parameter is usually chosen as $\Lambda = 2 \sim 3$. Each discretized region is denoted by j ($j = 0, 1, \cdots$). We denote the creation operator of the conduction electron for $\varepsilon_k > 0$ region as $a_{jm}^\dagger$ and that in $\varepsilon_k < 0$ region as $b_{jm}^\dagger$. All states of conduction electrons belonging to each discretized region are represented by just one state with the average energy E_j of the j-th region. According to this approximation, the Hamiltonian for the conduction electrons is written as

$$H_{\rm k} = \sum_{jm} E_j (a_{jm}^\dagger a_{jm} - b_{jm}^\dagger b_{jm}) \tag{2.27}$$

where

$$E_j = \frac{1}{2}(1 + \Lambda^{-1})\Lambda^{-j}. \tag{2.28}$$

The unit of the energies is the half width of band.

Next we define an operator f_{nm} which can be obtained through the unitary transformation from a_{jm} and b_{jm} as

$$f_{nm} = \sum_j (u_{nj} a_{jm} + v_{nj} b_{jm}), \tag{2.29}$$

where f_{nm} is a fermion operator satisfying

$$f_{nm} f_{nm}^\dagger + f_{nm}^\dagger f_{nm} = 1. \tag{2.30}$$

First we choose f_{0m} which couples with the local moment operator. Then we can obtain

$$u_{0j} = v_{0j} = \Big[\frac{1-\Lambda^{-1}}{2}\Big]^{1/2} \Lambda^{-j/2}. \tag{2.31}$$

Secondly, we determine the fermion operator in the outside orbital, f_{1m}, which is coupled with f_{0m}, from the commutation relation between f_{0m} and $H_{\rm k}$. Similarly, we can obtain f_{nm} for arbitrary number n through this procedure. Finally $H_{\rm k}$ is rewritten as

$$\sum_{nm} \varepsilon_n (f_{nm}^\dagger f_{n+1,m} + f_{n+1,m}^\dagger f_{nm}) \tag{2.32}$$

where

$$\varepsilon_n = \frac{1}{2}(1+\Lambda^{-1})\Lambda^{-n/2}(1-\Lambda^{-n-1})(1-\Lambda^{-2n-1})^{-1/2}(1-\Lambda^{-2n-3})^{-1/2}. \tag{2.33}$$

If n is large enough, we can approximate ε_n as

$$\varepsilon_n = \frac{1}{2}(1+\Lambda^{-1})\Lambda^{-n/2} \tag{2.34}$$

It is allowed for our problem to apply this relation of ε_n to all n. As a result of the above procedure, we have the hopping type of Hamiltonian:

$$H = \frac{1+\Lambda^{-1}}{2}\left[\sum_{n=0}^{\infty} \Lambda^{-n/2} \sum_m (f_{nm}^\dagger f_{n+1,m} + f_{n+1,m}^\dagger f_{nm}) + H_0\right]. \tag{2.35}$$

For example, H_0 for the multi-channel exchange Hamiltonian (2.25) is reduced to

$$H_0 = -\tilde{J} \sum_{ss'\mu} f_{0s'\mu}^\dagger f_{0s\mu} (\boldsymbol{\sigma})_{s's} \cdot \boldsymbol{S}, \tag{2.36}$$

and

$$\tilde{J} = \frac{2J}{1+\Lambda^{-1}}. \tag{2.37}$$

In practice, we keep the coefficient of the term

$$\sum_m (f^\dagger_{nm} f_{n+1,m} + f^\dagger_{n+1,m} f_{nm}) \tag{2.38}$$

as unity. Then one can truncate higher energy levels, since the energy scale for the lowest states is of the order of unity at every renormalization step. Let us define

$$H_N = \Lambda^{(N-1)/2}\Big[\sum_{n=0}^{N-1} \Lambda^{-n/2} \sum_m (f^\dagger_{nm} f_{n+1,m} + f^\dagger_{n+1,m} f_{nm}) + H_0\Big]. \tag{2.39}$$

Then H is expressed with H_N as

$$H = \lim_{N\to\infty} \frac{1}{2}(1+\Lambda^{-1})\Lambda^{-(N-1)/2} H_N. \tag{2.40}$$

We can also obtain the recursion relation as

$$H_{N+1} = \Lambda^{1/2} H_N + \sum_m (f^\dagger_{Nm} f_{N+1,m} + f^\dagger_{N+1,m} f_{Nm}). \tag{2.41}$$

Finally we briefly touch on the relation between the renormalization step and the temperature. The temperature is practically defined by calculating the impurity susceptibility and specific heat. If the total spin is a good quantum number, the impurity susceptibility is given by

$$T\chi_{\rm imp} = \lim_{N\to\infty}\left[\frac{{\rm Tr} J^2_{z,N} \exp(-\beta_N H_N)}{{\rm Tr}\exp(-\beta_N H_N)} - \frac{{\rm Tr}(J^0_{z,N})^2 \exp(-\beta_N H^0_N)}{{\rm Tr}\exp(-\beta_N H^0_N)}\right], \tag{2.42}$$

where $J_{z,N}$ is the z component of the total spin. For H^0_N and $J^0_{z,N}$, the impurity part is excluded from H_N and $J_{z,N}$, respectively. β_N is defined as

$$\beta_N = \frac{1}{2}(1+\Lambda)\Lambda^{-(N-1)/2}/k_{\rm B}T \tag{2.43}$$

where $k_{\rm B}$ is Boltzmann constant. If β_N is nearly equal to unity, only excited states of H_N with the order of unity are important in the trace. Corresponding to this, a temperture T_N is defined by

$$k_{\rm B}T_N = \frac{1}{2}(1+\Lambda)\Lambda^{-(N-1)/2}/\beta_N. \tag{2.44}$$

Then the lowest energy excitations of H_N are of the order of $k_{\rm B}T_N$, since the lowest energy scale for H_N is the order of unity.

2.2.2 Numerical Diagonalization

The NRG calculation starts from the bases obtained by the diagonalizing H_0. In general H_0 does not explicitly preserve the magnitude and the z component of the total spin. In this case the number of total electrons is the only conserved quantity that can be used to index representing the eigenstates.

Next, in order to obtain the matrix elements of H_1, we use the states given by the direct product of the eigenstates of H_0 and the states of conduction electrons filled in the first orbital. The latter states are also classified with the number of conduction electrons filled in the orbital. The eigenvalues and eigenstates of H_1 are determined by diagonalization. Then we calculate the matrix elements of H_2 with the recursion relation (2.41) by using the bases formed from the eigenstates of H_1 and the states of conduction electrons filled in the second orbital. Repeating this procedure, we determine the eigenvalues and eigenstates of H_N.

Here we briefly show how to construct the matrix elements of H_{N+1} by using the solution of H_N. The states of conduction electrons filled in the $(N+1)$-th orbital are expressed by a combination of $f^\dagger_{N+1,m}$. For example, if m has the four degree of freedom (four scattering channels including spin), they are expressed with sixteen binary numbers with four figures as

$$0000,\ 0001,\ 0010,\ \cdots,\ 1110,\ 1111. \tag{2.45}$$

The numbers 0 and 1 correspond, respectively, absence and presence of an electron in each orbital. Moreover these binary numbers are represented by $\alpha_{N+1} = 0 \sim 15$ in order and the state of fermions filled in the $(N+1)$ orbital is expressed as $|\alpha_{N+1}\rangle$. If we represent the eigenstates of H_N by $|k_N\rangle$ and have $N_{\rm tot}$ states at the N-th NRG step, the number of the bases $|\alpha_{N+1}\rangle \otimes |k_N\rangle$ for H_{N+1} amounts to $16N_{\rm tot}$. The matrix elements of H_{N+1} are given by a direct calculation of

$$\langle \alpha'_{N+1}, k'_N | f^\dagger_{Nm} f_{N+1,m} + f^\dagger_{N+1,m} f_{Nm} | \alpha_{N+1}, k_N \rangle, \tag{2.46}$$

where $|\alpha_{N+1}, k_N\rangle$ and $|\alpha'_{N+1}, k'_N\rangle$ are the bases of H_{N+1}. For the total number of electrons Q_N, the state $|k_N\rangle$ has been already obtained as a linear combination of the bases of H_{N-1} in the following way:

$$|k_{Q_N}\rangle = \sum C(k_{Q_N}; \alpha_{N-1}, k_{N-1}) |\alpha_{N-1}\rangle |k_{N-1}\rangle, \tag{2.47}$$

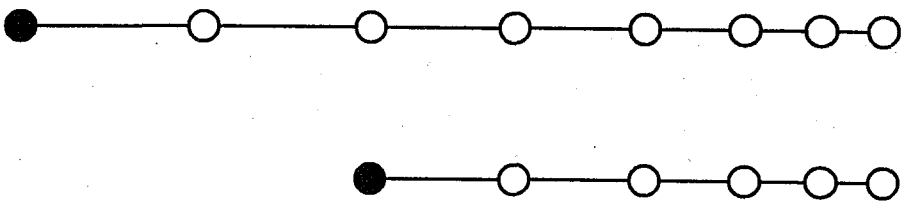

Figure 2.5: A graphical representation of H_N. The full circle represents a local spin, while the open ones represent orbitals of conduction electrons whose number is N. The distance between the empty circles corresponds to the magnitude of integral of electron transfer between them. The distance at the right side is always taken to be unity, independent of N. The chain expands towards the left as N increases.

where $C(k_{Q_N}; \alpha_{N-1}, k_{N-1})$ is the expansion coefficient. The matrix elements of H_{N+1} are given by a sum of the products of $C(k_{Q_N}; \alpha_{N-1}, k_{N-1})$ from $|k_{Q_N}\rangle$ and that from $|k'_{Q_N}\rangle$.

As mentioned above, the eigenvalues and eigenstates of H_N can be obtained by using the recursion relation (2.41). However, we are inevitably confronted with the difficulty that the matrix dimension of H_N becomes so large as N increases that it expands beyond the computational capacity of computer. In the NRG method, we leave only low energy eigenstates of H_N at each NRG step. For the next H_{N+1}, this cut-off restricts the maximum dimension of the matrices for diagonalization. It does not affect the low energy part so seriously because of the logarithmic discretization. In practice we obtain the eigenvalues for each Q_N, arrange all the eigenvalues of H_N in the order of energy and leave the eigenstates smaller than $N_{\rm cut}$. We note that $N_{\rm cut}$ should be chosen to take care of the degeneracy of the eigenstates. The eigenvalues in the high energy region is not reliable since the higher excited states have been discarded, while those in the low energy region are not reliable either if N is fixed to a finite value. The larger $N_{\rm cut}$ is, the better accuracy is expected for the eigenstates in the wide energy region at each NRG step.

Finally we summarize technical points in the NRG method.

- One has to check carefully the eigenvalues with the almost same value. If they

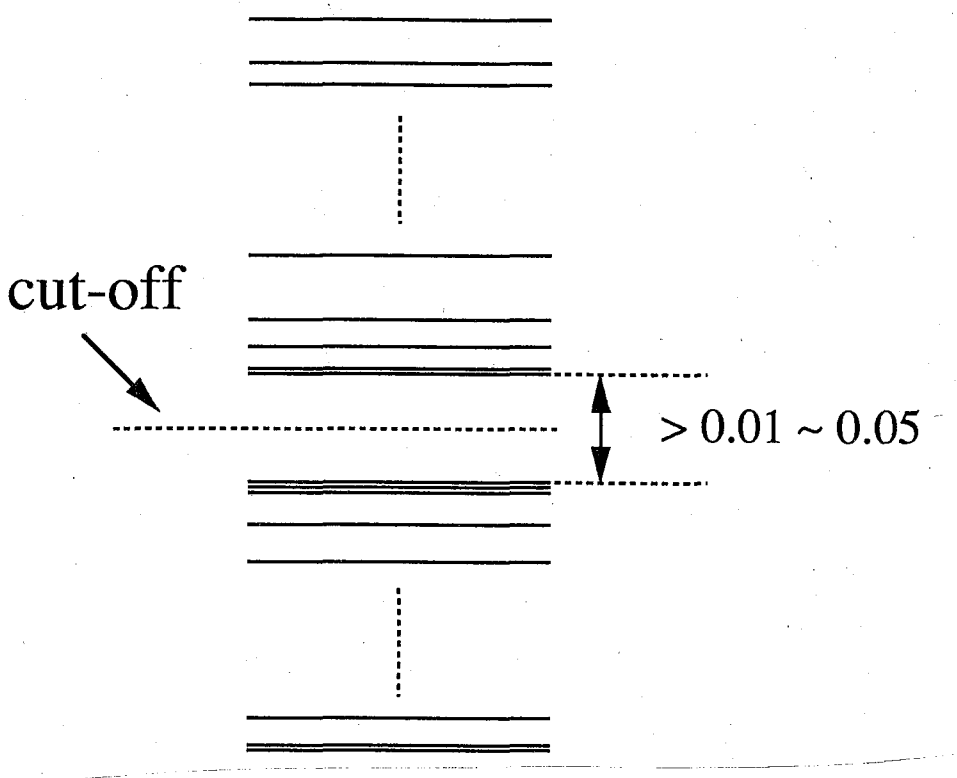

Figure 2.6: Cut-off of eigenvalues of H_N. Energy is measured vertically.

are within the numerical accuracy, it is likely that they belongs to a degenerate level. If so, one should put the same eigenvalue to them; otherwise numerical error may arise.

- In some cases $N_{\rm cut}$ cannot be taken so large because of the computational capacity of computer. In taking the cut-off, one had better take care of a difference of energy between the lowest discarded state and the highest kept state; otherwise the cut-off may give rise to error. The difference of energy is set larger than $0.01 \sim 0.05$ for our problem.

- To achieve efficiency, the vectorized calculation should be performed with a supercomputer. Much of CPU time are consumed for the diagonalization of the matrix. The maximum dimension of the matrix to be diagonalized depends on $N_{\rm cut}$ and the number of scattering channel of conduction electrons m including spin. It amounts to $\sim 1800 \times 1800$ for $N_{\rm cut} \sim 500$ and 4 channels; $\sim 4000 \times 4000$ for $N_{\rm cut} \sim 300$ and 6 channels.

2.2.3 Analysis of Energy Eigenvalues

Here we discuss the change of the energy eigenvalues of H_N with the increase of N. The energy levels are measured from the lowest energy at each NRG step. They finally become constant as N becomes large enough and keep the same values in the region of larger N. This means that H_N is approaching a fixed point.

First we consider the case of free conduction electrons (only hopping terms in (2.39)). This case turns out to be one-particle problem. H_N can be expressed with $N \times N$ matrix per scattering channel m, which is exactly diagonalized and written as

$$\left.\begin{array}{ll} H_N^0 = \sum_m \sum_{i=1}^{(N+1)/2} \eta_i (g_{im}^\dagger g_{im} + h_{im}^\dagger h_{im}) & (N+1: \text{ even}) \\ H_N^0 = \sum_m \left[\eta_0' g_0^\dagger g_0 + \sum_{i=1}^{N/2} \eta_i' (g_{im}^\dagger g_{im} + h_{im}^\dagger h_{im}) \right] & (N+1: \text{ odd}) \end{array}\right\} \tag{2.48}$$

Here $g_{im}^\dagger$ and g_{im} are the creation and annihilation operators for the quasi-particles with the i-th positive energy eigenvalue η_i and the channel m. $h_{im}^\dagger$ is the creation operator for holes defined as

$$h_{im}^\dagger = g_{im} \tag{2.49}$$

This relationship is guaranteed by the particle-hole symmetry. When N is large enough, low energy levels are independent of N. As a result of the numerical diagonalization, they can be obtained as the following series of energies which depend on whether N is even or odd for $\Lambda = 2$:

$$\left.\begin{array}{l} \eta_1 = 0.6555, \quad \eta_2 = 1.976, \quad \cdots, \quad \eta_i = 2^{i-1} \\ \eta_0' = 0, \quad \eta_1' = 1.297, \quad \eta_2' = 2.827, \quad \cdots, \quad \eta_i' = 2^{i-1/2} \end{array}\right\} \tag{2.50}$$

For large i, the energies are generally given by as $\eta_i = \Lambda^{i-1}$ and $\eta_i' = \Lambda^{i-1/2}$.

Next we take H_0 in (2.39) into account together and here treat the well-known one-channel case where m is restricted to only spin degree of freedom in (2.36). The parameters are taken as $\tilde{J} = -0.3$, $\Lambda = 2$ and $N_{\text{cut}} = 1000$. The behavior of energy eigenvalues depends on whether N is even or odd The low-lying energy levels are shown in Fig. 2.7 for even-number and odd-number renormalization steps. The eigenstates are characterized by the total number of electrons (Q_N), the magnitude and the z component of total spin (S_N and $S_{z,N}$ respectively). The total number is measured from the number of electrons at half filling. The ground state has $Q_N = 0$

for both even-number and odd-number renormalization steps. As far as the weak exchange coupling is considered, the energy levels in the small N region can be explained by weakly coupling the electrons with the local spin. For small $|\tilde{J}|$, the first excitation energy is nearly zero. This region is called the free-spin fixed point. The sufficiently large N region, on the other hand, corresponds to the strong coupling fixed point, where $|\tilde{J}|$ can be regarded as infinity. It means that a local singlet is formed on the 0-th site where one conduction electron and the local spin are combined strongly. Therefore the low-lying energy levels are equivalent to filling electrons in one-particle energy levels shown in Fig. 2.8. We actually find that the one-particle energy levels at even-number renormalization step are equal to η_i for odd N in (2.48), while those at odd-number renormalization step agree with η_i' for even N in (2.48). The ground state is given by filling electrons up to the Fermi energy level. In Fig. 2.7 (a), the ground state has $Q_N = 0$, $S_N = 0$ and $S_{z,N} = 0$. η_1 is the first excited state, which corresponds to $Q_N = 1$ and $Q_N = -1$. This state has four-fold degeneracy, including the degree of freedom of spin. The second excited energy level equals to $2\eta_1$, which corresponds to $Q_N = 2$, $Q_N = -2$ and both one-particle and one-hole excitation ($Q_N = 0$). The excited state has six-fold degeneracy since the last state has four possibilities due to spin degeneracy. In Fig. 2.7 (b), a one-particle energy level lies just Fermi energy level, so that the ground state is four-fold degenerate: It consists of two-fold $Q_N = 0$ state, a $Q_N = 1$ one and a $Q_N = -1$ one. The excited states can be obtained similarly to Fig. 2.7 (a). According to this analysis, for one-channel exchange model, the free-spin fixed point moves to the strong coupling fixed point as the renormalization proceeds. For this we conclude that the local spin is quenched and Fermi liquid realizes at low temperatures. However this is not the case for the two-channel or multi-channel exchange model which satisfies $N_{\rm ch} > 2S$ as discussed in Section 4.1. The NRG analysis on this problem will be described later.

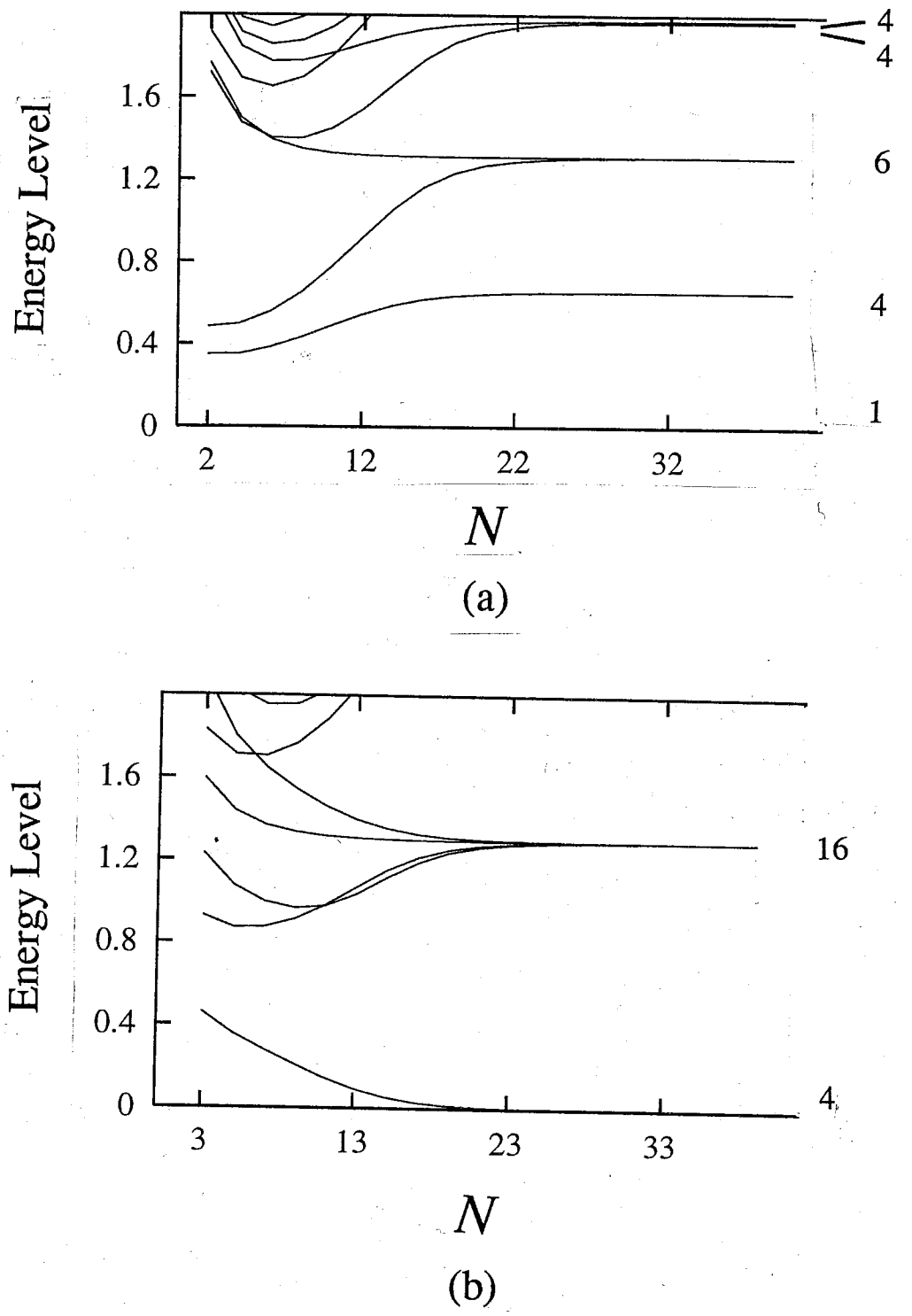

Figure 2.7: The low-lying NRG levels for the one-channel Kondo model for the antiferromagnetic coupling $J = -0.3$. $\Lambda = 2$ is taken and ~ 1000 states are kept: (a) even-number and (b) odd-number renormalization steps. The numbers at the right side represent the degrees of degeneracy.

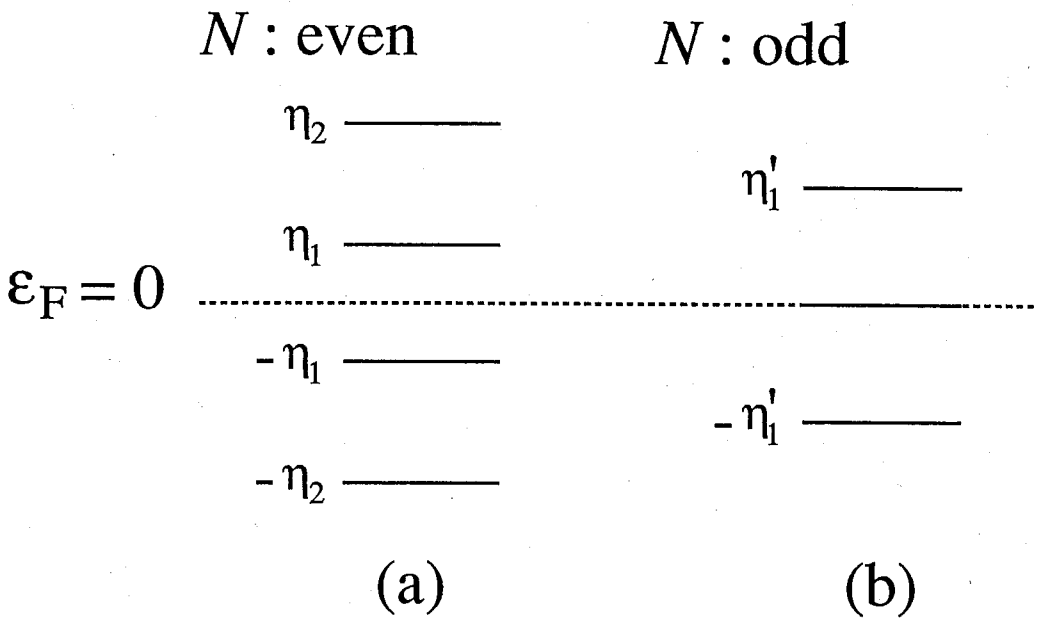

Figure 2.8: The one-particle energy levels at the fixed point where $\tilde{J} = -\infty$ for (a) even-number and (b) odd-number renormalization steps.

Chapter 3

Effective Exchange Interaction Due to Orbitally Degenerate Impurities

3.1 Extended Anderson Model

As mentioned in Chapter 1, we wish to examine the Kondo effect due to orbitally degenerate impurities in which various interactions among plural local f-electrons play an important role. Such a situation might be realized in U-based compounds. Although many intraatomic interactions must be taken into account in order to have a realistic atomic structure, we start first from the extended Anderson model in the absence of crystal field, which is written as

$$H = H_{\rm k} + H_f + H_{\rm mix}, \tag{3.1}$$

$$H_{\rm k} = \sum_{ks} \varepsilon_k a_{ks}^\dagger a_{ks}, \tag{3.2}$$

$$H_f = \varepsilon_f n_f + \frac{U}{2}(n_f^2 - n_f) - \frac{J_{\rm H}}{2}(2\boldsymbol{S}_f^2 + \frac{n_f^2}{2} - 2n_f) + H_{\rm so}, \tag{3.3}$$

$$H_{\rm mix} = \sum_{kms} \left(v_k a_{ks}^\dagger f_{ms} + {\rm h.c.}\right). \tag{3.4}$$

Here $H_{\rm k}$ and H_f represent the energy of conduction electrons and that of local f-electrons, respectively; $H_{\rm mix}$ is the mixing Hamiltonian between conduction and local f-electrons. $a_{ks}^\dagger$ and $f_{ms}^\dagger$ are the creation operators for conduction and local electrons, respectively. k, m and s denote the wave vector, orbital channel and spin ($=\uparrow,\downarrow$), respectively. n_f and $\boldsymbol{S}_f$ are the local f-electron number and the local

spin, respectively, which are defined with the creation and annihilation operators of f-electrons as

$$n_f \equiv \sum_{ms} f^\dagger_{ms} f_{ms}, \tag{3.5}$$

$$\boldsymbol{S}_f \equiv \sum_{mss'} f^\dagger_{ms} \Big(\frac{\boldsymbol{\sigma}}{2}\Big)_{ss'} f_{ms'}, \tag{3.6}$$

where $\boldsymbol{\sigma}$ is the Pauli matrix. $H_{\rm so}$ is the spin-orbit coupling in the $5f$-orbital

$$H_{\rm so} = \lambda \sum_{mm'ss'} f^\dagger_{ms} \big(\boldsymbol{L}\big)_{mm'} \cdot \Big(\frac{\boldsymbol{\sigma}}{2}\Big)_{ss'} f_{m's'}, \tag{3.7}$$

where $\boldsymbol{L}$ is the orbital angular momentum operator with $L = 3$ and m represents L_z. The second and third terms in H_f are the direct and exchange Coulomb interactions between local electrons on the impurity atom, respectively. They are equivalent to [18]

$$\frac{U}{2} \sum_{\substack{m_1 m_2 \\ s_1 s_2}} f^\dagger_{m_1 s_1} f^\dagger_{m_2 s_2} f_{m_2 s_2} f_{m_1 s_1} + \frac{J_{\rm H}}{2} \sum_{\substack{m_1 m_2 \\ s_1 s_2}} f^\dagger_{m_1 s_1} f^\dagger_{m_2 s_2} f_{m_1 s_2} f_{m_2 s_1}. \tag{3.8}$$

It is difficult to describe exactly the eigenstates of local f-electrons in which λ and $J_{\rm H}$ are comparable in magnitude as in heavy atoms like U. For simplicity, we choose the j-j coupling scheme, assuming $U > \lambda > J_{\rm H}$. This gives the same ground state as the Russell-Saunders coupling scheme for $U > J_{\rm H} > \lambda$. Since λ is positive and large, the subspace with $J = L - S = 3 - 1/2 = 5/2$ is chosen for one electron states and $J = L + S = 7/2$ is discarded. The multiplets are formed from the electrons within $J = 5/2$. The eigenstates are distinguished by the total angular momentum $\boldsymbol{J}$; the energy levels are separated from each other by $J_{\rm H}$. According to this scheme, the ground state of local f-electrons corresponds to the quantum number of $J = 5/2$, $J = 4$ and $J = 9/2$ for f^1, f^2 and f^3 configurations, respectively. For conduction electrons, it is reasonable to restrict exclusively to partial waves with the total angular momentum $j = 5/2$, since the mixing is expected to be particularly strong between the conduction band and the impurity orbital with the same symmetry. Then it is useful to introduce the creation operator of conduction electrons in the spherical wave representation as

$$a^\dagger_{klms} = (-i)^l \frac{kR}{\sqrt{6\pi}} \int d\Omega_k Y_l^m(\Omega_k) a^\dagger_{ks}, \tag{3.9}$$

where Y_l^m is the spherical harmonic and we choose $l = 3$ for f-symmetry. R represents the radius of the spherical crystal. To take into account the spin-orbit interaction, $a^\dagger_{k,3,m,s}$ is transformed to $j = l + s = 7/2$ and $j = l - s = 5/2$ operators as

$$a^\dagger_{k,7/2,M} = \sqrt{\frac{1}{2} + \frac{M}{7}}\, a^\dagger_{k,3,M-1/2,\uparrow} + \sqrt{\frac{1}{2} - \frac{M}{7}}\, a^\dagger_{k,3,M+1/2,\downarrow}, \tag{3.10}$$

$$a^\dagger_{k,5/2,M} = -\sqrt{\frac{1}{2} - \frac{M}{7}}\, a^\dagger_{k,3,M-1/2,\uparrow} + \sqrt{\frac{1}{2} + \frac{M}{7}}\, a^\dagger_{k,3,M+1/2,\downarrow}, \tag{3.11}$$

where M is the z component for $j = 7/2$ or $j = 5/2$. After these transformations the Hamiltonian (3.1) is rewritten as

$$H_{\rm k} = \sum_{km} \varepsilon_k a^\dagger_{km} a_{km}, \tag{3.12}$$

$$H_f = E_f n_f + \frac{U}{2}(n_f^2 - n_f) - \frac{J_{\rm H}}{2}\Big(2[\boldsymbol{S}_f^2]_{J=5/2} + \frac{n_f^2}{2} - 2n_f\Big), \tag{3.13}$$

$$H_{\rm mix} = \sum_{km} \Big(v_k a^\dagger_{km} f_m + {\rm h.c.}\Big). \tag{3.14}$$

Here m $(= 5/2, 3/2, \cdots, -5/2)$ is the z component of $\boldsymbol{j}$ $(j = 5/2)$ for conduction electrons or that of $\boldsymbol{J}$ $(J = 5/2)$ for the local f-electrons. E_f means $E_f = \varepsilon_f - 2\lambda$. $[\boldsymbol{S}_f^2]_{J=5/2}$ represents a projection of $\boldsymbol{S}_f^2$ onto the multiplet which consists of only local electrons with $J_i = 5/2$ (i is the index of the local electron). Namely, the total angular momentum of the multiplet with n electrons is determined by $\boldsymbol{J} = \boldsymbol{J}_1 + \boldsymbol{J}_2 + \cdots + \boldsymbol{J}_n$ where every $\boldsymbol{J}_i$ has the magnitude of 5/2. Although the multiplet is no longer pure eigenstate of $\boldsymbol{S}_f^2$, one can write it within the restriction as

$$[\boldsymbol{S}_f^2]_{J=5/2} = \frac{3}{4} n_f + \frac{1}{49}(\boldsymbol{J}^2 - \frac{35}{4} n_f). \tag{3.15}$$

This relation is derived in Appendix B.

3.2 Derivation of Effective Exchange Hamiltonian

Now we derive an effective exchange Hamiltonian from the simplified Anderson Hamiltonian (3.12), (3.13) and (3.14) via the Schrieffer-Wolff transformation, assuming $|E_f|$ and U are much larger than v_k. The configuration of the most stable

unperturbed state is assumed to be f^n. The stability condition is then given by

$$[E_f + (n-1)U](E_f + nU) < 0, \tag{3.16}$$

if $J_{\rm H} \ll U$. Here the Fermi energy is taken as the origin of energy.

We will treat the effective exchange interaction only within the ground state of this configuration, which can be justified if the Hund coupling $J_{\rm H}$ is so large that one can neglect the contribution from the excited states. On the other hand, we consider all the intermediate states for f^{n-1} and f^{n+1} configurations, which are connected by the electron transfer between conduction and local electrons.

The eigenstates for f^n configuration given by H_f have the following energy:

$$E(n, J_i) = E_f n + \frac{1}{2}(U - \frac{J_{\rm H}}{2})(n^2 - n) - \frac{J_{\rm H}}{49}\{J_i(J_i+1) - \frac{35}{4}n\}, \tag{3.17}$$

where n is the electron number and J_i represents the total angular momentum of the i-th eigenstate. The ground state is given by the maximum J among J_i's: $J = 5/2$ for $n = 1$, $J = 4$ for $n = 2$ and $J = 9/2$ for $n = 3$. If the Schrieffer-Wolff transformation is applied to second order of v_k, we can obtain an effective exchange interaction between conduction electrons and the local ground states $|n, J, M\rangle$ where M represents $J_z = J, J-1, \cdots, -J$. Formally the Hamiltonian takes the following form:

$$H_{\rm ex} = \sum_{\substack{kk' \\ mm'}} a^\dagger_{k'm'} a_{km} \Big[\sum_i I(n-1, J_i)\; T_{m'm}(n-1, J_i) - \sum_j I(n+1, J_j)\; T_{m'm}(n+1, J_j) \Big]. \tag{3.18}$$

where $I(n-1, J_i)$ and $I(n+1, J_j)$ are the couplings of the exchange interaction via the intermediate states with f^{n-1} and f^{n+1}, respectively. They are given by

$$I(n-1, J_i) = \frac{|v_{k_{\rm F}}|^2}{E(n-1, J_i) - E(n, J)} > 0, \tag{3.19}$$

$$I(n+1, J_j) = \frac{|v_{k_{\rm F}}|^2}{E(n+1, J_j) - E(n, J)} > 0, \tag{3.20}$$

where conduction electrons corresponding to $\varepsilon_k \simeq \varepsilon_{k_{\rm F}} = 0$ are considered.

$T_{m'm}$ represents the transition matrix with respect to M. The matrix elements $T_{m'm}$ are given as

$$\big(T_{m'm}(n-1, J_i)\big)_{M'M} = \langle n, J, M' | f^\dagger_m | n-1, J_i, M_i \rangle \langle n-1, J_i, M_i | f_{m'} | n, J, M \rangle,$$

(3.21)

$$\Big(T_{m'm}(n+1,J_j)\Big)_{M'M} = \langle n,J,M'|f_{m'}|n+1,J_j,M_j\rangle\langle n+1,J_j,M_j|f_m^\dagger|n,J,M\rangle,$$

(3.22)

where $M_i = M - m' = M' - m$ and $M_j = M + m = M' + m'$. $|n-1,J_i,M_i\rangle$ and $|n+1,J_j,M_j\rangle$ are the eigenstates for f^{n-1} and f^{n+1}, respectively.

Next we introduce a unitary transformation to $T_{m'm}(n-1,J_i)$ and $T_{m'm}(n+1,J_j)$ in order to describe them in terms of irreducible tensor operators $J_q^{(p)}$ in rotation group, which have been defined by (2.9) and (2.10). The relationship between $T_{m'm}$ and $J_q^{(p)}$ can be written down as follows:

$$T_{-5/2,5/2} = -C_5 J_5^{(5)}, \tag{3.23}$$

$$\begin{pmatrix} \frac{1}{\sqrt{2}} & \frac{1}{\sqrt{2}} \\ \frac{1}{\sqrt{2}} & -\frac{1}{\sqrt{2}} \end{pmatrix} \begin{pmatrix} T_{-3/2,5/2} \\ T_{-5/2,3/2} \end{pmatrix} = \begin{pmatrix} C_4 J_4^{(4)} \\ C_5 J_4^{(5)} \end{pmatrix}, \tag{3.24}$$

$$\begin{pmatrix} \frac{\sqrt{10}}{6} & \frac{2}{3} & \frac{\sqrt{10}}{6} \\ \frac{1}{\sqrt{2}} & 0 & -\frac{1}{\sqrt{2}} \\ \frac{\sqrt{2}}{3} & -\frac{\sqrt{5}}{3} & \frac{\sqrt{2}}{3} \end{pmatrix} \begin{pmatrix} T_{-1/2,5/2} \\ T_{-3/2,3/2} \\ T_{-5/2,1/2} \end{pmatrix} = -\begin{pmatrix} C_3 J_3^{(3)} \\ C_4 J_3^{(4)} \\ C_5 J_3^{(5)} \end{pmatrix}, \tag{3.25}$$

$$\begin{pmatrix} \frac{\sqrt{5}}{2\sqrt{7}} & \frac{3}{2\sqrt{7}} & \frac{3}{2\sqrt{7}} & \frac{\sqrt{5}}{2\sqrt{7}} \\ \frac{\sqrt{5}}{2\sqrt{3}} & \frac{1}{2\sqrt{3}} & -\frac{1}{2\sqrt{3}} & -\frac{\sqrt{5}}{2\sqrt{3}} \\ \frac{3}{2\sqrt{7}} & -\frac{\sqrt{5}}{2\sqrt{7}} & -\frac{\sqrt{5}}{2\sqrt{7}} & \frac{3}{2\sqrt{7}} \\ \frac{1}{2\sqrt{3}} & -\frac{\sqrt{5}}{2\sqrt{3}} & \frac{\sqrt{5}}{2\sqrt{3}} & -\frac{1}{2\sqrt{3}} \end{pmatrix} \begin{pmatrix} T_{1/2,5/2} \\ T_{-1/2,3/2} \\ T_{-3/2,1/2} \\ T_{-5/2,-1/2} \end{pmatrix} = \begin{pmatrix} C_2 J_2^{(2)} \\ C_3 J_2^{(3)} \\ C_4 J_2^{(4)} \\ C_5 J_2^{(5)} \end{pmatrix}, \tag{3.26}$$

$$\begin{pmatrix} \frac{1}{\sqrt{7}} & \frac{2\sqrt{2}}{\sqrt{35}} & \frac{3}{\sqrt{35}} & \frac{2\sqrt{2}}{\sqrt{35}} & \frac{1}{\sqrt{7}} \\ \frac{\sqrt{5}}{\sqrt{14}} & \frac{1}{\sqrt{7}} & 0 & -\frac{1}{\sqrt{7}} & -\frac{\sqrt{5}}{\sqrt{14}} \\ \frac{1}{\sqrt{3}} & -\frac{1}{\sqrt{30}} & -\frac{2}{\sqrt{15}} & -\frac{1}{\sqrt{30}} & \frac{1}{\sqrt{3}} \\ \frac{1}{\sqrt{7}} & -\frac{5}{\sqrt{70}} & 0 & \frac{5}{\sqrt{70}} & -\frac{1}{\sqrt{7}} \\ \frac{1}{\sqrt{42}} & -\frac{\sqrt{5}}{\sqrt{21}} & \frac{\sqrt{10}}{\sqrt{21}} & -\frac{\sqrt{5}}{\sqrt{21}} & \frac{1}{\sqrt{42}} \end{pmatrix} \begin{pmatrix} T_{3/2,5/2} \\ T_{1/2,3/2} \\ T_{-1/2,1/2} \\ T_{-3/2,-1/2} \\ T_{-5/2,-3/2} \end{pmatrix} = -\begin{pmatrix} C_1 J_1^{(1)} \\ C_2 J_1^{(2)} \\ C_3 J_1^{(3)} \\ C_4 J_1^{(4)} \\ C_5 J_1^{(5)} \end{pmatrix}, \tag{3.27}$$

$$\begin{pmatrix} \frac{1}{\sqrt{6}} & \frac{1}{\sqrt{6}} & \frac{1}{\sqrt{6}} & \frac{1}{\sqrt{6}} & \frac{1}{\sqrt{6}} & \frac{1}{\sqrt{6}} \\ \frac{5}{\sqrt{70}} & \frac{3}{\sqrt{70}} & \frac{1}{\sqrt{70}} & -\frac{1}{\sqrt{70}} & -\frac{3}{\sqrt{70}} & -\frac{5}{\sqrt{70}} \\ \frac{5}{2\sqrt{21}} & -\frac{1}{2\sqrt{21}} & -\frac{2}{\sqrt{21}} & -\frac{2}{\sqrt{21}} & -\frac{1}{2\sqrt{21}} & \frac{5}{2\sqrt{21}} \\ \frac{5}{6\sqrt{5}} & -\frac{7}{6\sqrt{5}} & -\frac{2}{3\sqrt{5}} & \frac{2}{3\sqrt{5}} & \frac{7}{6\sqrt{5}} & -\frac{5}{6\sqrt{5}} \\ \frac{1}{2\sqrt{7}} & -\frac{3}{2\sqrt{7}} & \frac{1}{\sqrt{7}} & \frac{1}{\sqrt{7}} & -\frac{3}{2\sqrt{7}} & \frac{1}{2\sqrt{7}} \\ \frac{1}{6\sqrt{7}} & -\frac{5}{6\sqrt{7}} & \frac{5}{3\sqrt{7}} & -\frac{5}{3\sqrt{7}} & \frac{5}{6\sqrt{7}} & -\frac{1}{6\sqrt{7}} \end{pmatrix} \begin{pmatrix} T_{5/2,5/2} \\ T_{3/2,3/2} \\ T_{1/2,1/2} \\ T_{-1/2,-1/2} \\ T_{-3/2,-3/2} \\ T_{-5/2,-5/2} \end{pmatrix}$$

$$= \begin{pmatrix} C_0\mathbf{1} \\ C_1 J_0^{(1)} \\ C_2 J_0^{(2)} \\ C_3 J_0^{(3)} \\ C_4 J_0^{(4)} \\ C_5 J_0^{(5)} \end{pmatrix}. \tag{3.28}$$

Here $\mathbf{1}$ denotes the unit matrix. $C_0, C_1, \cdots, C_5$ are constants which are given in Tables 3.1–3.3. In fact, the matrix elements of the above unitary matrices correspond to those of $j_{-q}^{(p)}$ for conduction electrons with $j = 5/2$. It leads to the following tensorial expression:

$$\sum_{p,q} A'_p (-1)^q j_{-q}^{(p)} J_q^{(p)} \tag{3.29}$$

for both of $T_{m'm}(n-1, J_i)$ and $T_{m'm}(n+1, J_j)$. The difference among the transition matrices appears only in the coefficient A'_p.

Finally we combine $T_{m'm}(n-1, J_i)$ and $T_{m'm}(n+1, J_j)$ to obtain the effective exchange Hamiltonian. For the f^n configuration, the coupling for each p ($p > 0$) can be expressed with $J_{0,p}(n)$ as

$$J_{0,p}(1) = \alpha_p(1) I(0,0) + \beta_p(1) I(2,0) + \gamma_p(1) I(2,2) + \delta_p(1) I(2,4), \tag{3.30}$$

$$J_{0,p}(2) = \alpha_p(2) I(1,\frac{5}{2}) + \beta_p(2) I(3,\frac{3}{2}) + \gamma_p(2) I(3,\frac{5}{2}) + \delta_p(2) I(3,\frac{9}{2}), \tag{3.31}$$

$$J_{0,p}(3) = \alpha_p(3) I(2,2) + \beta_p(3) I(2,4) + \gamma_p(3) I(4,2) + \delta_p(3) I(4,4). \tag{3.32}$$

Here the coefficients $\alpha_p(n)$, $-\beta_p(n)$, $-\gamma_p(n)$ and $-\delta_p(n)$ are related to C_p and are the values in the first, second, third and fourth columns, respectively, in Tables 3.1 (for $n = 1$) and 3.2 (for $n = 2$). For $n = 3$, $\alpha_p(3)$, $\beta_p(3)$, $-\gamma_p(3)$ and $-\delta_p(3)$ are the values in Table 3.3. For example, we have

$$\alpha_1(3) = \frac{5}{14}, \quad \alpha_2(3) = \frac{25}{672}, \quad \alpha_3(3) = \frac{15}{28}, \quad \alpha_4(3) = \frac{1}{3528}, \quad \alpha_5(3) = \frac{3}{28}. \tag{3.33}$$

The coefficients $\beta_p(n)$, $\gamma_p(n)$ and $\delta_p(n)$ for $n = 1$ and 2, and all coefficients for $n = 3$ are related to the Hund coupling. For $n = 1$ and 2, $\beta_p(n) + \gamma_p(n) + \delta_p(n) = 1$ is satisfied for each p. Therefore $J_{0,p}$ takes the same positive coupling constant

$$J_0 = -\frac{|v_{k_F}|^2 U}{[E_f + (n-1)U](E_f + nU)}, \tag{3.34}$$

if the Hund coupling $J_{\rm H}$ vanishes. Here the ε_k-dependence of J_0 is neglected and $k_{\rm F}$ represents the wave number at the Fermi sea. Similarly, for $n = 3$, $\alpha_p(3) + \beta_p(3) = \gamma_p(3) + \delta_p(3) = 1$ is satisfied for each odd p. Then J_0 can be also given by $J_{0,p}$ for each odd p if $J_{\rm H} = 0$.

After the calculations as mentioned above, the Hamiltonian for f^1, f^2 and f^3 ground states is given to second order of v_k by the following form:

$$H = H_{\rm k} + H_f + H_{\rm ex}, \tag{3.35}$$

$$H_{\rm ex} = J_0 \sum_{\substack{kk' \\ mm'}} a^\dagger_{k'm'} a_{km} T_{m'm}, \tag{3.36}$$

where

$$T_{m'm} = \frac{2}{35}\Big[\sum_{p=1}^{5}\sum_{q=-p}^{p}(-1)^q A_p (j^{(p)}_{-q})_{m'm} J^{(p)}_q + A_0\Big]$$

with $m' - m = -q$. The coefficients A_p are related to Clebsch-Gordan coefficients. The Hund coupling is contained not in J_0 but in A_p. $j^{(p)}_{-q}$ and $J^{(p)}_q$ represent the tensor operators for conduction and local f-electrons, respectively. Namely, the former is formed with $j = 5/2$ and the latter with the local angular moment $\boldsymbol{J}$. When $J_{\rm H}$ vanishes, A_p's take the following values:

$$A_1 = 1,\ A_2 = \frac{5}{24},\ A_3 = \frac{7}{162},\ A_4 = \frac{1}{90},\ A_5 = \frac{2}{405}, \tag{3.37}$$

for f^1 configuration ($J = 5/2$),

$$A_1 = 1,\ A_2 = \frac{5}{84},\ A_3 = -\frac{1}{324},\ A_4 = -\frac{1}{630},\ A_5 = -\frac{1}{2835}, \tag{3.38}$$

for f^2 configuration ($J = 4$),

$$A_1 = 1,\ A_2 = 0,\ A_3 = -\frac{1}{162},\ A_4 = 0,\ A_5 = \frac{2}{8505}, \tag{3.39}$$

for f^3 configuration ($J = 9/2$). Since the Hund coupling is actually finite, the value of A_p shifts from the above value by $\alpha J_{\rm H}/U$ ($< A_p$) for a small $J_{\rm H}/U$, where α is also related to Clebsch-Gordan coefficients.

Our Hamiltonian written with tensor operators is convenient to study the effect of the crystal field in a systematic way.

	$T_{m'm}(0,0)$	$T_{m'm}(0,4)$	$T_{m'm}(2,4)$	$T_{m'm}(4,4)$
$\sqrt{6}C_0$	1	1/3	5/3	3
$(\sqrt{70}/2)C_1$	1	−1/3	−23/21	3/7
$2\sqrt{21}C_2$	1	1/3	1/6	−3/2
$9\sqrt{5}C_3$	1	−1/3	29/42	−19/14
$15\sqrt{7}C_4$	1	1/3	−5/6	−1/2
$(45\sqrt{7}/2)C_5$	1	−1/3	−25/42	−1/14

Table 3.1: C_p's in (3.23)–(3.28) for f^1 configuration.

	$T_{m'm}(1,5/2)$	$T_{m'm}(3,3/2)$	$T_{m'm}(3,5/2)$	$T_{m'm}(3,9/2)$
$(\sqrt{6}/2)C_0$	1	4/21	1/2	55/42
$(\sqrt{70}/2)C_1$	1	−5/21	−1/2	−11/42
$7\sqrt{21}C_2$	1	10/21	1/2	−83/42
$-126\sqrt{5}C_3$	1	20/21	−1/2	−61/42
$-105\sqrt{7}C_4$	1	−4/21	1/2	−55/42
$-315\sqrt{7}C_5$	1	2/21	−1/2	−25/42

Table 3.2: C_p's in (3.23)–(3.28) for f^2 configuration.

	$T_{m'm}(2,2)$	$T_{m'm}(2,4)$	$T_{m'm}(4,2)$	$T_{m'm}(4,4)$
$(\sqrt{6}/3)C_0$	3/14	11/14	3/14	11/14
$(\sqrt{70}/2)C_1$	5/14	9/14	−5/14	−9/14
$(5\sqrt{21}/12)C_2$	25/672	−25/672	25/672	−25/672
$63\sqrt{5}C_3$	15/28	−43/28	−15/28	43/28
$(\sqrt{7}/6)C_4$	1/3528	−1/3528	1/3528	−1/3528
$(945\sqrt{7}/2)C_5$	3/28	25/28	−3/28	−25/28

Table 3.3: C_p's in (3.23)–(3.28) for f^3 configuration. All C_p's vanish for $T_{m'm}(2,0)$ and $T_{m'm}(4,0)$.

Chapter 4

Kondo Effect Due to Doublet State

In this chapter we wish to discuss differences of the Kondo effect between Kramers and non-Kramers doublets. In particular we focus our attention on the number of scattering channels and the stability of Fermi liquid and non-Fermi liquid at low temperatures.

It is well known that, whether one has Kramers doublets or not depends on the number of local electrons: we have the former case for odd number and the latter for even. This shows up typically in connection with f^2 and f^3 configurations in the presence of cubic crystal field. f^2 and f^3 also correspond to U^{4+} and U^{3+}, respectively. We discuss the f^2 case first and then turn to the f^3 case. The case of tetragonal and hexagonal crystal fields are also studied for f^2.

4.1 Kondo Effect Due to f^2 Non-Kramers Doublet

For f^2 configuration, the degenerate ground states without the crystal field are characterized by the total angular momentum: $J = 4$ and $J_z = 4, 3, \cdots, -4$. The perturbation due to cubic crystal field lifts the degeneracy. If the lowest state becomes non-Kramers doublet, it is given by $|\Gamma_3\pm\rangle$, which are written as

$$|\Gamma_3+\rangle = \frac{\sqrt{42}}{12}|4\rangle - \frac{\sqrt{15}}{6}|0\rangle + \frac{\sqrt{42}}{12}|-4\rangle, \tag{4.1}$$

$$|\Gamma_3-\rangle = \frac{1}{\sqrt{2}}|2\rangle + \frac{1}{\sqrt{2}}|-2\rangle. \tag{4.2}$$

Both of them can be distinguished in terms of quadrupolar moment (irreducible tensor operator of rank 2)

$$3J_z^2 - J(J+1) = 2J_0^{(2)}, \tag{4.3}$$

and have the following properties:

$$\langle \Gamma_3 \pm | J_z | \Gamma_3 \pm \rangle = 0, \tag{4.4}$$

$$\langle \Gamma_3 \pm | J_\pm^n | \Gamma_3 \mp \rangle = 0 \quad (n : \text{odd}). \tag{4.5}$$

We express the non-Kramers doublet $|\Gamma_3 \pm\rangle$ with a pseudo-spin operator with 1/2 as

$$S_+|\Gamma_3-\rangle = |\Gamma_3+\rangle, \quad S_-|\Gamma_3+\rangle = |\Gamma_3-\rangle, \tag{4.6}$$

$$S_z|\Gamma_3+\rangle = \frac{1}{2}|\Gamma_3+\rangle, \quad S_z|\Gamma_3-\rangle = -\frac{1}{2}|\Gamma_3-\rangle. \tag{4.7}$$

The effective exchange Hamiltonian is obtained by calculating $\langle \Gamma_3 \pm | J_q^{(p)} | \Gamma_3 \pm \rangle$ and $\langle \Gamma_3 \pm | J_q^{(p)} | \Gamma_3 \mp \rangle$ in (3.36); the scattering of conduction electrons is expressed with $j_q^{(p)}$ in the following way:

$$H_{\text{ex}} = J_0 \sum_{mm'}^{kk'} a_{k'm'}^\dagger a_{km} [(T_\perp)_{m'm} S_- + (T_\perp^\dagger)_{m'm} S_+ + (T_z)_{m'm} S_z + (T_0)_{m'm}], \tag{4.8}$$

where $T_\perp$, T_z and T_0 are linear combinations of $\{j_q^{(p)}\}$, which are defined as

$$T_\perp = -\frac{\sqrt{2}}{147}(j_2^{(2)} + j_{-2}^{(2)}) - \frac{\sqrt{10}}{630}(j_2^{(3)} - j_{-2}^{(3)}) - \frac{4\sqrt{30}}{2205}(j_2^{(4)} + j_{-2}^{(4)}), \tag{4.9}$$

$$T_z = \frac{4}{147} j_0^{(2)} - \frac{8}{441} j_0^{(4)} + \frac{4\sqrt{70}}{2205}(j_4^{(4)} + j_{-4}^{(4)}), \tag{4.10}$$

$$T_0 = -\frac{1}{630} j_0^{(4)} - \frac{\sqrt{70}}{8820}(j_4^{(4)} + j_{-4}^{(4)}), \tag{4.11}$$

for $J_{\text{H}} = 0$. These are written down explicitly with 6×6 matrices as

$$T_\perp = -\frac{1}{84} \begin{pmatrix} & & 5\sqrt{30} & & & \\ & & & -3\sqrt{6} & & \\ 3\sqrt{30} & & & & -5\sqrt{6} & \\ & -5\sqrt{6} & & & & 3\sqrt{30} \\ & & -3\sqrt{6} & & & \\ & & & 5\sqrt{30} & & \end{pmatrix}, \tag{4.12}$$

$$T_z = \frac{4}{21}\begin{pmatrix} 0 & & & & \sqrt{5} & \\ & 2 & & & & \sqrt{5} \\ & & -2 & & & \\ & & & -2 & & \\ \sqrt{5} & & & & 2 & \\ & \sqrt{5} & & & & 0 \end{pmatrix}, \tag{4.13}$$

$$T_0 = -\frac{1}{84}\begin{pmatrix} 1 & & & & \sqrt{5} & \\ & -3 & & & & \sqrt{5} \\ & & 2 & & & \\ & & & 2 & & \\ \sqrt{5} & & & & -3 & \\ & \sqrt{5} & & & & 1 \end{pmatrix}, \tag{4.14}$$

where the blanks in these matrices should be filled in with 0's. For conduction electrons, the spherical symmetric basis of the operator has been transformed to the cubic symmetric one in the following way:

$$\begin{aligned} a^\dagger_{k,\Gamma_7\mp} &= \sqrt{\frac{1}{6}}a^\dagger_{k,\pm 5/2} - \sqrt{\frac{5}{6}}a^\dagger_{k,\mp 3/2}, \\ a^\dagger_{k,\Gamma_8\pm 2} &= \sqrt{\frac{5}{6}}a^\dagger_{k,\pm 5/2} + \sqrt{\frac{1}{6}}a^\dagger_{k,\mp 3/2}, \\ a^\dagger_{k,\Gamma_8\pm 1} &= a^\dagger_{k,\pm 1/2}. \end{aligned} \tag{4.15}$$

Then, within the non-Kramers doublet, the effective exchange Hamiltonian in the absence of crystal field (3.36) is reduced as follows:

$$H_{\rm ex}(\Gamma_3) = H_{\rm iso} + H_{\rm aniso} + H_{\rm pot}, \tag{4.16}$$

$$\begin{aligned} H_{\rm iso} = \frac{8}{21}J_0\sum_{kk'}\Big\{ & -(a^\dagger_{k',\Gamma_8+2}a_{k,\Gamma_8+1} + a^\dagger_{k',\Gamma_8-2}a_{k,\Gamma_8-1})S_- \\ & -(a^\dagger_{k',\Gamma_8+1}a_{k,\Gamma_8+2} + a^\dagger_{k',\Gamma_8-1}a_{k,\Gamma_8-2})S_+ \\ & +\Big[(a^\dagger_{k',\Gamma_8+2}a_{k,\Gamma_8+2} - a^\dagger_{k',\Gamma_8+1}a_{k,\Gamma_8+1}) \\ & +(a^\dagger_{k',\Gamma_8-2}a_{k,\Gamma_8-2} - a^\dagger_{k',\Gamma_8-1}a_{k,\Gamma_8-1})\Big]S_z\Big\}, \end{aligned} \tag{4.17}$$

$$\begin{aligned} H_{\rm aniso} = J_0\sum_{kk'}\Big\{ & -\frac{5}{42}\Big[(a^\dagger_{k',\Gamma_8+2}a_{k,\Gamma_8+1} - a^\dagger_{k',\Gamma_8+1}a_{k,\Gamma_8+2}) \\ & +(a^\dagger_{k',\Gamma_8-2}a_{k,\Gamma_8-1} - a^\dagger_{k',\Gamma_8-1}a_{k,\Gamma_8-2})\Big](S_+ - S_-) \\ & -\frac{2\sqrt{5}}{21}\Big[(a^\dagger_{k',\Gamma_7-}a_{k,\Gamma_8+1} + a^\dagger_{k',\Gamma_8+1}a_{k,\Gamma_7-}) \end{aligned}$$

$$+ (a^\dagger_{k',\Gamma_7+} a_{k,\Gamma_8-1} + a^\dagger_{k',\Gamma_8-1} a_{k,\Gamma_7+})\Big](S_+ + S_-)$$
$$- \frac{4\sqrt{5}}{21}\Big[(a^\dagger_{k',\Gamma_7-} a_{k,\Gamma_8+2} + a^\dagger_{k',\Gamma_8+2} a_{k,\Gamma_7-})$$
$$+ (a^\dagger_{k',\Gamma_7+} a_{k,\Gamma_8-2} + a^\dagger_{k',\Gamma_8-2} a_{k,\Gamma_7+})\Big] S_z\Big\}. \tag{4.18}$$

$$H_{\rm pot} = \frac{1}{42} J_0 \sum_{kk'} \Big[- (a^\dagger_{k',\Gamma_8+2} a_{k,\Gamma_8+2} + a^\dagger_{k',\Gamma_8-2} a_{k,\Gamma-2})$$
$$- (a^\dagger_{k',\Gamma_8+1} a_{k,\Gamma_8+1} + a^\dagger_{k',\Gamma_8-1} a_{k,\Gamma_8-1})$$
$$+ 2(a^\dagger_{k',\Gamma_7+} a_{k,\Gamma_7+} + a^\dagger_{k',\Gamma_7-} a_{k,\Gamma_7-})\Big] \tag{4.19}$$

Here the last part $H_{\rm pot}$ is the potential scattering, which is ignored in the following discussion. Through the above calculation, the Hund coupling $J_{\rm H}$ has been taken to be zero. It actually appears in the coupling constants since f^3 configuration can be taken into account together with f^1. Even if $J_{\rm H}$ remains finite, however, it does not change the form of this Hamiltonian and only modifies the coupling constants in the Hamiltonian. We have also neglected the splitting of f^1 states due to the crystal field, whose effect only gives rise to difference between the coupling constant J_0 in $H_{\rm iso}$ and that in $H_{\rm aniso}$. This can be justified for a weak crystal field. The first part of the Hamiltonian $H_{\rm iso}$ is the isotropic two-channel exchange interaction, which is the same as what Cox derived by assuming that the lowest Γ_7 doublet for f^1 is left as the only intermediate state of the exchange interaction under a strong crystal field [23]. The coupling is antiferromagnetic since $J_0 > 0$ holds. The second part $H_{\rm aniso}$ is the anisotropic exchange interaction for the partial waves with three kinds of symmetries: Γ_7-, Γ_8+2 and Γ_8+1 belong to one channel, while Γ_7+, Γ_8-2 and Γ_8-1 make the other channel. This interaction arises since Γ_8 quartet as well as Γ_7 doublet is taken into account for f^1. Both channels do not mix with each other. The first term in $H_{\rm aniso}$ has the form of $\sigma_y S_y$ and the second one corresponds to $\sigma_x S_x$. The last term cannot be compared to the usual exchange interaction.

Next we examine the low temperature physics of the exchange model, using the NRG method. As we have done in the Section 2.2, we treat the hopping-type Hamiltonian (which can be derived by following Wilson) with a recursion relation as

$$H_{N+1} = \Lambda^{1/2} H_N + \sum_{\sigma\mu} \Big[(f^\dagger_{N+1,\sigma\mu} f_{N\sigma\mu} + g^\dagger_{N+1,\mu} g_{N\mu}) + \text{h.c.} \Big], \tag{4.20}$$

and

$$H_0 = H_{0,\mathrm{iso}} + H_{0,\mathrm{aniso}}, \tag{4.21}$$

$$H_{0,\mathrm{iso}} = J_\alpha \sum_\mu \Big[- f^\dagger_{0\uparrow\mu} f_{0\downarrow\mu} S_- - f^\dagger_{0\downarrow\mu} f_{0\uparrow\mu} S_+ + (f^\dagger_{0\uparrow\mu} f_{0\uparrow\mu} - f^\dagger_{0\downarrow\mu} f_{0\downarrow\mu}) S_z \Big], \tag{4.22}$$

$$H_{0,\mathrm{aniso}} = \sum_\mu \Big[J_\beta (f^\dagger_{0\uparrow\mu} f_{0\downarrow\mu} - f^\dagger_{0\downarrow\mu} f_{0\uparrow\mu})(S_+ - S_-) + J_\gamma (g^\dagger_{0\mu} f_{0\downarrow\mu} + f^\dagger_{0\downarrow\mu} g_{0\mu})(S_+ + S_-) + J_\delta (g^\dagger_{0\mu} f_{0\uparrow\mu} + f^\dagger_{0\uparrow\mu} g_{0\mu}) S_z \Big]. \tag{4.23}$$

Here σ (=$\uparrow, \downarrow$) represents a pseudo-spin with 1/2 corresponding to the quadrupolar moment. μ (=1,2) is the channel index and one of the two channels is the time-reversal partner of the other. $f^\dagger_{1\uparrow}$, $f^\dagger_{1\downarrow}$ and $g^\dagger_1$ correspond to $a^\dagger_{\Gamma_8+2}$, $a^\dagger_{\Gamma_8+1}$ and $a^\dagger_{\Gamma_7-}$, respectively, while $f^\dagger_{2\uparrow}$, $f^\dagger_{2\downarrow}$ and $g^\dagger_2$ correspond to $a^\dagger_{\Gamma_8-2}$, $a^\dagger_{\Gamma_8-1}$ and $a^\dagger_{\Gamma_7+}$, respectively. The conventional two-channel model can be obtained if only $H_{0,\mathrm{iso}}$ is left, which leads to the result that the fixed point belongs to a non-Fermi liquid type. J_α reaches a finite value J^*_α, whether J_α is weak or not, as shown by Fig. 4.1. In this case it is allowed to omit $g^\dagger_\mu$ in (4.20), since the exchange interaction is not connected with $g^\dagger_\mu$. Λ is taken to be 3 and $\sim$ 300 low-lying states are kept at each renormalization step. The reason why it is called non-Fermi liquid is that the ground state has the degeneracy derived from the local moment. The NRG energy levels at the fixed point is understood by considering that the local moment still remains. Although this interaction is isotropic, anisotropy becomes irrelevant and the same fixed point can be obtained as a result of renormalization [52, 53].

Let us turn to the stability problem of the fixed point against the perturbation of $H_{0,\mathrm{aniso}}$. Λ is also taken to be 3 and $\sim$ 500 low-lying states are kept at each renormalization step in this case. In Fig. 4.2 the low-lying energy levels are shown for even NRG steps. One notices immediately that the degeneracy of the energy levels given by $H_{0,\mathrm{iso}}$ is lifted by the perturbation at the initial step, but it is recovered gradually as the NRG step proceeds. The low-lying energy levels at the fixed point of our model are identified with those given by the conventional two-channel model.

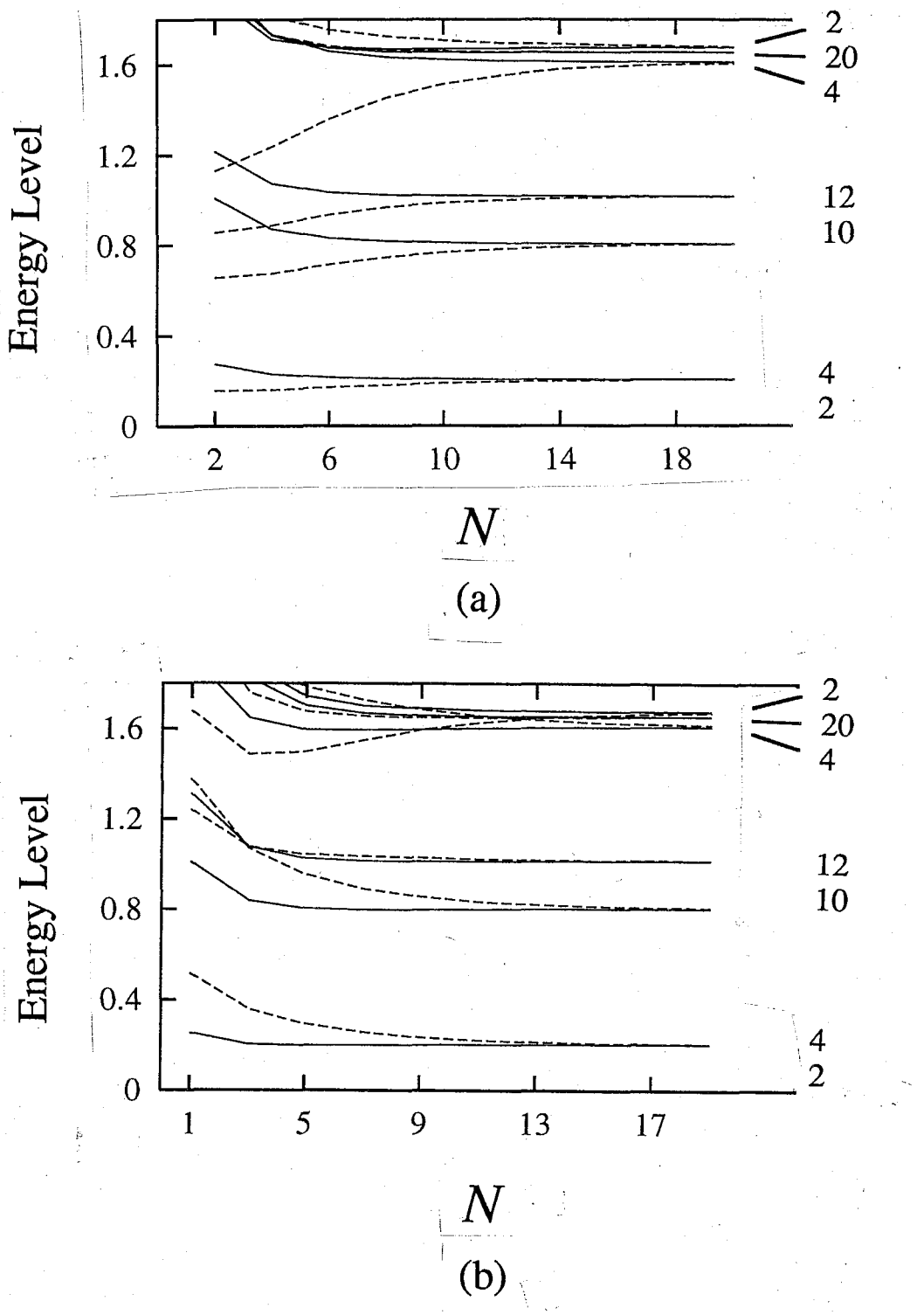

Figure 4.1: The low-lying NRG energy levels for $H_{\rm iso}$; $J_\alpha = 1.0$ (solid line) and $J_\alpha = 0.4$ (broken line) at (a) even-number renormalization steps and (b) odd-number renormalization steps. The numbers at the right side represent the degrees of degeneracy.

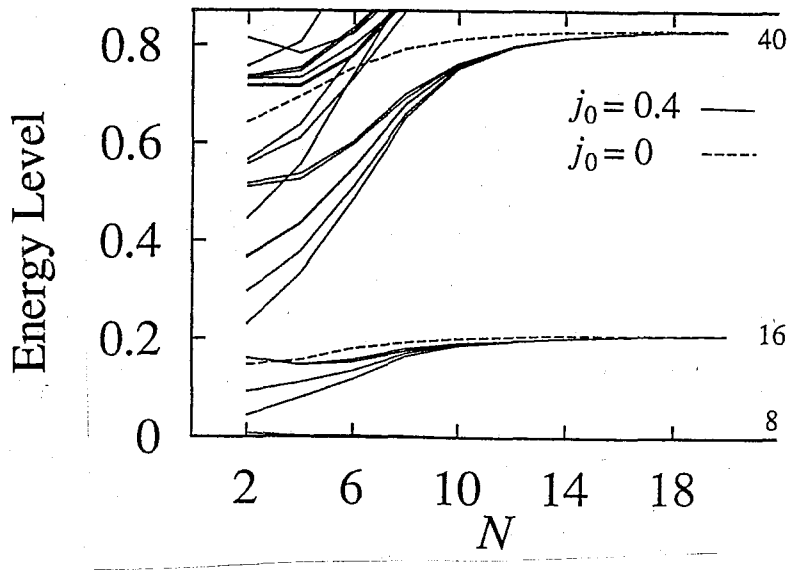

Figure 4.2: The low-lying NRG energy levels for the case $J_\alpha = 0.4$, $J_\beta = -(5/16)j_0$, $J_\gamma = -(\sqrt{5}/4)j_0$ and $J_\delta = -(\sqrt{5}/2)j_0$ at even-number renormalization steps. The numbers at the right side represent the degrees of degeneracy.

At even NRG steps the degeneracy of every energy level is four times that of the corresponding energy level in Fig. 4.1 (a). It is evident that the conduction electron denoted by $g_\mu^\dagger$ has no direct coupling with the local moment. It means that J_β, J_γ and $J_\delta \to 0$ as $J_\alpha \to J_\alpha^*$. We conclude from this that the perturbation is irrelevant and the non-Fermi liquid fixed point is stable. This conclusion is still valid if the Hund coupling $J_{\rm H}$ is finite, since its effect simply gives rise to a slight modification of the bare values of the couplings J_α, J_β, J_γ and J_δ.

This argument holds also for the case of the f^2 ground state for tetragonal or hexagonal crystal field [54]. For the tetragonal case, the doublet state is given by $|\Gamma_5\pm\rangle$ in Table 2.3. To describe the doublet we can introduce spin 1/2 operator in the same way as in the cubic case. After calculating the matrix elements related to $J_q^{(p)}$ in $H_{\rm ex}$ (3.36), we obtain the effective exchange interaction due to the doublet in

the same form as (4.8). In this case $T_\perp$ and T_z for $|\Gamma_{t5}^{(1)}\rangle$ are obtained as

$$T_\perp = \frac{\sqrt{42}}{98}\alpha\beta\Big(j_{-2}^{(2)} - \frac{2\sqrt{15}}{45}j_{-2}^{(4)}\Big) + \frac{5\sqrt{6}}{294}\beta^2\Big(j_2^{(2)} + \frac{2\sqrt{15}}{25}j_2^{(4)}\Big), \tag{4.24}$$

$$T_z = -\frac{12}{35}\alpha^2\Big(j_0^{(1)} + \frac{7}{324}j_0^{(3)} + \frac{11}{162}j_0^{(5)}\Big) + \frac{4}{35}\beta^2\Big(j_0^{(1)} + \frac{1}{12}j_0^{(3)} - \frac{1}{6}j_0^{(5)}\Big) + \frac{2\sqrt{10}}{315}\alpha\beta\Big(j_4^{(5)} + j_{-4}^{(5)}\Big). \tag{4.25}$$

For the conduction electrons, the creation operators are transformed to the new ones with 1/2 pseudo-spin σ (=$\uparrow, \downarrow$) and channel index μ (=1,2) defined as

$$a_{k\uparrow 1}^\dagger = \frac{\sqrt{5}\beta a_{k,5/2}^\dagger + \sqrt{7}\alpha a_{k,-3/2}^\dagger}{\sqrt{7\alpha^2+5\beta^2}}, \quad a_{k\downarrow 1}^\dagger = a_{k,1/2}^\dagger,$$
$$a_{k\uparrow 2}^\dagger = a_{k,-1/2}^\dagger, \quad a_{k\downarrow 2}^\dagger = \frac{\sqrt{5}\beta a_{k,-5/2}^\dagger + \sqrt{7}\alpha a_{k,3/2}^\dagger}{\sqrt{7\alpha^2+5\beta^2}}. \tag{4.26}$$

and

$$b_{k1}^\dagger = \frac{\sqrt{7}\alpha a_{k,5/2}^\dagger - \sqrt{5}\beta a_{k,-3/2}^\dagger}{\sqrt{7\alpha^2+5\beta^2}},$$
$$b_{k2}^\dagger = \frac{\sqrt{7}\alpha a_{k,-5/2}^\dagger - \sqrt{5}\beta a_{k,3/2}^\dagger}{\sqrt{7\alpha^2+5\beta^2}}. \tag{4.27}$$

Finally we obtain the effective exchange Hamiltonian in terms of these operators and 1/2 spin operator as

$$\begin{aligned} H_{\rm ex} = J_0 \sum_{kk'\mu} \Big[& \frac{\beta\sqrt{2(7\alpha^2+5\beta^2)}}{7}(a_{k'\uparrow\mu}^\dagger a_{k\downarrow\mu} S_- + a_{k'\downarrow\mu}^\dagger a_{k\uparrow\mu} S_+) \\ & + \frac{1}{2}(a_{k'\uparrow\mu}^\dagger a_{k\uparrow\mu} - a_{k'\downarrow\mu}^\dagger a_{k\downarrow\mu}) S_z \Big] \\ + J_0 \sum_{kk'} & \left(-\frac{7\alpha^2+3\beta^2}{14}\right) \Big[\sum_\sigma (a_{k'\sigma 1}^\dagger a_{k\sigma 1} - a_{k'\sigma 2}^\dagger a_{k\sigma 2}) \\ & + 2(b_{k'1}^\dagger b_{k1}^\dagger - b_{k'2}^\dagger b_{k2}) \Big] S_z \end{aligned} \tag{4.28}$$

Here the potential scattering is also ignored. The NRG analysis was carried out by adding the last term related to S_z to the anisotropic two-channel exchange model. The result shows that the extra term is marginal irrelevant and the non-Fermi liquid fixed point discussed above is still stable. Thus, within this model, the isotropic two-channel exchange model holds at low temperatures.

For the hexagonal case, there are two kinds of doublets, $|\Gamma_{h5}\rangle$ and $|\Gamma_{h6}\rangle$ as shown in Table 2.4. For the former, the effective exchange Hamiltonian is given by taking $\alpha = \pm 1$ and $\beta = 0$ in the exchange Hamiltonian (4.28). For the latter, it is more complicated than the above and is given for $|\Gamma_{h6}^{(1)}\rangle$ as

$$
\begin{aligned}
H_{\rm ex} = J_0 \sum_{kk'} \Bigg\{ & -\frac{\sqrt{70}\alpha\beta}{14}[(a^\dagger_{k'5/2}a_{k1/2} + a^\dagger_{k'-1/2}a_{k-5/2})S_- \\
& + (a^\dagger_{k'1/2}a_{k5/2} + a^\dagger_{k'-5/2}a_{k-1/2})S_+] \\
& + \frac{3\sqrt{14}\alpha\beta}{14}[(a^\dagger_{k'1/2}a_{k-3/2} + a^\dagger_{k'3/2}a_{k-1/2})S_- \\
& + (a^\dagger_{k'-3/2}a_{k1/2} + a^\dagger_{k'-1/2}a_{k3/2})S_+] \\
& - \frac{3\sqrt{5}\beta^2}{14}[(a^\dagger_{k'-3/2}a_{k5/2} + a^\dagger_{k'-5/2}a_{k3/2})S_- \\
& + (a^\dagger_{k'-3/2}a_{k5/2} + a^\dagger_{k'-5/2}a_{k3/2})S_+] \\
& + \Big[\Big(\alpha^2 - \frac{9}{14}\beta^2\Big)(a^\dagger_{k'5/2}a_{k5/2} - a^\dagger_{k'-5/2}a_{k-5/2}) \\
& + \Big(\alpha^2 - \frac{5}{14}\beta^2\Big)(a^\dagger_{k'3/2}a_{k3/2} - a^\dagger_{k'-3/2}a_{k-3/2}) \\
& + \frac{2}{7}\beta^2(a^\dagger_{k'1/2}a_{k1/2} - a^\dagger_{k'-1/2}a_{k-1/2})\Big]S_z\Bigg\}
\end{aligned}
\tag{4.29}
$$

If the intermediate state for f^1 is restricted to the lowest state, for example, $|\pm 3/2\rangle$, only the first exchange term remains and the diagonal terms related to S_z is modified. In this case we have the same form of the effective exchange Hamiltonian as (4.28). Adding the second and third terms to the exchange Hamiltonian as a perturbation, we carried out the NRG study. The results show that the perturbation is not relevant and the non-Fermi liquid is still stable.

In this chapter, all the f^1 states have been taken into account for a weak crystal field. The NRG study has shown that the additional terms coming from higher intermediate states are not relevant.

4.2 Kondo Effect Due to f^3 Kramers Doublet

We now turn to the f^3 case obeying the Hund's rule. The cubic crystal field lifts the degeneracy of $J = 9/2$ ground state, leading to the Kramers doublet $|\Gamma_6\pm\rangle$ as a

candidate of the lowest state; it has the following form:

$$|\Gamma_6\pm\rangle = \frac{3}{2\sqrt{6}}|\pm 9/2\rangle + \frac{\sqrt{14}}{2\sqrt{6}}|\pm 1/2\rangle + \frac{1}{2\sqrt{6}}|\mp 7/2\rangle. \tag{4.30}$$

The two state can be distinguished by the average of J_z:

$$\langle\Gamma_6 \pm |J_z|\Gamma_6\pm\rangle = \pm\frac{11}{6}, \tag{4.31}$$

$$\langle\Gamma_6 \pm |J_\pm^n|\Gamma_6\mp\rangle = 0 \quad (n : \text{even}). \tag{4.32}$$

To take into account the Hund coupling $J_{\rm H}$, we introduce two couplings which are defined with $I(n \pm 1, J_i)$ given in (3.19) and (3.20) as

$$J_0 = \frac{1}{2}[I(2,2) + I(2,4) + I(4,2) + I(4,4)] > 0, \tag{4.33}$$

$$J_1 = -\frac{1}{2}[I(2,2) - I(2,4) + I(4,2) - I(4,4)] > 0 \quad \left(\sim \frac{J_{\rm H}}{U} J_0\right), \tag{4.34}$$

where J_0 can be also given by $J_{0,p}$ in (3.32) for each odd p if $J_{\rm H} = 0$.

As we have done in Section 4.1, the Kramers doublet $|\Gamma_6\pm\rangle$ can be expressed with $S = 1/2$ spin operator. Finally we obtain an effective exchange Hamiltonian as

$$H_{\rm ex}(\Gamma_6) = H_{{\rm ex},J_0} + H_{{\rm ex},J_1}, \tag{4.35}$$

$$\begin{aligned} H_{{\rm ex},J_i} = J_i \sum_{mm'}^{kk'} a^\dagger_{k'm'} a_{km} [&(T_{\perp i})_{m'm} S_- + (T^\dagger_{\perp i})_{m'm} S_+ \\ &+ (T_{z,i})_{m'm} S_z + (T_{0,i})_{m'm}], \end{aligned} \tag{4.36}$$

where

$$T_{\perp 1} = -\left(\frac{11\sqrt{2}}{105} j_1^{(1)} + \frac{\sqrt{3}}{405} j_1^{(3)} + \frac{\sqrt{30}}{567} j_1^{(5)}\right) - \left(\frac{\sqrt{5}}{405} j_{-3}^{(3)} - \frac{\sqrt{35}}{2835} j_{-3}^{(5)}\right) - \frac{\sqrt{7}}{315} j_5^{(5)}, \tag{4.37}$$

$$T_{z,1} = \left(\frac{22}{105} j_0^{(1)} - \frac{4}{405} j_0^{(3)} + \frac{38}{2835} j_0^{(5)}\right) + \frac{\sqrt{70}}{945}(j_4^{(5)} + j_{-4}^{(5)}), \tag{4.38}$$

$$\begin{aligned} T_{\perp 2} = &-\left(\frac{22\sqrt{2}}{735} j_1^{(1)} + \frac{29\sqrt{3}}{5670} j_1^{(3)} + \frac{11\sqrt{30}}{7938} j_1^{(5)}\right) - \left(29\frac{\sqrt{5}}{5670} j_{-3}^{(3)} - \frac{11\sqrt{35}}{39690} j_{-3}^{(5)}\right) \\ &- \frac{11\sqrt{7}}{4410} j_5^{(5)}, \end{aligned} \tag{4.39}$$

$$T_{z,2} = \left(\frac{44}{735} j_0^{(1)} - \frac{58}{2835} j_0^{(3)} + \frac{209}{19845} j_0^{(5)}\right) + \frac{11\sqrt{70}}{13230}(j_4^{(5)} + j_{-4}^{(5)}), \tag{4.40}$$

$$T_{0,2} = -\frac{1}{180} j_0^{(4)} - \frac{\sqrt{70}}{2520}(j_4^{(4)} + j_{-4}^{(4)}), \tag{4.41}$$

and $T_{0,1} = 0$. If we use 6×6 matrices, the following expressions are obtained:

$$T_{\perp 1} = \frac{1}{6}\begin{pmatrix} & \sqrt{5} & & & 3 & \\ & & 0 & & & \\ & & & 4 & & \\ 0 & & & & 0 & \\ & -1 & & & & \sqrt{5} \\ & & 0 & & & \end{pmatrix}, \tag{4.42}$$

$$T_{z,1} = \frac{1}{6}\begin{pmatrix} 3 & & & & \sqrt{5} & \\ & 1 & & & & -\sqrt{5} \\ & & 4 & & & \\ & & & -4 & & \\ \sqrt{5} & & & & -1 & \\ & -\sqrt{5} & & & & -3 \end{pmatrix}, \tag{4.43}$$

$$T_{\perp 2} = \frac{1}{84}\begin{pmatrix} & 9\sqrt{5} & & & & 33 \\ & & -10\sqrt{2} & & & \\ & & & 26 & & \\ -2\sqrt{10} & & & & -10\sqrt{2} & \\ & -19 & & & & 9\sqrt{5} \\ & & -2\sqrt{10} & & & \end{pmatrix}, \tag{4.44}$$

$$T_{z,2} = \frac{1}{84}\begin{pmatrix} 3 & & & & 11\sqrt{5} & \\ & 9 & & & & -11\sqrt{5} \\ & & 46 & & & \\ & & & -46 & & \\ 11\sqrt{5} & & & & -9 & \\ & -11\sqrt{5} & & & & -3 \end{pmatrix}, \tag{4.45}$$

$$T_0 = -\frac{1}{24}\begin{pmatrix} 1 & & & \sqrt{5} & & \\ & -3 & & & \sqrt{5} & \\ & & 2 & & & \\ & & & 2 & & \\ \sqrt{5} & & & & -3 & \\ & \sqrt{5} & & & & 1 \end{pmatrix}, \tag{4.46}$$

where the blanks in these matrices should be filled in with 0's similarly to (4.12), (4.13) and (4.14). Then, within the Kramers doublet, the effective Hamiltonian can be expressed with the cubic symmetric basis of the operators for the conduction electrons as:

$$H_{\mathrm{ex},J_0} = J_0 \sum_{kk'} \Big\{ -\frac{1}{3}\Big[a^\dagger_{k',\Gamma_7-} a_{k,\Gamma_7+} S_- + a^\dagger_{k',\Gamma_7+} a_{k,\Gamma_7-} S_+ + (a^\dagger_{k',\Gamma_7-} a_{k,\Gamma_7-} - a^\dagger_{k',\Gamma_7+} a_{k,\Gamma_7+}) S_z \Big]$$

$$
\begin{aligned}
&+\frac{2}{3}\Big[a^{\dagger}_{k',\Gamma_8+2}a_{k,\Gamma_8-2}S_- + a^{\dagger}_{k',\Gamma_8-2}a_{k,\Gamma_8+2}S_+ \\
&+(a^{\dagger}_{k',\Gamma_8+2}a_{k,\Gamma_8+2} - a^{\dagger}_{k',\Gamma_8-2}a_{k,\Gamma_8-2})S_z\Big] \\
&+\frac{2}{3}\Big[a^{\dagger}_{k',\Gamma_8+1}a_{k,\Gamma_8-1}S_- + a^{\dagger}_{k',\Gamma_8-1}a_{k,\Gamma_8+1}S_+ \\
&+(a^{\dagger}_{k',\Gamma_8+1}a_{k,\Gamma_8+1} - a^{\dagger}_{k',\Gamma_8-1}a_{k,\Gamma_8-1})S_z\Big]\Big\}, \qquad (4.47)
\end{aligned}
$$

$$
\begin{aligned}
H_{\mathrm{ex},J_1} = J_1\sum_{kk'}\Big\{ &-\frac{19}{63}\Big[a^{\dagger}_{k',\Gamma_7-}a_{k,\Gamma_7+}S_- + a^{\dagger}_{k',\Gamma_7+}a_{k,\Gamma_7-}S_+ \\
&+(a^{\dagger}_{k',\Gamma_7-}a_{k,\Gamma_7-} - a^{\dagger}_{k',\Gamma_7+}a_{k,\Gamma_7+})S_z\Big] \\
&+\Big[\frac{59}{126}(a^{\dagger}_{k',\Gamma_8+2}a_{k,\Gamma_8-2}S_- + a^{\dagger}_{k'\Gamma_8-2}a_{k,\Gamma_8+2}S_+) \\
&+\frac{29}{126}(a^{\dagger}_{k',\Gamma_8+2}a_{k,\Gamma_8+2} - a^{\dagger}_{k',\Gamma_8-2}a_{k,\Gamma_8-2})S_-\Big] \\
&+\Big[\frac{13}{42}(a^{\dagger}_{k',\Gamma_8+1}a_{k,\Gamma_8-1}S_- + a^{\dagger}_{k',\Gamma_8-1}a_{k,\Gamma_8+1}S_+ \\
&+\frac{23}{42}(a^{\dagger}_{k',\Gamma_8+1}a_{k,\Gamma_8+1} - a^{\dagger}_{k',\Gamma_8-1}a_{k,\Gamma_8-1})S_z\Big]\Big\} \\
+J_1\sum_{kk'}\Big\{ &\frac{2\sqrt{5}}{63}\Big[(a^{\dagger}_{k',\Gamma_7-}a_{k,\Gamma_8-2} + a^{\dagger}_{k',\Gamma_8+2}a_{k,\Gamma_7+})S_- \\
&+(a^{\dagger}_{k',\Gamma_8-2}a_{k,\Gamma_7-} + a^{\dagger}_{k',\Gamma_7+}a_{k,\Gamma_8+2})S_+\Big] \\
&+\frac{2\sqrt{15}}{63}\Big[(a^{\dagger}_{k',\Gamma_8-1}a_{k,\Gamma_7-} + a^{\dagger}_{k',\Gamma_7+}a_{k,\Gamma_8+1})S_- \\
&+(a^{\dagger}_{k',\Gamma_7-}a_{k,\Gamma_8-1} + a^{\dagger}_{k',\Gamma_8+1}a_{k,\Gamma_7+})S_+\Big] \\
&-\frac{5\sqrt{3}}{63}\Big[(a^{\dagger}_{k',\Gamma_8-2}a_{k,\Gamma_8+1} + a^{\dagger}_{k',\Gamma_8-1}a_{k,\Gamma_8+2})S_- \\
&+(a^{\dagger}_{k',\Gamma_8+1}a_{k,\Gamma_8-2} + a^{\dagger}_{k',\Gamma_8+2}a_{k,\Gamma_8-1})S_+\Big] \\
&-\frac{4\sqrt{5}}{63}\Big[(a^{\dagger}_{k',\Gamma_7-}a_{k,\Gamma_8+2} - a^{\dagger}_{k',\Gamma_7+}a_{k,\Gamma_8-2}) \\
&+(a^{\dagger}_{k',\Gamma_8+2}a_{k,\Gamma_7-} - a^{\dagger}_{k',\Gamma_8-2}a_{k,\Gamma_7+})\Big]S_z\Big\}, \qquad (4.48)
\end{aligned}
$$

where potential scattering terms have been ignored. Here we have taken account of the Hund coupling J_{H} whose contribution is contained in H_{ex,J_1}, where J_1 becomes smaller with the decrease of J_{H}/U. On the other hand, we have neglected the splitting of f^2 and f^4 states due to the crystal field since it is considered to be much small compared with that due to the Hund coupling in real systems. When J_{H} vanishes,

there remains only H_{ex,J_0}, which is a three-channel exchange model, but the coupling related to $\Gamma_7\pm$ is ferromagnetic and the other two couplings related to $\Gamma_8 \pm 2$ and $\Gamma_8 \pm 1$ are antiferromagnetic and identical. Therefore it turns out to be the same as the two-channel model in Section 4.1, since the ferromagnetic exchange is irrelevant as can be proved by the NRG analysis. The first part and the second part of H_{ex,J_1} represent, respectively, the anisotropic exchange in time-reversal pairs only and the mixing of channels for conduction electrons.

We now apply the NRG method to (4.47) and (4.48). Explicitly, we study the following Hamiltonian:

$$H_{N+1} = \Lambda^{1/2} H_N + \sum_{\sigma\nu} (f^\dagger_{N+1,\sigma\nu} f_{N,\sigma\nu} + \mathrm{h.c.}) \tag{4.49}$$

and

$$H_0 = H_{0,\mathrm{sp}} + H_{0,\mathrm{ch}}, \tag{4.50}$$

$$\begin{aligned} H_{0,\mathrm{sp}} = \sum_\nu \Big[& J_{\perp\nu} (f^\dagger_{0\uparrow\nu} f_{0\downarrow\nu} S_- + f^\dagger_{0\downarrow\nu} f_{0\uparrow\nu} S_+) \\ & + J_{z\nu} (f^\dagger_{0\uparrow\nu} f_{0\uparrow\nu} - f^\dagger_{0\downarrow\nu} f_{0\downarrow\nu}) S_z \Big], \end{aligned} \tag{4.51}$$

$$\begin{aligned} H_{0,\mathrm{ch}} = {} & K_1 \Big[(f^\dagger_{0\uparrow1} f_{0\downarrow2} + f^\dagger_{0\uparrow2} f_{0\downarrow1}) S_- + (f^\dagger_{0\downarrow2} f_{0\uparrow1} + f^\dagger_{0\downarrow1} f_{0\uparrow2}) S_+ \Big] \\ & + K_2 \Big[(f^\dagger_{0\downarrow3} f_{0\uparrow1} + f^\dagger_{0\downarrow1} f_{0\uparrow3}) S_- + (f^\dagger_{0\uparrow1} f_{0\downarrow3} + f^\dagger_{0\uparrow3} f_{0\downarrow1}) S_+ \Big] \\ & + K_3 \Big[(f^\dagger_{0\downarrow2} f_{0\uparrow3} + f^\dagger_{0\downarrow3} f_{0\uparrow2}) S_- + (f^\dagger_{0\uparrow3} f_{0\downarrow2} + f^\dagger_{0\uparrow2} f_{0\downarrow3}) S_+ \Big] \\ & + K_4 \Big[(f^\dagger_{0\uparrow1} f_{0\uparrow2} - f^\dagger_{0\downarrow1} f_{0\downarrow2}) + (f^\dagger_{0\uparrow2} f_{0\uparrow1} - f^\dagger_{0\downarrow2} f_{0\downarrow1}) \Big] S_z. \end{aligned} \tag{4.52}$$

Here $H_{0,\mathrm{sp}}$ and $H_{0,\mathrm{ch}}$ represent, respectively, the exchange only in spin and the exchange in channel for conduction electrons. σ is the $1/2$ pseudo-spin corresponding to the magnetic moment. ν (=1,2,3) is the channel index and a time-reversal pair of electrons belong to each channel. $f^\dagger_{\uparrow1}$, $f^\dagger_{\downarrow1}$, $f^\dagger_{\uparrow2}$, $f^\dagger_{\downarrow2}$, $f^\dagger_{\uparrow3}$ and $f^\dagger_{\downarrow3}$ correspond to $a^\dagger_{\Gamma_7-}$, $a^\dagger_{\Gamma_7+}$, $a^\dagger_{\Gamma_8+2}$, $a^\dagger_{\Gamma_8-2}$, $a^\dagger_{\Gamma_8+1}$ and $a^\dagger_{\Gamma_8-1}$, respectively.

We have examined the exchange model for some typical cases. Λ has been taken to be 3. The lowest $200 \sim 300$ states are kept at each step. Technically one has to be careful in the truncation of states, since it depends on the degree of degeneracy of the highest few states. This problem becomes important near the fixed point because of the presence of a large number of degenerate states.

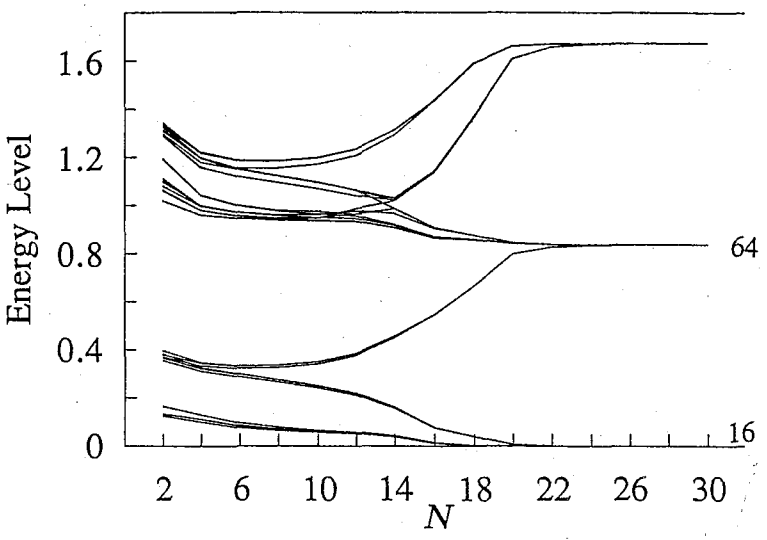

Figure 4.3: The low-lying NRG energy levels for the case $J_{\perp 1} = J_{z1} = -0.5$, $J_{\perp 2} = J_{\perp 3} = J_{z2} = J_{z3} = 1.0$, $K_1 = K_2 = 0.4$ and $K_3 = K_4 = -0.4$ at even-number renormalization steps. The numbers at the right side represent the degrees of degeneracy.

First we treat only $H_{0,\mathrm{sp}}$ (which corresponds to $J_{\mathrm{H}} = 0$) and change the couplings in various ways, keeping the constraint that $J_{\perp 1} = J_{z1} < 0$ and $J_{\perp 2}, J_{z2}, J_{\perp 3}, J_{z3} > 0$. For the case $J_{\perp 2} = J_{\perp 3}$ and $J_{z2} = J_{z3}$, the NRG result shows that the low temperature behavior at a stable fixed point is identified with a non-Fermi liquid, since we have two equivalent relevant couplings in the present case. The situation is the same as in the conventional two-channel exchange model. On the other hand, if the anisotropy is added to the couplings, namely, $J_{\perp 2} \neq J_{\perp 3}$ and $J_{z2} \neq J_{z3}$, the system becomes Fermi liquid which is also given by the standard one-channel model.

Next we examine the stability of the fixed point against the perturbation of $H_{0,\mathrm{ch}}$. In Fig. 4.3 the low-lying energy levels are shown for even renormalization steps. It shows that the fixed point becomes Fermi liquid type, even if $J_{\perp 2} = J_{\perp 3}$ and $J_{z2} = J_{z3}$ This means that the non-Fermi liquid fixed point is unstable. From the above argument we conclude that the Hund coupling gives the channel anisotropy,

which causes the channel reduction at low temperatures, and the system becomes Fermi liquid.

Chapter 5

Influence of Local Excited States on Kondo Effect

In the previous chapter, we have examined the Kondo effect due to doublet state only and have clarified the difference between Kramers and non-Kramers doublets. It has been shown that the Fermi liquid is not realized at low temperatures for f^2 configuration. In this chapter, whether the non-Fermi liquid for f^2 is stable or not is studied in more realistic cases where the excited states are taken into account as well as the ground doublet state. It is shown that the effect of the excited states cannot be ignored in general since it tends to stabilize the Fermi liquid depending on the coupling constants of the effective exchange interaction and the crystal field splitting of the localized states.

5.1 Model for Strong Crystal Field

In this section we wish to discuss a model for f^2 configuration in the presence of a tetragonal or hexagonal crystal field. The local f-electron levels studied here are shown schematically in Fig. 5.1. For simplicity we keep within the f^2 configuration only the non-Kramers doublet ground state and the first singlet excited state; it is assumed that the former is magnetically coupled with the latter. It is evident that there are more crystal-field excited states in general. The singlet excited state represents those excited states, although there is just one in our model.

We first examine how such a situation is realized in a real atom. To study the effect of the crystal field on the Kondo effect with minimum elements, we restrict

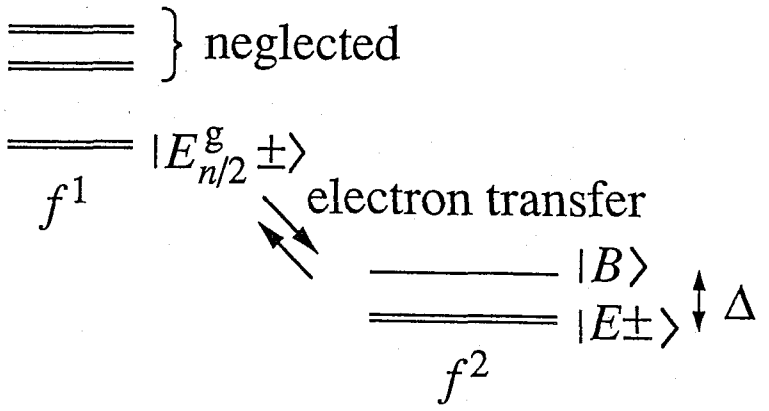

Figure 5.1: The local f-electron states which are considered in our model for a strong crystal field. The f^2 configuration consists of the ground doublet and the first excited singlet with splitting Δ. The intermediate states of f^1 configuration are restricted to the lowest doublet state.

the local f-electron states to the doublet ground state (whose energy is taken as the origin) and the first excited state which is a singlet and higher than the ground state by Δ:

$$|E_\pm\rangle = \alpha|\mp 3\rangle + \beta|\pm 1\rangle, \quad |B\rangle = \frac{1}{\sqrt{2}}|2\rangle + \frac{1}{\sqrt{2}}|-2\rangle. \tag{5.1}$$

For the tetragonal field $|E_\pm\rangle$ and $|B\rangle$ correspond to $|\Gamma^{(1)}_{t5}\pm\rangle$ and $|\Gamma^{(1)}_{t3}\rangle$ respectively in Table 2.3. For the hexagonal field we take

$$|E_\pm\rangle = \alpha|\pm 4\rangle + \beta|\mp 2\rangle, \quad |B\rangle = \frac{1}{\sqrt{2}}|3\rangle + \frac{1}{\sqrt{2}}|-3\rangle. \tag{5.2}$$

$|E_\pm\rangle$ and $|B\rangle$ correspond to $|\Gamma^{(1)}_{h6}\pm\rangle$ and $|\Gamma^{(1)}_{h3}\rangle$ respectively in Table 2.4). Here $|m\rangle$ represents the eigenstate of J_z $(= 4, 3, \cdots, -4)$. The coefficients α and β depend on the crystal field parameters and satisfy $\alpha^2 + \beta^2 = 1$.

The effective exchange Hamiltonian (3.36) gives transitions among the doublet ground state and the singlet excited state. It is convenient to describe the matrix elements of $H_{\rm ex}$, $\langle E_\pm|H_{\rm ex}|E_\pm\rangle$, $\langle E_\pm|H_{\rm ex}|E_\mp\rangle$ and $\langle E_\pm|H_{\rm ex}|B\rangle$, with the following operators [55]:

$$S_z = \frac{1}{2}(|E_+\rangle\langle E_+| - |E_-\rangle\langle E_-|), \quad S_+ = |E_+\rangle\langle E_-|, \quad S_- = |E_-\rangle\langle E_+|,$$

$$m_+ = |E_+\rangle\langle B| + |B\rangle\langle E_-|, \quad m_- = |B\rangle\langle E_+| + |E_-\rangle\langle B|, \tag{5.3}$$
$$\tilde{m}_+ = |E_+\rangle\langle B| - |B\rangle\langle E_-|, \quad \tilde{m}_- = |B\rangle\langle E_+| - |E_-\rangle\langle B|,$$

where $\boldsymbol{S}$ represents a pseudo-spin with $1/2$ describing the doublet ground state; both $m_\pm$ and $\tilde{m}_\pm$ are operators which couple the doublet with the singlet excited state. As will be shown later, the exchange coupling in our model is changed by α and β, and it leads to competition among various exchange interactions and Δ.

Calculating $\langle E_\pm|J_q^{(p)}|E_\pm\rangle$, $\langle E_\pm|J_q^{(p)}|E_\mp\rangle$ and $\langle E_\pm|J_q^{(p)}|B\rangle$, we obtain an effective exchange Hamiltonian within the doublet ground state and the singlet excited state for the tetragonal case as

$$H = H_{\rm k} + H_{\rm l} + H_{\rm ex}, \tag{5.4}$$
$$H_{\rm k} = \sum_{km} \varepsilon_k a_{km}^\dagger a_{km}, \tag{5.5}$$
$$H_{\rm l} = \Delta|B\rangle\langle B|, \tag{5.6}$$

$$\begin{aligned} H_{\rm ex} = J_0 \sum_{\substack{kk' \\ mm'}} a_{k'm'}^\dagger a_{km} \big[& (T_{\perp 1})_{m'm} S_- + (T_{\perp 1}^\dagger)_{m'm} S_+ + (T_z)_{m'm} S_z \\ & + (T_{\perp 2})_{m'm} m_- + (T_{\perp 2}^\dagger)_{m'm} m_+ \\ & + (T_{\perp 3})_{m'm} \tilde{m}_- + (T_{\perp 3}^\dagger)_{m'm} \tilde{m}_+ \big], \end{aligned} \tag{5.7}$$

Here $T_{\perp 1}$ and T_z have been given by (4.24) and (4.25), respectively. $T_{\perp 2}$ and $T_{\perp 3}$, which are related to the excited singlet state, are defined as

$$\begin{aligned} T_{\perp 2} = \alpha \Big[& \frac{\sqrt{14}}{35}\Big(j_{-1}^{(1)} - \frac{\sqrt{6}}{108} j_{-1}^{(3)} + \frac{\sqrt{15}}{54} j_{-1}^{(5)}\Big) - \frac{1}{105} j_{-5}^{(5)}\Big] \\ & + \beta \Big[\frac{3\sqrt{2}}{35}\Big(j_{-1}^{(1)} + \frac{\sqrt{6}}{162} j_{-1}^{(3)} + \frac{\sqrt{15}}{162} j_{-1}^{(5)}\Big) + \frac{\sqrt{5}}{378}\Big(j_3^{(3)} - \frac{2\sqrt{7}}{5} j_3^{(5)}\Big)\Big], \end{aligned} \tag{5.8}$$
$$T_{\perp 3} = -\alpha \cdot \frac{5\sqrt{42}}{1176}\Big(j_{-1}^{(2)} + \frac{2\sqrt{30}}{75} j_{-1}^{(4)}\Big) + \beta\Big[\frac{9\sqrt{6}}{1176}\Big(j_{-1}^{(2)} + \frac{4\sqrt{30}}{45} j_{-1}^{(4)}\Big) - \frac{\sqrt{35}}{1470} j_3^{(4)}\Big]. \tag{5.9}$$

The potential scattering terms have been ignored in (5.7). It is convenient to transform the basis of the creation operator $a_{km}^\dagger$ as follows:

$$\frac{1}{\sqrt{7\alpha^2 + 5\beta^2}}\big(\sqrt{5}\beta a_{k,\pm 5/2}^\dagger + \sqrt{7}\alpha a_{k,\mp 3/2}^\dagger\big), \tag{5.10}$$
$$\frac{1}{\sqrt{7\alpha^2 + 5\beta^2}}\big(\sqrt{7}\alpha a_{k,\pm 5/2}^\dagger - \sqrt{5}\beta a_{k,\mp 3/2}^\dagger\big); \tag{5.11}$$

$a^{\dagger}_{k,\pm 1/2}$ is kept not transformed. The exchange Hamiltonian (5.7) can be reduced to a simpler form by using the new basis.

In the present model every orbital channel participates in the exchange interaction, so that the exchange terms related to $m_{\pm}$ and $\tilde{m}_{\pm}$ are complicated. To make the model simpler, we restrict the intermediate states of the exchange process to the lowest Kramers doublet in f^1 configuration. This is the same restriction as in Cox's model [23], which can be justified for a strong crystal field (see Fig. 1.5). Moreover, for simplicity, we consider the case where the eigenstates for f^1 are given by

$$|E^{(1)}_{3/2}\pm\rangle = \frac{1}{\sqrt{7\alpha^2+5\beta^2}}\Big(\sqrt{5}\beta|\pm 5/2\rangle + \sqrt{7}\alpha|\mp 3/2\rangle\Big), \tag{5.12}$$

$$|E^{(2)}_{3/2}\pm\rangle = \frac{1}{\sqrt{7\alpha^2+5\beta^2}}\Big(\sqrt{7}\alpha|\pm 5/2\rangle - \sqrt{5}\beta|\mp 3/2\rangle\Big), \tag{5.13}$$

$$|E_{1/2}\pm\rangle = |\pm 1/2\rangle, \tag{5.14}$$

for the tetragonal crystal field. This can be realized if the crystal field parameters satisfy

$$\frac{B^0_4}{B^0_2} < \frac{9}{170} \quad \text{or} \quad \frac{B^0_4}{B^0_2} > \frac{3}{10}\ . \tag{5.15}$$

The ratio of the energies for $|E^{(1)}_{3/2}\pm\rangle$, $|E^{(2)}_{3/2}\pm\rangle$ and $|E_{1/2}\rangle$ is obtained as

$$E(E^{(1)}_{3/2}) : E(E^{(2)}_{3/2}) : E(E_{1/2}) = 2(7\alpha^2+4\beta^2) : -7 : -(7\alpha^2+\beta^2). \tag{5.16}$$

Then, if the conditions

$$B^0_2 > 0, \quad \frac{B^0_4}{B^0_2} < \frac{1}{8} \tag{5.17}$$

are also satisfied, $|E^{(2)}_{3/2}\pm\rangle$ is selected as the lowest state within f^1 and it is also reasonable to choose $|E\pm\rangle$ and $|B\rangle$ for f^2. The derivation of the conditions are given in Appendix C. The above discussion for the tetragonal case is also applicable to the hexagonal one with minor modifications. The only difference is that the eigenstates for f^1 are independent of those for f^2, namely, of α and β in $|E\pm\rangle$, so that the basis of the creation operator $a^{\dagger}_{km}$ need not be transformed. The energy levels are given by the crystal field parameters as

$$\begin{aligned} E(E_{5/2}) &= 10B^0_2 + 60B^0_4, \\ E(E_{3/2}) &= -2B^0_2 - 180B^0_4, \\ E(E_{1/2}) &= -8B^0_2 + 120B^0_4. \end{aligned} \tag{5.18}$$

	(a)	(b)	(c)
$a_{k\uparrow 1}$	$\dfrac{\sqrt{5}\beta a_{k,5/2}+\sqrt{7}\alpha a_{k,-3/2}}{\sqrt{7\alpha^2+5\beta^2}}$	$a_{k,3/2}$	$a_{k,-3/2}$
$a_{k\downarrow 1}$	$a_{k,1/2}$	$a_{k,-1/2}$	$a_{k,5/2}$
$a_{k\uparrow 2}$	$a_{k,-1/2}$	$a_{k,1/2}$	$a_{k,-5/2}$
$a_{k\downarrow 2}$	$\dfrac{\sqrt{5}\beta a_{k,-5/2}+\sqrt{7}\alpha a_{k,3/2}}{\sqrt{7\alpha^2+5\beta^2}}$	$a_{k,-3/2}$	$a_{k,3/2}$

Table 5.1: The representation of $a_{k\sigma\mu}$ ($\sigma=\uparrow,\downarrow$, $\mu=1,2$) (a) for the tetragonal crystal field, (b) for the case $|B_4^0|/|B_2^0|<3/10$ and (c) for the case $|B_4^0|/|B_2^0|>3/10$ for the hexagonal crystal field.

When $B_2^0<0$ and $B_4^0<0$ are satisfied, it is possible to regard $|E\pm\rangle$ and $|B\rangle$ as the ground state and the first excited state for f^2, respectively. For f^1, the ground state becomes $|E_{5/2}\rangle$ for $|B_4^0|/|B_2^0|<3/10$ and $|E_{1/2}\rangle$ for $|B_4^0|/|B_2^0|>3/10$.

For the strong crystal field, one can conclude from the above argument that conduction electrons affected by the exchange interaction are only two kinds of pairs of partial waves. We finally obtain an effective Hamiltonian for both the tetragonal and hexagonal crystal fields in the same form:

$$H = H_{\rm k} + H_{\rm I} + H_{\rm ex}$$

$$H_{\rm k} = \sum_{k\sigma\mu} \varepsilon_k a^\dagger_{k\sigma\mu} a_{k\sigma\mu}, \tag{5.19}$$

$$H_{\rm I} = \Delta |B\rangle\langle B|, \tag{5.20}$$

$$H_{\rm ex} = H_{\rm sp} + H_{\rm ch} + H_{\rm sc}, \tag{5.21}$$

where

$$\begin{aligned} H_{\rm sp} = \sum_{kk'\mu} \Big[& J_{\perp,0}(a^\dagger_{k'\uparrow\mu} a_{k\downarrow\mu} S_- + a^\dagger_{k'\downarrow\mu} a_{k\uparrow\mu} S_+) \\ & + J_{z,0}(a^\dagger_{k'\uparrow\mu} a_{k\uparrow\mu} - a^\dagger_{k'\downarrow\mu} a_{k\downarrow\mu}) S_z \Big], \end{aligned} \tag{5.22}$$

$$H_{\rm ch} = \sum_{kk'\sigma} \Big[K_{z,0}(a^\dagger_{k'\sigma 1} a_{k\sigma 1} - a^\dagger_{k'\sigma 2} a_{k\sigma 2}) S_z$$

	(a)	(b)	(c)
$J_{\perp,0}$	$\frac{\beta}{7}\sqrt{2(7\alpha^2+5\beta^2)}$	$\frac{3}{14}\sqrt{14}\alpha\beta$	$-\frac{3}{14}\sqrt{5}\beta^2$
$J_{z,0}$	$\frac{1}{2}$	$\frac{1}{2}(\alpha^2+\frac{9}{14}\beta^2)$	$\frac{1}{2}\beta^2$
$K_{z,0}$	$-\frac{1}{14}(7\alpha^2+3\beta^2)$	$\frac{1}{2}(\alpha^2-\frac{9}{14}\beta^2)$	$-\frac{1}{7}\beta^2$
$K_{\perp,0}\ (=K_{\tilde{\perp},0})$	$\frac{\sqrt{2}\beta(3\sqrt{7}\alpha+5\beta)}{28\sqrt{7\alpha^2+5\beta^2}}$	$\frac{\sqrt{2}}{4}\alpha$	$\frac{\sqrt{35}}{28}\beta$
$I_{\perp,0}$	$\frac{1}{14}(3\sqrt{7}\alpha+5\beta)$	$\frac{3}{14}\sqrt{7}\beta$	$-\frac{3}{14}\sqrt{7}\beta$

Table 5.2: The coupling constants in $H_{\rm ex}$ (5.21) in units of J_0 (>0). (a), (b) and (c) correspond to the three cases in Table 5.1: $\alpha^2=(1+x)/2$ and $\beta^2=(1-x)/2$.

$$+K_{\perp,0}(a^\dagger_{k'\sigma 1}a_{k\sigma 2}m_- + a^\dagger_{k'\sigma 2}a_{k\sigma 1}m_+)\Big]$$
$$+\sum_{kk'}K_{\tilde{\perp},0}\Big[(a^\dagger_{k'\uparrow 1}a_{k\uparrow 2}-a^\dagger_{k'\downarrow 1}a_{k\downarrow 2})\tilde{m}_- + (a^\dagger_{k'\uparrow 2}a_{k\uparrow 1}-a^\dagger_{k'\downarrow 2}a_{k\downarrow 1})\tilde{m}_+\Big], \tag{5.23}$$

$$H_{\rm sc}=\sum_{kk'}I_{\perp,0}(a^\dagger_{k'\uparrow 2}a_{k\downarrow 1}m_- + a^\dagger_{k'\downarrow 1}a_{k\uparrow 2}m_+). \tag{5.24}$$

Here $H_{\rm sp}$ represents the exchange process in spin of conduction electrons and within the doublet ground state. Except for the $K_{z,0}$ term, $H_{\rm ch}$ corresponds to the exchange in channel of conduction electrons and in ground and excited states of local f-electrons. $H_{\rm sc}$ represents the exchange in both spin and channel of conduction electrons and in the two levels of the f-electrons. σ ($=\uparrow,\downarrow$) and μ ($=1,2$) represent 1/2 pseudo-spin and channel index, respectively. Explicit representations of $a_{k\sigma\mu}$ are shown in Table 5.1. The coupling constants in $H_{\rm ex}$ are expressed by α and β, which are also given in Table 5.2 and shown in Fig. 5.2 where $\alpha^2=(1+x)/2$ and $\beta^2=(1-x)/2$ ($|x|<1$). If we suppress the terms containing $m_\pm$ or $\tilde{m}_\pm$, Cox's model for the tetragonal or hexagonal crystal field is recovered [54].

Having obtained the exchange Hamiltonian, let us examine the low temperature

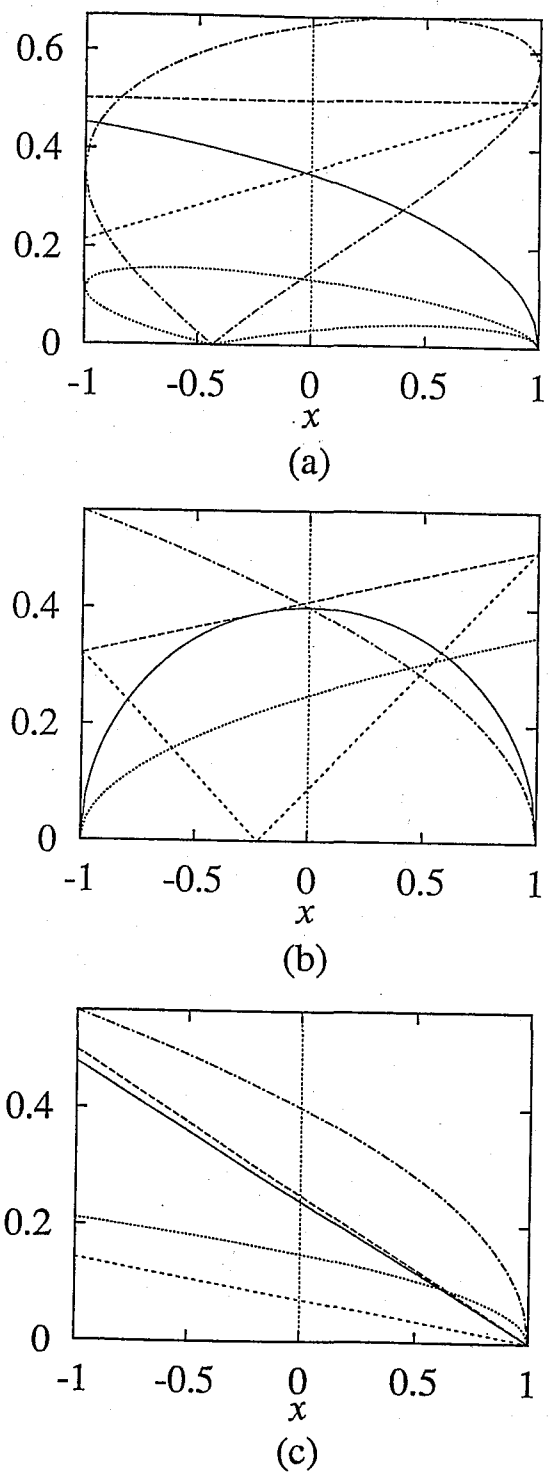

Figure 5.2: Various couplings of $H_{\rm ex}$ in (5.21) as a function of x. The explicit forms are presented in the columns (a), (b) and (c) of Table 5.2. The solid, dashed, half-dashed, dotted and dot-dashed lines represent $|J_{\perp,0}|$, $|J_{z,0}|$, $|K_{z,0}|$, $|K_{\perp,0}|$ and $|I_{\perp,0}|$, respectively.

physics of the model by using the NRG method. In the NRG method, the Hamiltonian is transformed to a hopping-type one with a recursion relation as

$$H_{N+1} = \Lambda^{1/2} H_N + \sum_{\sigma\mu} (f^\dagger_{N+1,\sigma\mu} f_{N\sigma\mu} + \text{h.c.}), \tag{5.25}$$

and

$$H_0 = H_{0,\text{l}} + H_{0,\text{sp}} + H_{0,\text{ch}} + H_{0,\text{sc}}, \tag{5.26}$$

$$H_{0,\text{l}} = \Delta |B\rangle\langle B|, \tag{5.27}$$

$$\begin{aligned} H_{0,\text{sp}} = \sum_{\mu} \big[& J_\perp (f^\dagger_{0\uparrow\mu} f_{0\downarrow\mu} S_- + f^\dagger_{0\downarrow\mu} f_{0\uparrow\mu} S_+) \\ & + J_z (f^\dagger_{0\uparrow\mu} f_{0\uparrow\mu} - f^\dagger_{0\downarrow\mu} f_{0\downarrow\mu}) S_z \big], \end{aligned} \tag{5.28}$$

$$\begin{aligned} H_{0,\text{ch}} = \sum_{\sigma} \big[& K_z (f^\dagger_{0\sigma 1} f_{0\sigma 1} - f^\dagger_{0\sigma 2} f_{0\sigma 2}) S_z \\ & + K_\perp (f^\dagger_{0\sigma 1} f_{0\sigma 2} m_- + f^\dagger_{0\sigma 2} f_{0\sigma 1} m_+) \big] \\ & + K_{\tilde{\perp}} \big[(f^\dagger_{0\uparrow 1} f_{0\uparrow 2} - f^\dagger_{0\downarrow 1} f_{0\downarrow 2}) \tilde{m}_- + (f^\dagger_{0\uparrow 2} f_{0\uparrow 1} - f^\dagger_{0\downarrow 2} f_{0\downarrow 1}) \tilde{m}_+ \big], \end{aligned} \tag{5.29}$$

$$H_{0,\text{sc}} = I_\perp (f^\dagger_{0\uparrow 2} f_{0\downarrow 1} m_- + f^\dagger_{0\downarrow 1} f_{0\uparrow 2} m_+), \tag{5.30}$$

where $f_{n\sigma\mu}$ is a new operator which is obtained from $a_{k\sigma\mu}$ via Wilson's logarithmic discretization of the conduction band. Energies are measured in units of half of the total conduction bandwidth. Λ is the logarithmic discretization factor and we take $\Lambda = 3$. In most calculations, the lowest ~ 500 states are kept at each renormalization step. If the exchange Hamiltonian is restricted to the first part H_{sp}, this model is equivalent to the two-channel exchange model discussed in Section 4.1. It leads to a fixed point which is of non-Fermi liquid type and isotropic; it means that $J_\perp$ and J_z reach the same finite value after a sufficient number of renormalization steps [52, 53].

Next we wish to discuss the role of $H_{0,\text{ch}}$, which is a new type of exchange interaction. We obtain the conventional two-channel model with $N_{\text{ch}} = 2S$ ($N_{\text{ch}} = 2, S = 1$) if $\Delta = 0$ and either $K_\perp = 0$ or $K_{\tilde{\perp}} = 0$ is satisfied. It results in the Fermi-liquid fixed point where the impurity moment is compensated completely. In our model, if Δ is small, the Fermi liquid is also realized though the relation $K_\perp = K_{\tilde{\perp}}$ has to be satisfied due to the crystal symmetry. Figures 5.3 and 5.4 give the low-lying NRG energy levels in this case. This is different from the $K_{\tilde{\perp}} = 0$ case because of the symmetry breaking of pseudo-spin. At the fixed point for $K_{\tilde{\perp}} = 0$, quasi-particle energy

levels have four-fold degeneracy related to pseudo-spin and channel. In the present case ($K_\perp = K_{\tilde{\perp}} \neq 0$), the degenerate energy levels for $K_{\tilde{\perp}} = 0$ are split into two due to the symmetry breaking as shown in Fig. 5.5. The splitting ΔE depends on the coupling constants and Δ: ΔE becomes small as $K_\perp$ $(= K_{\tilde{\perp}})$ increases, while as $K_\perp$ decreases, ΔE becomes so large that the first excited energy level for even NRG steps approaches zero, which is the origin of energy. It also takes the same value for both even and odd steps of the renormalization. Every level changes continuously with $K_\perp$. On the other hand, in the large-Δ region, the effect of the coupling $K_\perp$ becomes less important and only the K_z term is left. Then the system behaves like the ordinary Kondo model with an Ising-like exchange coupling.

Let us consider next both $H_{0,\mathrm{sp}}$ and $H_{0,\mathrm{ch}}$ together. In this case, the particle-hole symmetry is broken. For simplicity, we treat the case where $J_\perp = J_z$ $(= J)$, $K_\perp = K_{\tilde{\perp}}$ $(= K)$ and $K_z = I_\perp = 0$ are satisfied. Then the system depends on the parameters J, K and Δ. We obtain either the Fermi liquid region or the non-Fermi liquid region, depending on which of K and J is larger. The ground state is a singlet in the former and a doublet in the latter. The phase diagram is shown in Fig. 5.6, where Δ is fixed at 0.3. The critical point K_c, below which the excited singlet is negligible, depends on Δ. In Figs. 5.7 and 5.8 we show NRG energy levels near the ground state for the case where J and K are comparable in magnitude. Clearly, how to reach the final energy levels at the fixed point is different between these two cases, although both of them have almost the same energy levels at the initial NRG steps. For finite J and K, the particle-hole symmetry breaking lifts the degeneracy of the NRG energy levels for either $K = 0$ or $J = 0$. They are split into parts with the center of gravity kept constant. The splitting depends on both J and K. In Fig. 5.7, the local moment is considered to be still present. The NRG energy levels are the same as given by the two-channel model with a local spin 1/2, except for the splitting of energy levels due to the particle-hole symmetry breaking. However, in Fig. 5.8, the energy levels at the fixed point can be reproduced by assuming that the compensation of the local moment is achieved completely. Therefore the system becomes Fermi liquid whose states are described by filling electrons in one-particle energy levels such as shown in Fig. 5.5. In this case, the energy levels become asymmetric with respect to the Fermi level due to the particle-hole symmetry breaking. They actually shift

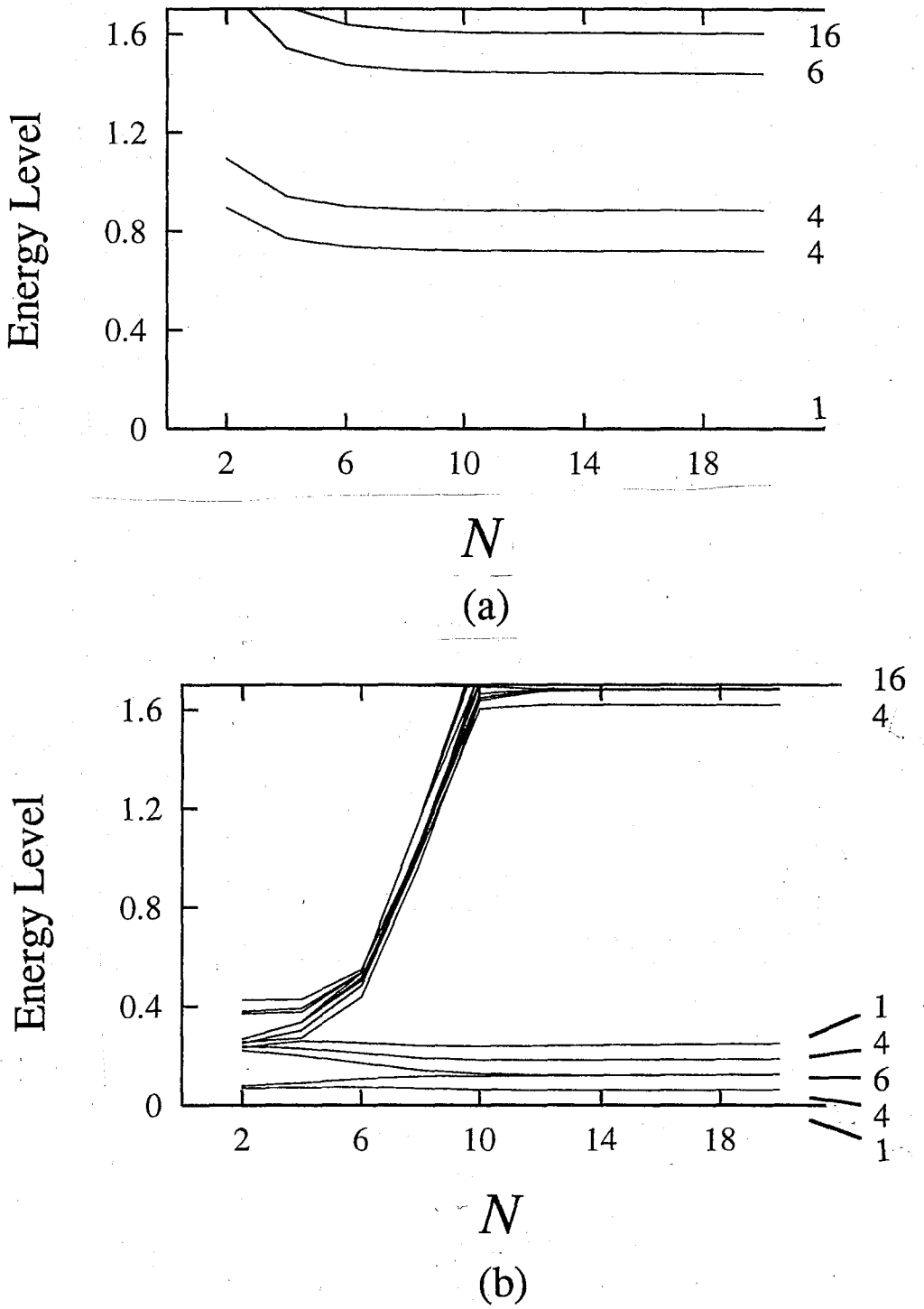

Figure 5.3: The low-lying NRG energy levels for only $H_{0,\mathrm{ch}}$, where $K_\perp = K_{\tilde{\perp}}$, $K_z = 0$ and $\Delta = 0$ are satisfied. (a) $K_\perp = 4.0$ and (b) $K_\perp = 0.1$ are given at even-number renormalization steps. The numbers at the right side represent the degrees of degeneracy.

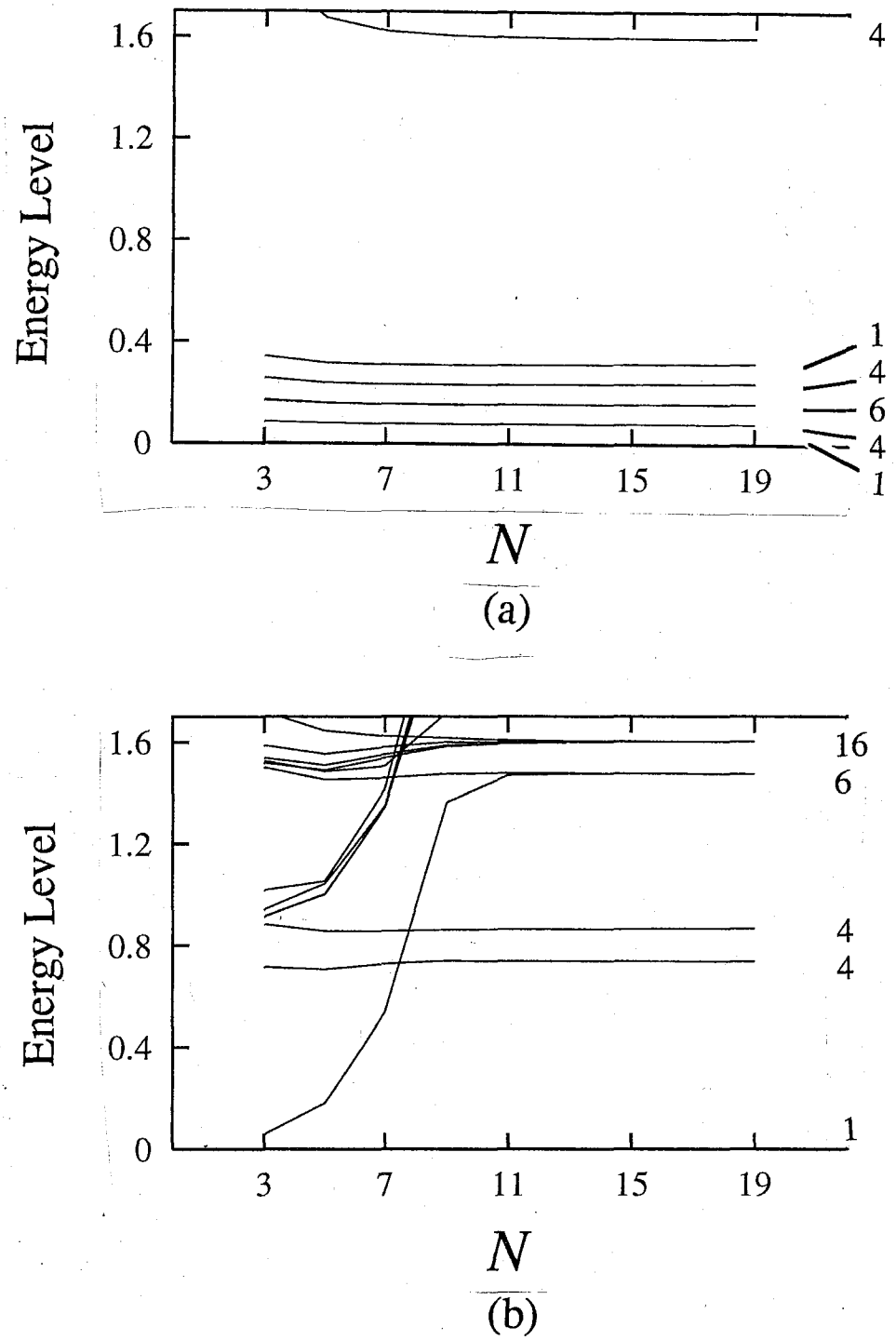

Figure 5.4: The low-lying NRG energy levels for only $H_{0,\mathrm{ch}}$, where $K_\perp = K_{\tilde{\perp}}$, $K_z = 0$ and $\Delta = 0$ are satisfied. (a) $K_\perp = 4.0$ and (b) $K_\perp = 0.1$ are given at odd-number renormalization steps. The numbers at the right side represent the degrees of degeneracy.

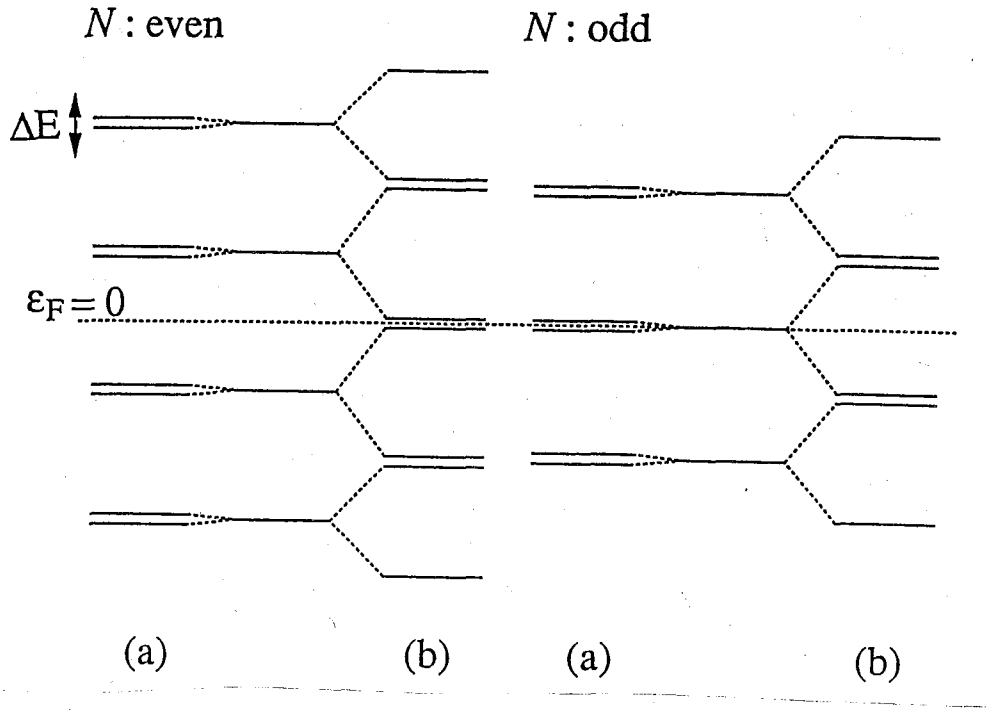

Figure 5.5: The one-particle energy levels at the Fermi-liquid fixed point where only $H_{0,\mathrm{ch}}$ is considered by satisfying $K_\perp = K_\parallel$: (a) for $K_\perp \gg 1$; (b) for $K_\perp \ll 1$. Energy is measured vertically. In both cases, each energy level is two-fold degenerate. It is different from the conventional two-channel model ($N_{\mathrm{ch}} = 2$, $S = 1$), which has four-fold degenerate energy levels.

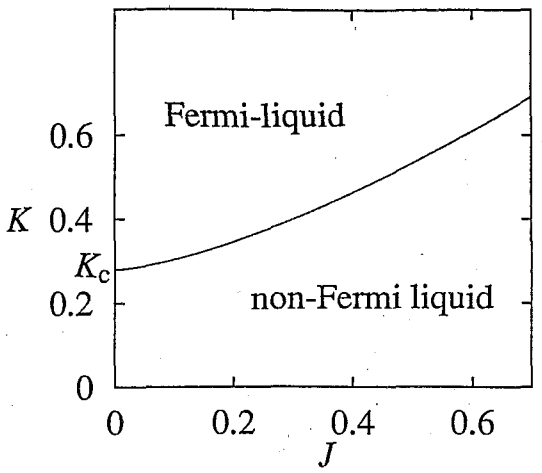

Figure 5.6: The phase diagram of the stability region of the Fermi and non-Fermi liquids. Here Δ is fixed at $\Delta = 0.3$ and K_{c} ($\simeq 0.28$) represents the critical point. The magnitude of K_{c} increases with the increase of Δ.

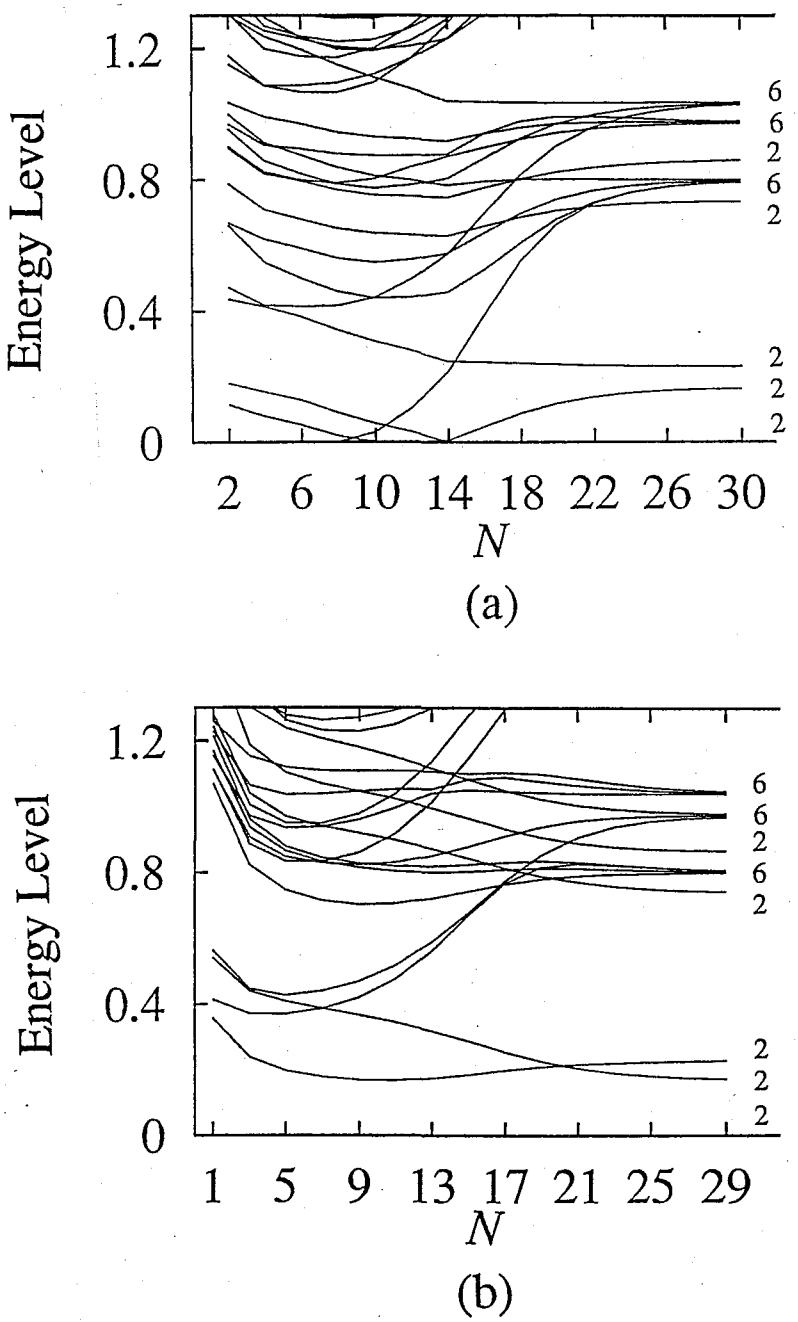

Figure 5.7: The low-lying NRG energy levels for $J = 0.4$: (a) even-number and (b) odd-number renormalization steps. K and Δ are chosen as $K = 0.6$ and $\Delta = 0.9$. The numbers at the right side denote the degrees of degeneracy.

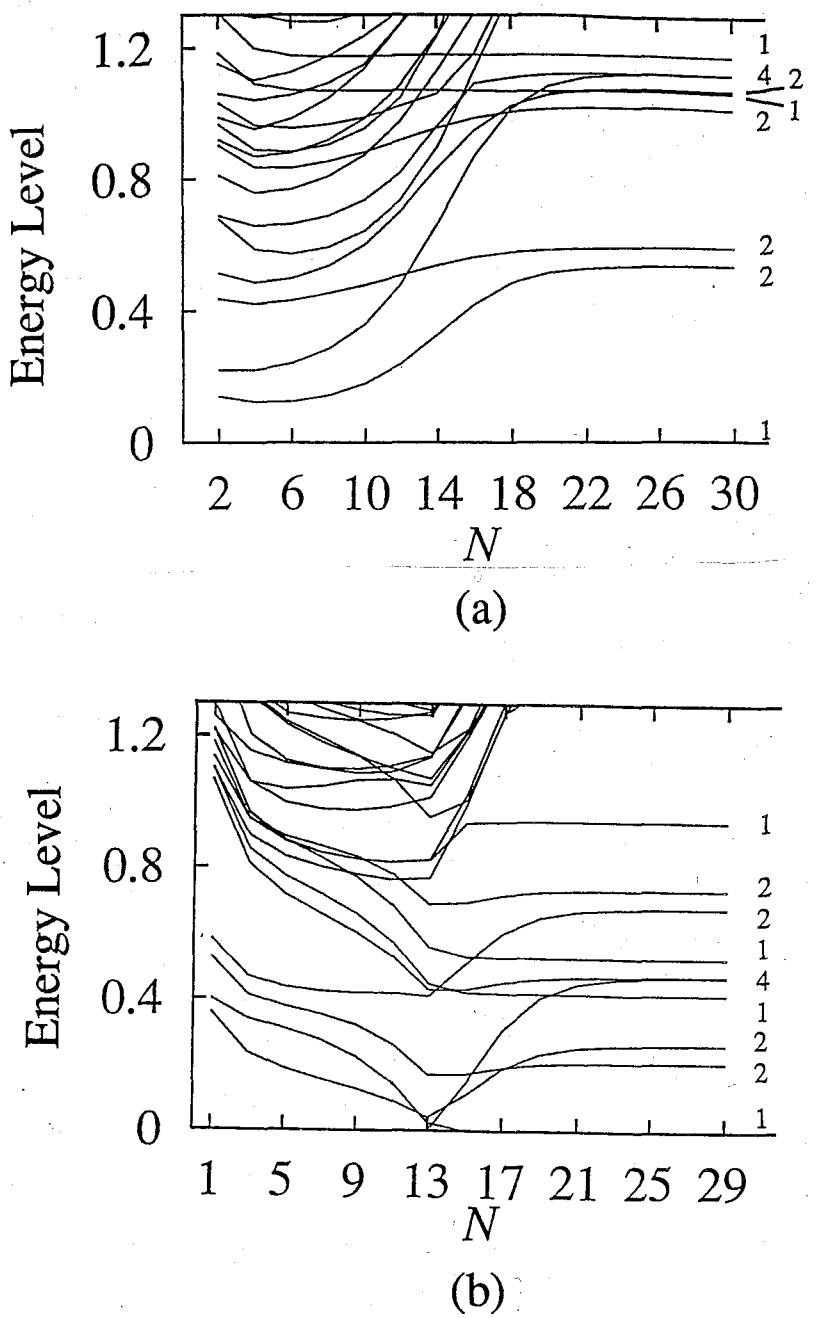

Figure 5.8: The low-lying NRG energy levels for $J = 0.38$: (a) even-number and (b) odd-number renormalization steps. K and Δ are chosen as $K = 0.6$ and $\Delta = 0.9$. The numbers at the right side denote the degrees of degeneracy.

downwards from the ones in the symmetric case. The presence of $H_{0,\mathrm{sc}}$, which we have neglected in the above discussion, does not change the phase diagram of Fermi liquid vs. non-Fermi liquid qualitatively.

In real systems, the coupling constants in H_0 depend on the crystal field parameters as shown in Table 5.2 and Fig. 5.2. We conclude that the non-Fermi liquid is dominant over the Fermi liquid all over x for the tetragonal field (Fig. 5.2 (a)) as well as for the hexagonal field satisfying $|B_4^0|/|B_2^0| > 3/10$ (Fig. 5.2 (c)), since $K_\perp$ is smaller than $J_\perp$ or $I_\perp$. However, the Fermi liquid is dominant in the range $x > 0.6$ in case $|B_4^0|/|B_2^0| < 3/10$ is satisfied for the hexagonal crystal field (Fig. 5.2 (b)).

5.2 Extension to Singlet Ground State

The above discussion can be extended to negative Δ [55, 56]. In this case the ground state is the singlet state $|B\rangle$ and the excited state is the doublet state $|E\rangle$ for f^2 configuration. The Fermi liquid region spreads more widely as Δ becomes smaller. When $\Delta = 0$, K_c goes to zero. For a negative Δ, the $K = 0$ line is separated into two regions as shown in Fig. 5.9: The local singlet $|B\rangle$ and free conduction electrons are realized independently in the region where J is smaller than J_c; for larger J, on the other hand, the fixed point is non-Fermi liquid type discussed above. The Fermi liquid region is connected with the former region continuously. This is understood from Fig. 5.10, where J is taken to be zero. The first and second excited energy levels for $K \neq 0$ are very close to those for the free-electron case ($K = 0$) as K approaches to zero, especially in the case where Δ is negative.

Let us understand Fig. 5.10, where the one-particle energy levels are in the same way as (2.48). For $K = 0$ and $\Lambda = 3$, the one-particle energy levels are

$$\left.\begin{array}{l} \eta_1 = 0.8000, \quad \eta_2 = 2.997, \quad \cdots, \quad \eta_i = 3^{i-1} \\ \eta_0' = 0, \quad \eta_1' = 1.696, \quad \eta_2' = 5.196, \quad \cdots, \quad \eta_i' = 3^{i-1/2} \end{array}\right\} \tag{5.31}$$

This means that the localized state is in the singlet state denoted by $|B\rangle$ and the conduction electrons have no coupling with the local electron. In fact the one-particle energy levels at the Fermi-liquid fixed point depend mainly on the initial coupling K and the crystal field splitting Δ. As K increases, they gradually changes until they reach the energy levels in (5.31) in which even-number renormalization step and

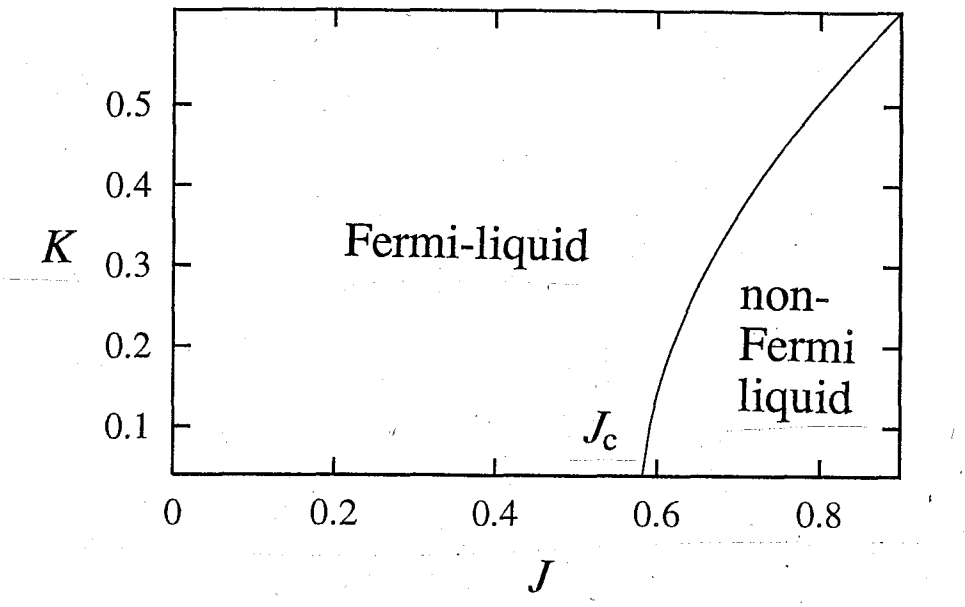

Figure 5.9: The phase diagram of the stability region of the Fermi and non-Fermi liquids. Here Δ is fixed at $\Delta = -0.5$ and J_c ($\simeq 0.58$) represents the critical point. The magnitude of J_c increases with the decrease of Δ.

odd-number one are completely exchanged when $K \to \infty$. The coupling J causes the particle-hole symmetry breaking. It is different from the strong coupling fixed point for the one-channel Kondo model which does not depend on the initial coupling: In the latter case, the magnitude of coupling becomes infinitely large as a result of renormalization.

To discuss the behavior in Fig. 5.10 more quantitatively, we study the effective Hamiltonian describing the one-particle energy levels at the fixed point for $J = 0$. It takes the following form:

$$H^*_N = H^*_{\mathrm{k},N} + H^*_{01,N} + H^*_{00,N}, \tag{5.32}$$

$$H^*_{\mathrm{k},N} = \Lambda^{(N-1)/2}\left[\sum_{n=1}^{N-1}\Lambda^{-n/2}\sum_{\sigma\mu}(f^{*\dagger}_{n\sigma\mu}f^*_{n+1,\sigma\mu} + f^{*\dagger}_{n+1,\sigma\mu}f^*_{n\sigma\mu})\right], \tag{5.33}$$

$$H^*_{01,N} = t^*_{01}\Lambda^{(N-1)/2}\sum_{\sigma\mu}(f^{*\dagger}_{0\sigma\mu}f^*_{1,\sigma\mu} + f^{*\dagger}_{1,\sigma\mu}f^*_{0\sigma\mu}), \tag{5.34}$$

$$\begin{aligned} H^*_{00,N} &= \varepsilon^*_{00}\Lambda^{(N+1)/2}\sum_{\mu\mu'}(\sigma_z)_{\mu'\mu}(f^{*\dagger}_{0\uparrow\mu'}f^*_{0\uparrow\mu} - f^{*\dagger}_{0\downarrow\mu'}f^*_{0\downarrow\mu}) \\ &\quad + t^*_{00}\Lambda^{(N+1)/2}\sum_{\mu}(f^{*\dagger}_{0\uparrow\mu}f^*_{0\downarrow\mu} + f^{*\dagger}_{0\downarrow\mu}f^*_{0\uparrow\mu}), \end{aligned} \tag{5.35}$$

where N is taken to be large enough. $f^{*\dagger}_{i\sigma\mu}$ represents the new creation operator defined at the fixed point, which is related to $f^{\dagger}_{i\sigma\mu}$ in (5.25). This effective Hamilto-

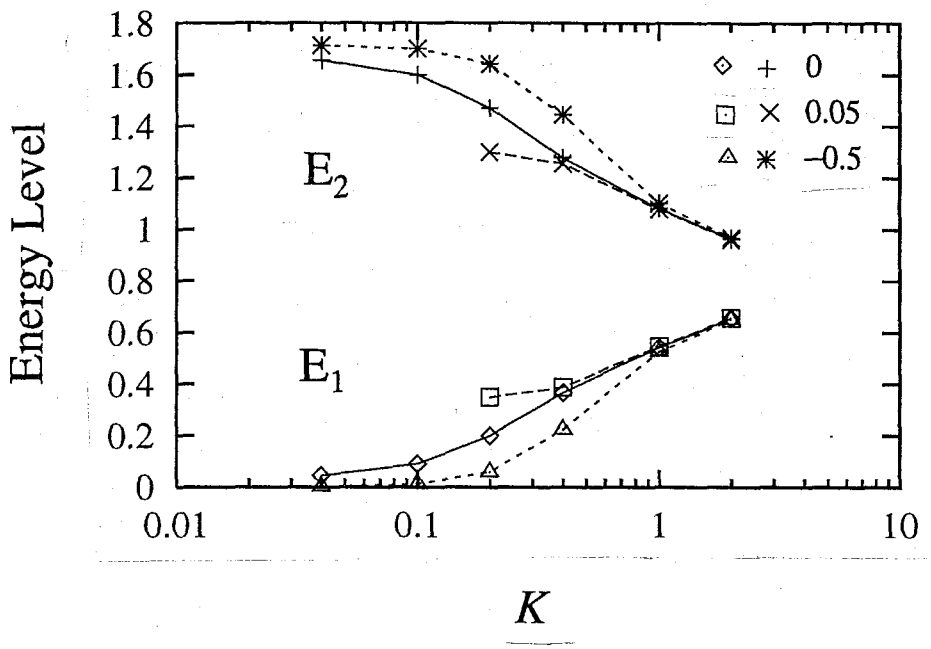

(a)

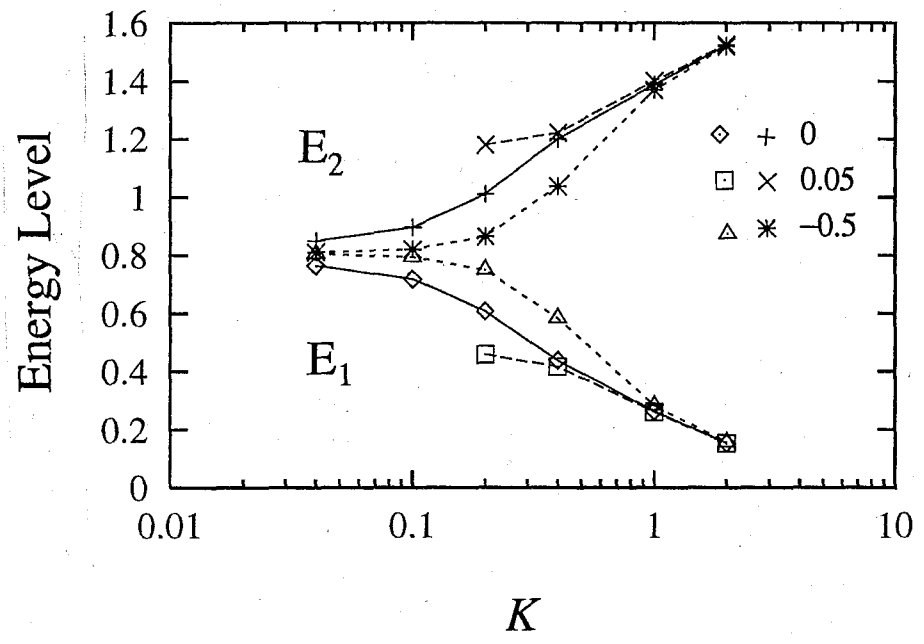

(b)

Figure 5.10: The dependence of the first (E_1) and second (E_2) excited one-particle energy levels on the coupling K, where only $H_{\rm ch}$ is considered. Δ is chosen as 0.05, 0 and -0.5: (a) even-number and (b) odd-number renormalization steps.

nian describes free conduction electrons, which are influenced by the potential on the zeroth site. The magnitude of potential energy is varied by the three coupling parameters t_{01}^*, t_{00}^* and ε_{00}^*, which are not independent of each other. If $A^* = \sqrt{\varepsilon_{00}^{*2} + t_{00}^{*2}}$ is defined, the energy levels depend only on A^*. On the other hand, if t_{01}^* are varied as $\tilde{t}_{01}^* = \alpha t_{01}^*$, rescaling with $\tilde{A}^* = \alpha^2 A^*$ leads to the same energy levels as with t_{01}^* and A^*. This relation holds well for low-lying energy levels. Then it is reasonable to take $t_{01}^* = 1$, $t_{00}^* = 0$ and $\varepsilon_{00}^* = A^*$. With this simplification, the effective Hamiltonian describing the one-particle energy levels is obtained as

$$H_N^* = \Lambda^{(N-1)/2} \left[\sum_{n=0}^{N-1} \Lambda^{-n/2} \sum_{\sigma\mu} (f_{n\sigma\mu}^{*\dagger} f_{n+1,\sigma\mu}^* + f_{n+1,\sigma\mu}^{*\dagger} f_{n\sigma\mu}^*) \right] + \varepsilon_{00}^* \Lambda^{(N+1)/2} \sum_{\sigma\sigma'\mu\mu'} (\sigma_z)_{\sigma'\sigma} (\sigma_z)_{\mu'\mu} f_{0\sigma'\mu'}^{*\dagger} f_{0\sigma\mu}^*, \tag{5.36}$$

where the energy levels depend only on one parameter ε_{00}^* when Λ is fixed. The dependence of energy levels on ε_{00}^* is shown in Fig. 5.11. Clearly, ε_{00}^* corresponds to the coupling K in Fig. 5.10 although the rescaling of ε_{00}^* is necessary to fit the energy levels with ones at the fixed point for each K completely. Practically ε_{00}^* can be determined by fitting the first excited state given by H_N^* with that given by the NRG calculation. By using the same value for ε_{00}^*, the second and higher energy levels also show a good agreement within less than 1 % error. It is clear that $\varepsilon_{00}^* = 0$ corresponds to the case $K = 0$, while $\varepsilon_{00}^* \to \infty$ corresponds to the case $K \to \infty$. The effect of the coupling J changes ε_{00}^* and brings about another parameter which is added to the second term in (5.36):

$$\varepsilon_{00}^* \Lambda^{(N+1)/2} \sum_{\sigma\sigma'\mu\mu'} (\sigma_z)_{\sigma'\sigma} (\sigma_z)_{\mu'\mu} f_{0\sigma'\mu'}^{*\dagger} f_{0\sigma\mu}^*, + \delta\varepsilon_{00}^* \Lambda^{(N+1)/2} \sum_{\sigma\mu} f_{0\sigma\mu}^{*\dagger} f_{0\sigma\mu}^*, \tag{5.37}$$

where the second term breaks the particle-hole symmetry. As discussed above, the conclusion is that the quenching of the local moment is influenced by both the local singlet state denoted by $|B\rangle$ which is independent of conduction electrons and the Kondo singlet state which is formed by the local moment coupled with the conduction electrons.

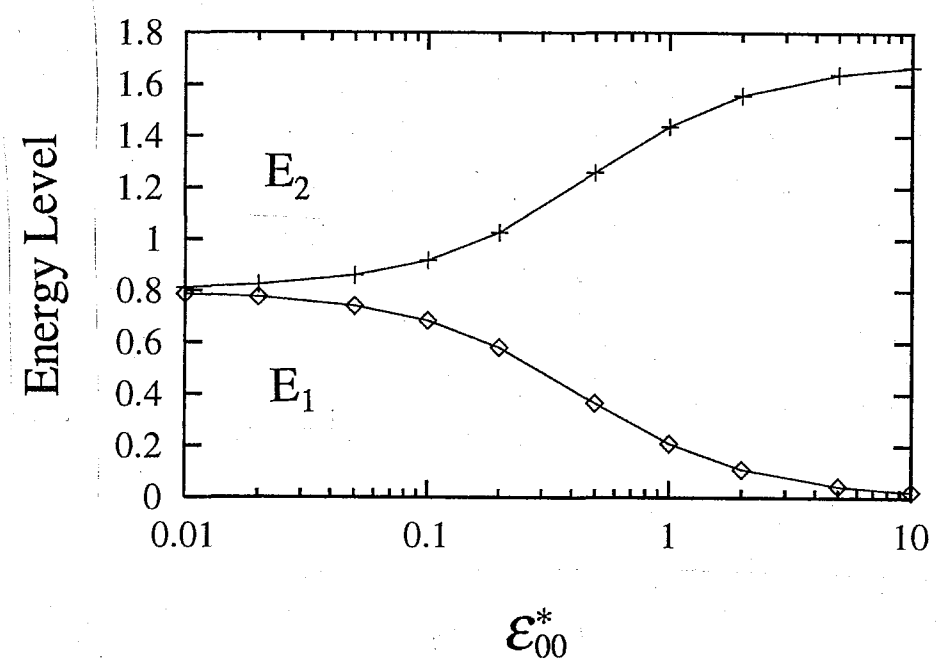

Figure 5.11: Dependence of one-particle energy levels on ε^*_{00} in the effective Hamiltonian (5.36). The first (E_1) and second (E_2) energy levels are shown. This should be compared with Fig. 5.10 (b).

5.3 Crossover Temperature

Let us closely look at the vicinity of the boundary between the Fermi and non-Fermi liquid regions in the phase diagram (Figs. 5.6 and 5.9). The point we wish to examine is the renormalization step (denoted by $N_{\rm cr}$) at which the lowest energy level changes from the singlet to the doublet (in the non-Fermi liquid region) or from the doublet to the singlet (in the Fermi liquid region). The change of the lowest state is found at an even-number step when the coupling constants J and K belong to the non-Fermi liquid region. In the Fermi liquid region, on the other hand, it occurs at an odd-number step. We find $N_{\rm cr}$ to be $N_{\rm cr} = 14$ in Fig. 5.7 and $N_{\rm cr} = 15$ in Fig. 5.8. The renormalization step is related to temperature as

$$T = \Lambda^{-N/2}. \tag{5.38}$$

We call the temperature corresponding to $N_{\rm cr}$ a crossover temperature $T_{\rm cr}$ here. To examine the behavior in the vicinity of the boundary, we change J close to the boundary, keeping K and Δ fixed. As shown in the Fig. 5.12, $N_{\rm cr}$ increases with a power law as $|J - J_{\rm b}|$ decreases. Here $J_{\rm b}$ is the value at the boundary. Therefore we conclude that the boundary is characterized by $T_{\rm cr} = 0$. The crossover temperature behaves as

$$T_{\rm cr} \propto |J - J_{\rm b}|^{\alpha}, \tag{5.39}$$

where the power is estimated approximately as $\alpha \simeq 9$ in Fig. 5.12 (a) and $\alpha \simeq 8$ in Fig. 5.12 (b). The implication of these values are not yet well understood. Further examination is needed.

The power-law behavior was previously found in the NRG study for the two-channel exchange model [53]. The channel anisotropy is a relevant perturbation breaking the non-Fermi liquid, so that it gives rise to the Fermi liquid. In this case a crossover temperature is defined as a renormalization step at which the NRG energy levels cross over to those at a Fermi liquid fixed point. Similarly to our model, the crossover temperature decreases with a power law as the anisotropy becomes smaller. In the latter case the origin of the power is well explained by the conformal field theory [57].

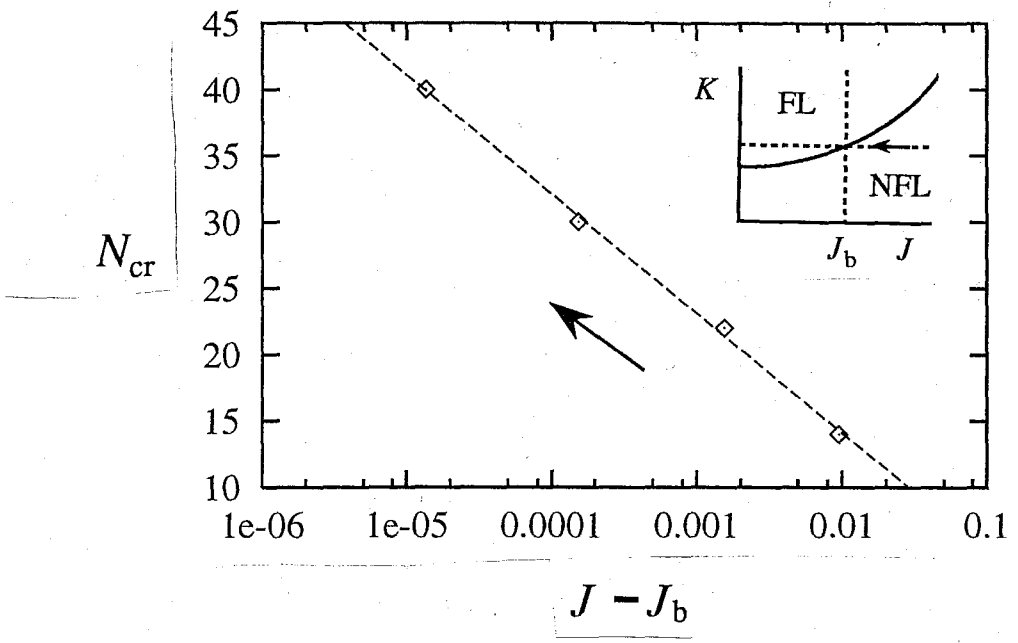

(a)

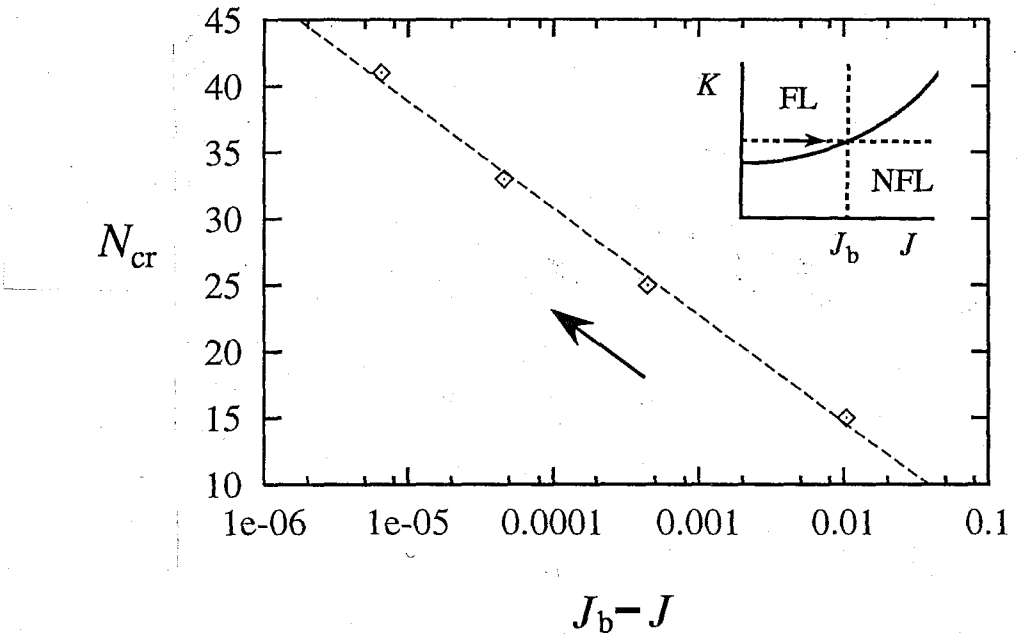

(b)

Figure 5.12: The dependence of N_{cr} ($\propto -\log T_{cr}$) as J approaches the boundary in (a) the non-Fermi liquid and (b) the Fermi liquid regions. K and Δ are fixed as $K = 0.6$ and $\Delta = 0.9$.

5.4 A More Generalized Treatment

In the previous sections, the intermediate state has been restricted only to the lowest state of f^1 configuration. This assumption has been introduced to make the exchange process simple. Let us relax this restriction here and discuss a more general case by checking the effective exchange interaction for the tetragonal crystal field. For the tetragonal case, we have obtained in (5.7) the exchange interaction in a tensorial expression. Then the creation operators for the conduction electrons $a^\dagger_{km}$ have been transformed to those defined in Table 5.1 by using pseudo-spin and channel. The higher excited states in f^1 give additional exchange terms to the effective Hamiltonian (5.21). They are the exchange between $a^\dagger_{k\sigma\mu}$ and $b^\dagger_{k\sigma}$. The latter is defined by

$$b^\dagger_{k\uparrow} = \frac{\sqrt{7}\alpha a^\dagger_{k,-5/2} - \sqrt{5}\beta a^\dagger_{k,3/2}}{\sqrt{7\alpha^2+5\beta^2}}, \tag{5.40}$$

$$b^\dagger_{k\downarrow} = \frac{\sqrt{7}\alpha a^\dagger_{k,5/2} - \sqrt{5}\beta a^\dagger_{k,-3/2}}{\sqrt{7\alpha^2+5\beta^2}}. \tag{5.41}$$

The Hamiltonian generalized for this case is then given by

$$H = H_{\rm k} + H_{\rm l} + H_{\rm ex}$$

$$H_{\rm k} = \sum_{k\sigma}\varepsilon_k(\sum_{\mu} a^\dagger_{k\sigma\mu}a_{k\sigma\mu} + b^\dagger_{k\sigma}b_{k\sigma}), \tag{5.42}$$

$$H_{\rm l} = \Delta|B\rangle\langle B|, \tag{5.43}$$

$$H_{\rm ex} = H^0_{\rm ex} + H_{\rm ex,add}, \tag{5.44}$$

where $H^0_{\rm ex}$ is equal to $H_{\rm ex}$ in (5.21) and $H_{\rm ex,add}$ is an additional term:

$$\begin{aligned} H_{\rm ex,add} &= K'_{z,0}(b^\dagger_{k'\uparrow}b_{k\uparrow} - b^\dagger_{k'\downarrow}b_{k\downarrow}) \\ &+ K'_{\perp 1,0}\sum_{kk'}\big[(b^\dagger_{k'\downarrow}a_{k\uparrow 2} + a^\dagger_{k'\downarrow 1}b_{k\uparrow})m_- + (a^\dagger_{k'\uparrow 2}b_{k\downarrow} + b^\dagger_{k'\uparrow}a_{k\downarrow 1})m_+ \\ &\quad + (b^\dagger_{k'\downarrow}a_{k\uparrow 2} - a^\dagger_{k'\downarrow 1}b_{k\uparrow})\tilde{m}_- + (a^\dagger_{k'\uparrow 2}b_{k\downarrow} - b^\dagger_{k'\uparrow}a_{k\downarrow 1})\tilde{m}_+\big] \\ &+ K'_{\perp 2,0}\sum_{kk'}\big[(b^\dagger_{k'\uparrow}a_{k\uparrow 1} + a^\dagger_{k'\downarrow 2}b_{k\downarrow})m_- + (a^\dagger_{k'\uparrow 1}b_{k\uparrow} + b^\dagger_{k'\downarrow}a_{k\downarrow 2})m_+ \\ &\quad + (b^\dagger_{k'\uparrow}a_{k\uparrow 1} - a^\dagger_{k'\downarrow 2}b_{k\downarrow})\tilde{m}_- + (a^\dagger_{k'\uparrow 1}b_{k\uparrow} - b^\dagger_{k'\downarrow}a_{k\downarrow 2})\tilde{m}_+\big]. \end{aligned} \tag{5.45}$$

Here the potential scattering has been ignored. The second and third exchange interactions come from via the intermediate states $|E^{(1)}_{3/2}\pm\rangle$ in (5.12) and $|E_{1/2}\pm\rangle$ in

(5.14), respectively, of f^1 configuration. If the Hund coupling is ignored and all the intermediate states are made up to one degenerate energy level for zero crystal field, the three coupling constants are related with each other as

$$K'_{z,0} = \alpha^2 + \frac{3}{7}\beta^2, \tag{5.46}$$

$$K'_{\perp 1,0} = \frac{\sqrt{10}\beta(\sqrt{7}\alpha - 3\beta)}{28\sqrt{7\alpha^2 + 5\beta^2}}, \tag{5.47}$$

$$K'_{\perp 2,0} = \frac{\sqrt{5}}{28}(\sqrt{7}\alpha - 3\beta), \tag{5.48}$$

where α and β are defined in (5.1). If the Hund coupling is nonvanishing and a small crystal field splitting is present, we expect a slight modification of the Hamiltonian.

We now apply the NRG calculation to the generalized model. For simplicity, only relevant terms are written down in the model Hamiltonian to discuss the NRG analysis:

$$H_{N+1} = \Lambda^{1/2} H_N + \sum_{\sigma\mu} \left[(f^\dagger_{N+1,\sigma\mu} f_{N\sigma\mu} + g^\dagger_{N+1,\mu} g_{N\mu}) + \text{h.c.} \right], \tag{5.49}$$

and

$$H_0 = H_{0,\text{l}} + H_{0,E} + H_{0,E+B}, \tag{5.50}$$

$$H_{0,\text{l}} = \Delta |B\rangle\langle B|, \tag{5.51}$$

$$H_{0,E} = J \sum_{\sigma\sigma'\mu} f^\dagger_{0\sigma'\mu} f_{0\sigma\mu} (\boldsymbol{\sigma})_{\sigma'\sigma} \cdot \boldsymbol{S}, \tag{5.52}$$

$$\begin{aligned} H_{0,E+B} = {} & K_\perp \Big[\sum_\sigma (f^\dagger_{0\sigma 1} f_{0\sigma 2} m_- + f^\dagger_{0\sigma 2} f_{0\sigma 1}) m_+ \\ & + (f^\dagger_{0\uparrow 1} f_{0\uparrow 2} - f^\dagger_{0\downarrow 1} f_{0\downarrow}) \tilde{m}_- + (f^\dagger_{0\uparrow 2} f_{0\uparrow 1} - f^\dagger_{0\downarrow 2} f_{0\downarrow 1}) \tilde{m}_+ \Big] \\ & + K'_{\perp 1} \Big[(g^\dagger_{0\downarrow} f_{0\uparrow 2} + f^\dagger_{0\downarrow 1} g_{0\uparrow}) m_- + (f^\dagger_{0\uparrow 2} g_{0\downarrow} + g^\dagger_{0\uparrow} f_{0\downarrow 1}) m_+ \\ & + (g^\dagger_{0\downarrow} f_{0\uparrow 2} - f^\dagger_{0\downarrow 1} g_{0\uparrow}) \tilde{m}_- + (f^\dagger_{0\uparrow 2} g_{0\downarrow} - g^\dagger_{0\uparrow} f_{0\downarrow 1}) \tilde{m}_+ \Big] \\ & + K'_{\perp 2} \Big[(g^\dagger_{0\uparrow} f_{0\uparrow 1} + f^\dagger_{0\downarrow 2} g_{0\downarrow}) m_- + (f^\dagger_{0\uparrow 1} g_{0\uparrow} + g^\dagger_{0\downarrow} f_{0\downarrow 2}) m_+ \\ & + (g^\dagger_{0\uparrow} f_{0\uparrow 1} - f^\dagger_{0\downarrow 2} g_{0\downarrow}) \tilde{m}_- + (f^\dagger_{0\uparrow 1} g_{0\uparrow} - g^\dagger_{0\downarrow} f_{0\downarrow 2}) \tilde{m}_+ \Big], \end{aligned} \tag{5.53}$$

where $g^\dagger_{n\sigma}$ corresponds to $b^\dagger_{k\sigma}$ as $f^\dagger_{n\sigma\mu}$ to $a^\dagger_{k\sigma\mu}$. J_z is taken to be equal to $J_\perp$; they are represented by J as in the previous sections. In the NRG calculation, the lowest $200 \sim 300$ states are kept at each renomalization step although this number is too

small to achieve a sufficient quantitive accuracy. However the present truncation at $200 \sim 300$ does not affect qualitative results. The result of renormalization shows that whether a fixed point is of Fermi liquid type or not depends on two kinds of coupling constants. One ($J_{\perp,0}$) is connected with only $|E\pm\rangle$; the other ($K_{\perp,0}$, $K'_{\perp 1,0}$ or $K'_{\perp 2,0}$) is connected with both $|E\pm\rangle$ and $|B\rangle$. The magnitude of these relevant coupling constants is controlled by the crystal field, namely, α and β: $J_{\perp,0}$ and $K_{\perp,0}$ are given in Table 5.2 and the other couplings are given in (5.47) and (5.48). The dependence of the couplings on α and β is shown in Fig. 5.13, where both parameters are replaced by x, as in Fig. 5.2. x has been defined as $\alpha^2 = (1+x)/2$ and $\beta^2 = (1-x)/2$. We find that $K'_{\perp 2,0}$ is larger than $J_{\perp,0}$ for $x > 0.3$. The NRG result shows that the Fermi liquid is dominant over the non-Fermi liquid within this range. Notice that it was not possible for the tetragonal case in the previous discussion which is based on the model for a strong crystal field. The difference comes from higher intermediate states, which favor the Fermi liquid. If a stronger crystal field is introduced in this case, $K'_{\perp 2,0}$ is reduced and the Fermi liquid state is suppressed. However the Fermi liquid region still remains, since $K'_{\perp 2,0}$ is larger than $J_{\perp,0}$ as far as x is nearly equal to one and the crystal field is finite.

Let us discuss a more general case by changing the couplings arbitrarily. Figure 5.14 shows one-particle energy levels at the Fermi liquid fixed point. They depend on $K_\perp$, $K'_{\perp 1}$ and $K'_{\perp 2}$. Here J is fixed to zero. If only one of the three couplings is finite, we obtain energy levels in Fig. 5.14 (a). Every energy level is two-fold degenerate. The particle-hole symmetry is kept in this case. The same energy levels are also given by the NRG model in (5.25) and (5.26). Thus $K'_{\perp 1}$ and $K'_{\perp 2}$, which are related to the excited states of f^1, plays the same role as $K_\perp$. In Figs. 5.14 (b), (c) and (d), $K_\perp$ is fixed to zero and $K'_{\perp 1}$ and $K'_{\perp 2}$ are taken to be finite. One of them affects the energy levels in (a) which has been determined by the other. Compared with (a), the energy levels are shifted and the particle-hole symmetry is broken. In (d), some energy levels have four-fold degeneracy since a pair of energy levels in (c) merge with each other. This situation is present only when $K_\perp = 0$ and $K'_{\perp 1} = K'_{\perp 2}$ are satisfied. If $K_\perp$ is finite, the degeneracy is lifted as shown in Fig. 5.14 (e). Thus one-particle energy levels change continuously with the three couplings. If only one of the three couplings is larger than J in magnitude, the Fermi liquid wins over the

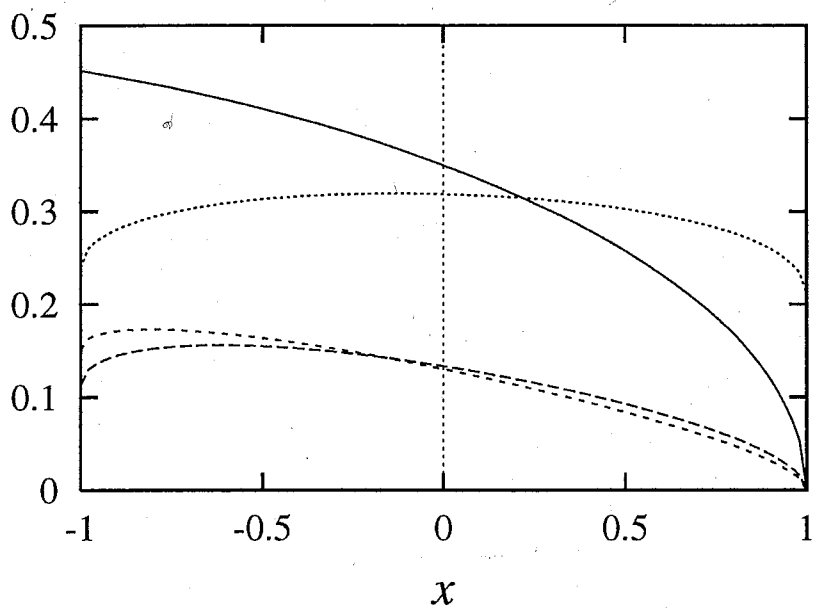

Figure 5.13: The magnitude of various relevant couplings of $H_{\rm ex}$ in (5.44) as a function of x. The explicit forms are presented for $J_{\perp,0}$ and $K_{\perp,0}$ in the column (a) of Table 5.2 and for $|K'_{\perp 1,0}|$ and $|K'_{\perp 2,0}|$ in (5.47) and (5.48), respectively. The solid, dashed, half-dashed and dotted lines represent $|J_{\perp,0}|$, $|K_{\perp,0}|$, $|K'_{\perp 1,0}|$ and $|K'_{\perp 2,0}|$, respectively.

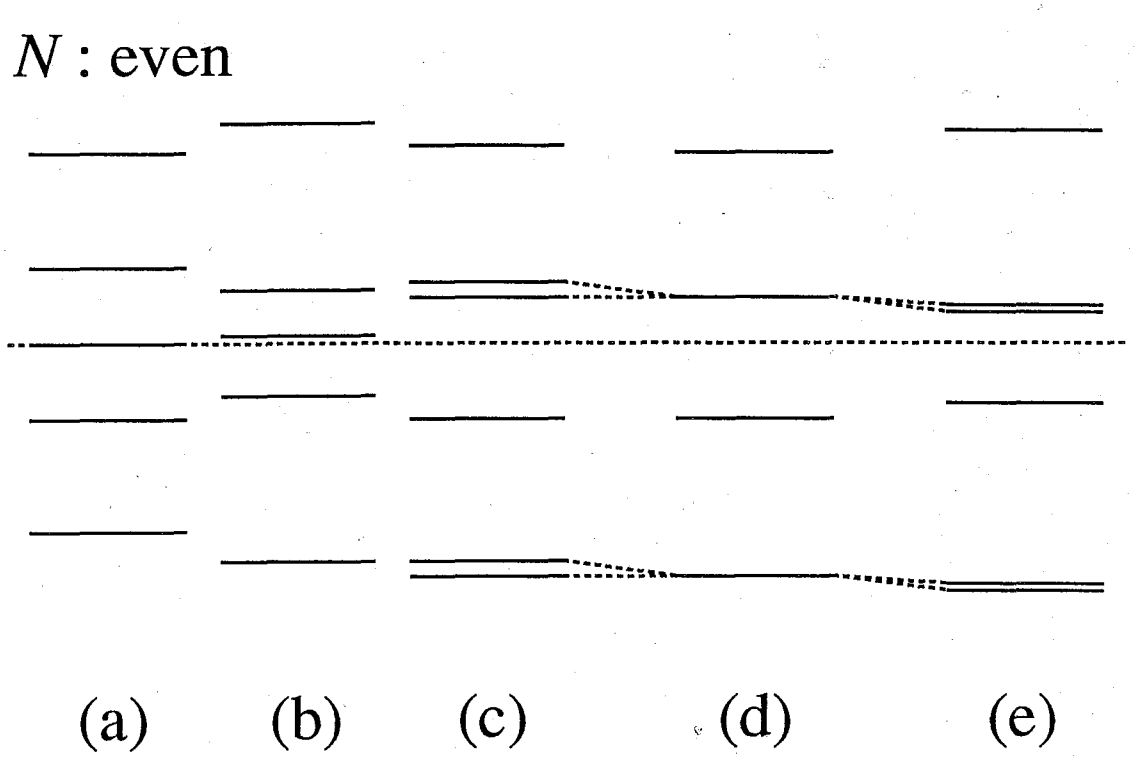

	(a)	(a)	(b)	(c)	(d)	(e)
$K_\perp$	0.6	0	0	0	0	0.2
$K'_{\perp 1}$(or $K'_{\perp 2}$)	0	0.6	0.6	0.6	0.6	0.6
$K'_{\perp 2}$(or $K'_{\perp 1}$)	0	0	0.4	0.5	0.6	0.6

Figure 5.14: One-particle energy levels at the Fermi liquid fixed point. This diagram shows the dependence on the couplings $K_\perp$, $K'_{\perp 1}$ and $K'_{\perp 2}$ at even-number renormalization steps. $J = 0$ and $\Delta = 0.3$ are chosen. Energy is measured vertically. For (a), the first and second excited states are $\simeq 0.5$ and $\simeq 1.2$, respectively. If J is finite, it shifts every energy level by a constant amount.

non-Fermi liquid. Qualitatively speaking, the role of J is to break the particle-hole symmetry at the Fermi liquid fixed point. The competition between the Fermi and non-Fermi liquids can be discussed in the same way as in Section 5.1.

In conclusion, due to the local excited states of f^1, the Fermi liquid can be dominant over the non-Fermi liquid. We note that the effect of the excited states in f^1 is not relevant unless the singlet is taken into account as well as the doublet for f^2 configuration. The excited state of f^2 plays the most important role to destabilize the non-Fermi liquid. Therefore it is reasonable to discuss the stability of the non-Fermi liquid by using the minimum model in (5.25) and (5.26).

Chapter 6

Conclusions

We have studied the Kondo effect due to orbitally degenerate $5f$ impurities in the presence of crystal field. This study has clarified the following issues:

(1) The difference between the Kondo effect due to a Kramers doublet and that due to a non-Kramers doublet.

(2) The stability of the non-Fermi liquid against realistic perturbations such as an effect of local excited states.

Let us summarize the main results in each Chapter.

In Chapter 3, an effective exchange interaction between the local moment and the conduction electrons has been derived in the absence of crystal field. Because of the orbital moment, the local moment is characterized not by spin $\boldsymbol{S}$ but by total angular momentum $\boldsymbol{J}$. The conduction electrons have been restricted to the partial waves with $j = 5/2$. It is based on the extended Anderson model with strong spin-orbit and Hund couplings. The effective exchange Hamiltonian is expressed in terms of the scalar product of tensor operators.

In Chapter 4, the crystal field was introduced and the effective exchange Hamiltonian was derived for the lowest f-electron state. For a cubic crystal field, we have discussed the difference of the Kondo effect between non-Kramers doublet in f^2 and Kramers doublet in f^3. We note that all the intermediate states are taken into account to derive the effective exchange Hamiltonian. New terms arise in addition to the terms in the conventional two-channel model. Whether they are relevant or not has been examined by using the NRG method. It has turned out that the

low temperature behavior can be described by the one-channel model for f^3. The NRG study has also shown that the Hund coupling is not important for the case of even-number f-electrons, while it causes the channel reduction for f^3. For f^2, the additional exchange terms are not relevant and the fixed point is the same as that in Cox's model. We have also checked that it holds for tetragonal and hexagonal cases.

In Chapter 5, the Kondo effect due to the non-Kramers doublet in f^2 has been further examined. A model for f^2 configuration has been studied for a tetragonal or hexagonal crystal field. The internal structure was simplified as the non-Kramers ground doublet and the first excited singlet. In this model for a strong crystal field, the channel-exchange terms appear in addition to the conventional two-channel model; the latter describes the exchange only in pseudo-spin (corresponding to the doublet ground state). On the other hand, the channel-exchange terms arise due to a coupling between the ground state doublet and the singlet excited state. The NRG study has shown that the new terms are so important that the system can become the Fermi liquid. It is due to competition between two kinds of exchange couplings, $J_\perp$ and $K_\perp$ $(= K_{\tilde{\perp}})$. Actually the relative magnitude of $J_\perp$ and $K_\perp$ $(= K_{\tilde{\perp}})$ depends on the crystal field parameters. The Fermi liquid can be realized in some region of the parameter space for the hexagonal crystal field, while for the tetragonal field case the non-Fermi liquid dominates over all the region.

We have also extended the model to the case of negative crystal field splitting Δ. In this case the singlet becomes the ground state; the Fermi liquid region becomes dominant. The nature of the Fermi liquid fixed point can be understood by considering a competition between the crystal-field singlet of f^2 and the local singlet state due to the Kondo effect. We have examined the boundary between the Fermi liquid and non-Fermi liquid regions. At the boundary, the crossover temperature $T_{\rm cr}$, at which the lowest NRG state changes from a doublet to a singlet or vice versa, vanishes. Finally higher intermediate states in f^1 configuration are taken into account for the tetragonal crystal field. The Fermi liquid becomes possible in this case due to an additional coupling connected with one of the higher f^1 states. Whether the Fermi liquid is stable or not depends on the crystal field parameters.

We have found in this study that not only the crystal-field ground state but also the excited states are important to realize the non-Fermi liquid state. Whether the

Fermi liquid is realized or not in realistic cases is not determined by a simple criterion based on the point group symmetry. The present study has shown that there is a difference of Kondo effect between even and odd number of f-electron systems. For even cases, we have found competition between the Fermi and non-Fermi liquids.

There are several problems left for future studies. First, it would be interesting to calculate physical quantities such as the magnetic susceptibility and the specific heat. They are expected to depend sensitively on the atomic structure of f-electron systems. Secondly, it is necessary to extend our study to the Anderson model, since the present work is limited to the strong coupling limit, which starts from large Coulomb interactions and small mixing. It is not evident that the strong coupling limit is smoothly connected with the weak coupling region.

Appendix A

Schrieffer-Wolff Transformation

The s-d exchange Hamiltonian (1.3) can be derived from the Anderson Hamiltonian (1.4) by assuming $|\varepsilon_0|$ and $U \ll |V_0|$. This can be carried out most conveniently by a canonical transformation. This procedure can be done by choosing a matrix S which satisfies the following relations:

$$\tilde{H} = e^S H e^{-S} = H_{\rm k} + H_0 + \frac{1}{2}[S, H_{\rm mix}] + O(|V_0|^3),$$
$$[H_{\rm k} + H_0, S] = H_{\rm mix}. \qquad \text{(A·1)}$$

In this case the most stable configuration is obtained by filling only one d-electron in the orbital: $n_{0s} = 1$. The matrix elements of S, which are determined by the equation (A·1) are as follows:

$$\langle ks; n_0 = n|S|0; n_0 = n+1\rangle = \frac{V_0}{\Delta E}\langle ks; n_0 = n|a^\dagger_{ks}a_{0s}|0; n_0 = n+1\rangle, \quad \text{(A·2)}$$
$$\langle 0; n_0 = n+1|S|ks; n_0 = n\rangle = -\frac{V_0}{\Delta E}\langle 0; n_0 = n+1|a^\dagger_{0s}a_{ks}|ks; n_0 = n\rangle, \text{(A·3)}$$
$$\Delta E = \langle ks; n_0 = n|H_{\rm k} + H_0|ks; n_0 = n\rangle$$
$$-\langle 0; n_0 = n+1|H_{\rm k} + H_0|0; n_0 = n+1\rangle, \qquad \text{(A·4)}$$

where the bracket denotes the following wave function:

$$|ks, k's'; n_0 = 0\rangle = a^\dagger_{ks}a^\dagger_{k's'}|{\rm F}\rangle, \qquad \text{(A·5)}$$
$$|ks; n_0 = 1\rangle = \begin{cases} a^\dagger_{ks}|{\rm F}\rangle|\uparrow\rangle, \\ a^\dagger_{ks}|{\rm F}\rangle|\downarrow\rangle, \end{cases} \qquad \text{(A·6)}$$
$$|0; n_0 = 2\rangle = |{\rm F}\rangle|\uparrow\downarrow\rangle. \qquad \text{(A·7)}$$

Here $|\mathrm{F}\rangle$ represents the Fermi sea. $|\uparrow\rangle$, $|\downarrow\rangle$ and $|\uparrow\downarrow\rangle$ represent the states for the localized electrons. The s-d exchange Hamiltonian is obtained up to the the second order of $|V_0|$ as

$$\begin{aligned}
&\langle k's';n_0=1|H_{sd}|ks;n_0=1\rangle \\
&\quad=\sum_{\varphi}\left[\frac{1}{2}\langle k's';n_0=1|S|\varphi\rangle\langle\varphi|H_{\mathrm{mix}}|ks;n_0=1\rangle\right. \\
&\qquad\left.-\frac{1}{2}\langle k's';n_0=1|H_{\mathrm{mix}}|\varphi\rangle\langle\varphi|S|ks;n_0=1\rangle\right], \qquad \text{(A·8)}
\end{aligned}$$

where φ's are possible intermediate states with $n=0$ or 2. Then the s-d exchange Hamiltonian is also expressed as (1.3) by using operators giving all the matrix elements in (A·8).

For plural localized electron systems, this transformation is also applicable straightforwardly although it is much complicated due to multiplets, which are formed by the Hund coupling.

Appendix B

Relation between the Exchange Interactions (3.15)

The equation (3.15) can be derived by directly applying the operator $\boldsymbol{S}_f^2$ to wave functions. Here we restrict ourselves to the f^2 case; however it can be easily extended to arbitrary f-electrons.

First we rewrite the eigenstates for total angular momentum $J = 4$ with one-particle states of $J = 5/2$. The eigenstate of J and J_z is represented by $|J_z,_J\rangle$ here. Then we obtain

$$|0_4\rangle = \frac{1}{\sqrt{14}}\Big(|5/2_{5/2}\rangle \otimes |-5/2_{5/2}\rangle + 3\,|3/2_{5/2}\rangle \otimes |-3/2_{5/2}\rangle + 2\,|1/2_{5/2}\rangle \otimes |-1/2_{5/2}\rangle\Big), \tag{B·1}$$

for $J = 4$ and $J_z = 0$. The one-particle states for $J = 5/2$ and $J = 7/2$ are obtained by making a linear combination with the states $L = 3$ and $S = 1/2$ (which we write as $|J_z, \sigma\rangle$ ($\sigma = \uparrow, \downarrow$) here). They are given by

$$|M_{7/2}\rangle = \sqrt{\frac{1}{2} + \frac{M}{7}}|M - 1/2, \uparrow\rangle + \sqrt{\frac{1}{2} - \frac{M}{7}}|M + 1/2, \downarrow\rangle, \tag{B·2}$$

$$|M_{5/2}\rangle = -\sqrt{\frac{1}{2} - \frac{M}{7}}|M - 1/2, \uparrow\rangle + \sqrt{\frac{1}{2} + \frac{M}{7}}|M + 1/2, \downarrow\rangle, \tag{B·3}$$

where M is the z component for $J = 7/2$ and $J = 5/2$. After using this transformation, the wave functions on the right side of (B·1) are expressed as

$$|5/2_{5/2}\rangle \otimes |-5/2_{5/2}\rangle = \frac{\sqrt{6}}{7}|2, \uparrow\rangle \otimes |-3, \uparrow\rangle + \frac{\sqrt{6}}{7}|3, \downarrow\rangle \otimes |-2, \downarrow\rangle$$

$$-\frac{1}{7}|2,\uparrow\rangle\otimes|-2,\downarrow\rangle-\frac{6}{7}|3,\downarrow\rangle\otimes|-3,\uparrow\rangle, \tag{B·4}$$

$$|3/2_{5/2}\rangle\otimes|-3/2_{5/2}\rangle=\frac{\sqrt{10}}{7}|1,\uparrow\rangle\otimes|-2,\uparrow\rangle+\frac{\sqrt{10}}{7}|2,\downarrow\rangle\otimes|-1,\downarrow\rangle$$
$$-\frac{2}{7}|1,\uparrow\rangle\otimes|-1,\downarrow\rangle-\frac{5}{7}|2,\downarrow\rangle\otimes|-2,\uparrow\rangle, \tag{B·5}$$

$$|1/2_{5/2}\rangle\otimes|-1/2_{5/2}\rangle=\frac{2\sqrt{3}}{7}|0,\uparrow\rangle\otimes|-1,\uparrow\rangle+\frac{2\sqrt{3}}{7}|1,\downarrow\rangle\otimes|0,\downarrow\rangle$$
$$-\frac{3}{7}|0,\uparrow\rangle\otimes|0,\downarrow\rangle-\frac{4}{7}|1,\downarrow\rangle\otimes|-1,\uparrow\rangle. \tag{B·6}$$

The total spin operator is given by $\boldsymbol{S}_f=\boldsymbol{S}_{f,1}+\boldsymbol{S}_{f,2}+\cdots+\boldsymbol{S}_{f,n}$ for f^n, where $\boldsymbol{S}_{f,i}$ is the spin operator for the i-th f-electron. Then $\boldsymbol{S}_f^2$ can be expressed as

$$\boldsymbol{S}_f^2=\frac{3}{4}n_f+\sum_{i\neq j}\boldsymbol{S}_{f,i}\cdot\boldsymbol{S}_{f,j}. \tag{B·7}$$

If we apply the second term on the right-hand side of (B·7) to a two-particle state, we obtain

$$\begin{aligned}&\boldsymbol{S}_{f,i}\cdot\boldsymbol{S}_{f,j}|m,\sigma\rangle\otimes|m',\sigma'\rangle\\&=\begin{cases}\dfrac{1}{4}|m,\sigma\rangle\otimes|m',\sigma'\rangle & (\sigma=\sigma'),\\[2ex] \dfrac{1}{2}|m,\sigma'\rangle\otimes|m',\sigma\rangle-\dfrac{1}{4}|m,\sigma\rangle\otimes|m',\sigma'\rangle & (\sigma\neq\sigma').\end{cases}\end{aligned} \tag{B·8}$$

After this operation is applied to (B·4), (B·5) and (B·6), the one-particle states with $L=3$ and $S=1/2$ are transformed back to those with $J=7/2$ and $J=5/2$. The state $\boldsymbol{S}_{f,1}\cdot\boldsymbol{S}_{f,2}|0_4\rangle$ is given by much lengthy combination of the two-particle states, which consist of $J=7/2$ and $J=5/2$ states. Assuming the $J=5/2$ states are much lower in energy than $J=7/2$ because of a strong spin-orbit interaction, we restrict one-particle states to $J=5/2$. Then we obtain

$$\begin{aligned}&[\boldsymbol{S}_{f,1}\cdot\boldsymbol{S}_{f,2}]_{J=5/2}|5/2_{5/2}\rangle\otimes|-5/2_{5/2}\rangle\\&=-\frac{25}{196}|5/2_{5/2}\rangle\otimes|-5/2_{5/2}\rangle+\frac{10}{196}|3/2_{5/2}\rangle\otimes|-3/2_{5/2}\rangle,\end{aligned} \tag{B·9}$$

$$\begin{aligned}&[\boldsymbol{S}_{f,1}\cdot\boldsymbol{S}_{f,2}]_{J=5/2}|3/2_{5/2}\rangle\otimes|-3/2_{5/2}\rangle\\&=\frac{10}{196}|5/2_{5/2}\rangle\otimes|-5/2_{5/2}\rangle-\frac{9}{196}|3/2_{5/2}\rangle|-3/2_{5/2}\rangle\\&\quad+\frac{16}{196}|1/2_{5/2}\rangle\otimes|-1/2_{5/2}\rangle,\end{aligned} \tag{B·10}$$

$$[\boldsymbol{S}_{f,1}\cdot\boldsymbol{S}_{f,2}]_{J=5/2}|1/2_{5/2}\rangle\otimes|-1/2_{5/2}\rangle$$
$$=\frac{16}{196}|3/2_{5/2}\rangle\otimes|-3/2_{5/2}\rangle-\frac{19}{196}|1/2_{5/2}\rangle\otimes|-1/2_{5/2}\rangle. \qquad \text{(B·11)}$$

From this we have

$$[\boldsymbol{S}_f^2]_{J=5/2}|0_4\rangle=\frac{5}{196}|0_4\rangle. \qquad \text{(B·12)}$$

The same procedure can be applied to the states of $J=2$ and $J=0$ for f^2 configuration. The result is as follows:

$$[\boldsymbol{S}_f^2]_{J=5/2}|0_2\rangle=-\frac{23}{196}|0_2\rangle, \qquad \text{(B·13)}$$

$$[\boldsymbol{S}_f^2]_{J=5/2}|0_0\rangle=-\frac{35}{196}|0_0\rangle. \qquad \text{(B·14)}$$

On the other hand, the exchange part is obtained as

$$\sum_{i\neq j}\boldsymbol{J}_i\cdot\boldsymbol{J}_j=J(J+1)-\frac{35}{4}n_f=\begin{cases}\dfrac{5}{2} & (J=4),\\ -\dfrac{23}{2} & (J=2),\\ -\dfrac{35}{2} & (J=0).\end{cases} \qquad \text{(B·15)}$$

Then it leads to the relation in (3.15).

Appendix C

Conditions (5.15) and (5.17)

The eigenstates in f^1 (5.12), (5.13) and (5.14) are obtained by diagonalizing the crystal field Hamiltonian. It can be expressed with the basis of J_z of $J = 5/2$ states ($|5/2\rangle$, $|3/2\rangle$, $\cdots$, $|-5/2\rangle$) in the following way:

$$H_{\rm tet} = \begin{pmatrix} H_{5/2,5/2} & & & & H_{5/2,-3/2} & \\ & H_{3/2,3/2} & & & & H_{3/2,-5/2} \\ & & H_{1/2,1/2} & & & \\ & & & H_{-1/2,-1/2} & & \\ H_{-3/2,5/2} & & & & H_{-3/2,-3/2} & \\ & H_{-5/2,3/2} & & & & H_{-5/2,-5/2} \end{pmatrix} \tag{C·1}$$

where the blanks should be filled in with 0's and

$$H_{5/2,5/2} = H_{-5/2,-5/2} = 10B_2^0 + 60B_4^0, \tag{C·2}$$

$$H_{3/2,3/2} = H_{-3/2,-3/2} = -2B_2^0 - 180B_4^0, \tag{C·3}$$

$$H_{1/2,1/2} = H_{-1/2,-1/2} = -8B_2^0 + 120B_4^0, \tag{C·4}$$

$$H_{5/2,-3/2} = H_{3/2,-5/2} = H_{-3/2,5/2} = H_{-5/2,3/2} = 12\sqrt{5}B_4^4. \tag{C·5}$$

Here B_6^0 and B_6^4 are not found since the operators O_6^0 and O_6^4 do nothing. On the other hand, it can be rewritten with the coefficients α and β in $|E_\pm\rangle$ as

$$H_{5/2,5/2} = H_{-5/2,-5/2} = (7\alpha^2 - 8\beta^2)B, \tag{C·6}$$

$$H_{3/2,3/2} = H_{-3/2,-3/2} = (-14\alpha^2 + 7\beta^2)B, \tag{C·7}$$

$$H_{1/2,1/2} = H_{-1/2,-1/2} = (7\alpha^2 + \beta^2)B, \tag{C·8}$$

$$H_{5/2,-3/2} = H_{3/2,-5/2} = H_{-3/2,5/2} = H_{-5/2,3/2} = -3\sqrt{35}\alpha\beta B. \tag{C·9}$$

where B is a constant representing the magnitude of crystal field. From (C·2)–(C·5) and (C·6)–(C·9), α, β and B can be expressed in terms of B_2^0 and B_4^0 as

$$\alpha^2 B = -\frac{2}{21}(9B_2^0 - 170B_4^0), \tag{C·10}$$

$$\beta^2 B = -\frac{2}{3}(3B_2^0 - 10B_4^0), \tag{C·11}$$

$$B = -\frac{20}{7}(B_2^0 - 8B_4^0), \tag{C·12}$$

and

$$(B_4^4)^2 = \frac{1}{36}(9B_2^0 - 170B_4^0)(3B_2^0 - 10B_4^0) > 0. \tag{C·13}$$

Thus (5.15) is the necessary condition for the states (5.12), (5.13) and (5.14) to be eigenstates. If the first condition in (5.15) is satisfied, $B < 0$ holds because of $\alpha^2 > 0$. On the other hand, the second condition leads to $B > 0$ because of $\beta^2 > 0$. The energies in (5.16) are actually expressed in units of B. Therefore the condition (5.17) gives $B < 0$, in which case $|E_{3/2}^{(2)}\pm\rangle$ becomes the lowest state in f^1.

Appendix D

List of Tensor Operators

Here we express tensor operators in terms of matrices. The resulting expression is used to derive effecting exchange Hamiltonians. The tensor operators we study are formed with the total angular momentum $\boldsymbol{J}$. They can be obtained from (2.9) and (2.10). The dimension of the matrix is 6×6 for $J = 5/2$, 9×9 for $J = 4$ and 10×10 for $J = 9/2$. The blanks in the following matrices should be filled in with 0's.

- Tensor operators based on $J = 5/2$

$$J_1^{(1)} = \frac{-1}{\sqrt{2}} \begin{pmatrix} 0 & \sqrt{5} & 0 & \cdots & \cdots & 0 \\ \vdots & \ddots & 2\sqrt{2} & \ddots & & \vdots \\ \vdots & & \ddots & 3 & \ddots & \vdots \\ \vdots & & & \ddots & 2\sqrt{2} & 0 \\ \vdots & & & & \ddots & \sqrt{5} \\ 0 & \cdots & \cdots & \cdots & \cdots & 0 \end{pmatrix} \qquad J_0^{(1)} = \frac{1}{2} \begin{pmatrix} 5 & 0 & \cdots & \cdots & \cdots & 0 \\ 0 & 3 & \ddots & & & \vdots \\ \vdots & \ddots & 1 & \ddots & & \vdots \\ \vdots & & \ddots & -1 & \ddots & \vdots \\ \vdots & & & \ddots & -3 & 0 \\ 0 & \cdots & \cdots & \cdots & 0 & -5 \end{pmatrix}$$

$$J_2^{(2)} = \frac{\sqrt{6}}{2} \begin{pmatrix} 0 & 0 & \sqrt{10} & 0 & \cdots & 0 \\ \vdots & & \ddots & 3\sqrt{2} & \ddots & \vdots \\ \vdots & & & \ddots & 3\sqrt{2} & 0 \\ \vdots & & & & \ddots & \sqrt{10} \\ \vdots & & & & & 0 \\ 0 & \cdots & \cdots & \cdots & \cdots & 0 \end{pmatrix} \qquad J_1^{(2)} = -\sqrt{6} \begin{pmatrix} 0 & \sqrt{5} & 0 & \cdots & \cdots & 0 \\ \vdots & \ddots & \sqrt{2} & \ddots & & \vdots \\ \vdots & & \ddots & 0 & \ddots & \vdots \\ \vdots & & & \ddots & -\sqrt{2} & 0 \\ \vdots & & & & \ddots & -\sqrt{5} \\ 0 & \cdots & \cdots & \cdots & \cdots & 0 \end{pmatrix}$$

$$J_0^{(2)} = \begin{pmatrix} 5 & 0 & \cdots & \cdots & \cdots & 0 \\ 0 & -1 & \ddots & & & \vdots \\ \vdots & \ddots & -4 & \ddots & & \vdots \\ \vdots & & \ddots & -4 & \ddots & \vdots \\ \vdots & & & \ddots & -1 & 0 \\ 0 & \cdots & \cdots & \cdots & 0 & 5 \end{pmatrix}$$

$$J_3^{(3)} = \frac{-3\sqrt{5}}{2}\begin{pmatrix} 0 & \cdots & 0 & \sqrt{10} & 0 & 0 \\ \vdots & & & \ddots & 4 & 0 \\ \vdots & & & & \ddots & \sqrt{10} \\ \vdots & & & & & 0 \\ \vdots & & & & & \vdots \\ 0 & \cdots & \cdots & \cdots & \cdots & 0 \end{pmatrix} \qquad J_2^{(3)} = \frac{3\sqrt{30}}{4}\begin{pmatrix} 0 & 0 & \sqrt{10} & 0 & \cdots & 0 \\ \vdots & & \ddots & \sqrt{2} & \ddots & \vdots \\ \vdots & & & \ddots & -\sqrt{2} & 0 \\ \vdots & & & & \ddots & -\sqrt{10} \\ \vdots & & & & & 0 \\ 0 & \cdots & \cdots & \cdots & \cdots & 0 \end{pmatrix}$$

$$J_1^{(3)} = \frac{-3\sqrt{3}}{2}\begin{pmatrix} 0 & 2\sqrt{5} & 0 & \cdots & \cdots & 0 \\ \vdots & \ddots & -\sqrt{2} & \ddots & & \vdots \\ \vdots & & \ddots & -4 & \ddots & \vdots \\ \vdots & & & \ddots & -\sqrt{2} & 0 \\ \vdots & & & & \ddots & 2\sqrt{5} \\ 0 & \cdots & \cdots & \cdots & \cdots & 0 \end{pmatrix} \qquad J_0^{(3)} = \frac{3}{2}\begin{pmatrix} 5 & 0 & \cdots & \cdots & \cdots & 0 \\ 0 & -7 & \ddots & & & \vdots \\ \vdots & \ddots & -4 & \ddots & & \vdots \\ \vdots & & \ddots & 4 & \ddots & \vdots \\ \vdots & & & \ddots & 7 & 0 \\ 0 & \cdots & \cdots & \cdots & 0 & -5 \end{pmatrix}$$

$$J_4^{(4)} = \frac{3\sqrt{70}}{2}\begin{pmatrix} 0 & \cdots & \cdots & 0 & \sqrt{5} & 0 \\ \vdots & & & & \ddots & \sqrt{5} \\ \vdots & & & & & 0 \\ \vdots & & & & & \vdots \\ \vdots & & & & & \vdots \\ 0 & \cdots & \cdots & \cdots & \cdots & 0 \end{pmatrix} \qquad J_3^{(4)} = \frac{-3\sqrt{35}}{2}\begin{pmatrix} 0 & \cdots & 0 & \sqrt{10} & 0 & 0 \\ \vdots & & & \ddots & 0 & 0 \\ \vdots & & & & \ddots & -\sqrt{10} \\ \vdots & & & & & 0 \\ \vdots & & & & & \vdots \\ 0 & \cdots & \cdots & \cdots & \cdots & 0 \end{pmatrix}$$

$$J_2^{(4)} = \frac{3\sqrt{10}}{4}\begin{pmatrix} 0 & 0 & 3\sqrt{10} & 0 & \cdots & 0 \\ \vdots & & \ddots & -5\sqrt{2} & \ddots & \vdots \\ \vdots & & & \ddots & -5\sqrt{2} & 0 \\ \vdots & & & & \ddots & 3\sqrt{10} \\ \vdots & & & & & 0 \\ 0 & \cdots & \cdots & \cdots & \cdots & 0 \end{pmatrix}$$

$$J_1^{(4)} = \frac{-3\sqrt{5}}{2}\begin{pmatrix} 0 & 2\sqrt{5} & 0 & \cdots & \cdots & 0 \\ \vdots & \ddots & -5\sqrt{2} & \ddots & & \vdots \\ \vdots & & \ddots & 0 & \ddots & \vdots \\ \vdots & & & \ddots & 5\sqrt{2} & 0 \\ \vdots & & & & \ddots & -2\sqrt{5} \\ 0 & \cdots & \cdots & \cdots & \cdots & 0 \end{pmatrix} \qquad J_0^{(4)} = \frac{15}{2}\begin{pmatrix} 1 & 0 & \cdots & \cdots & \cdots & 0 \\ 0 & -3 & \ddots & & & \vdots \\ \vdots & \ddots & 2 & \ddots & & \vdots \\ \vdots & & \ddots & 2 & \ddots & \vdots \\ \vdots & & & \ddots & -3 & 0 \\ 0 & \cdots & \cdots & \cdots & 0 & 1 \end{pmatrix}$$

$$J_5^{(5)} = \frac{-45\sqrt{7}}{2}\begin{pmatrix} 0 & \cdots & \cdots & \cdots & 0 & 1 \\ \vdots & & & & & 0 \\ \vdots & & & & & \vdots \\ \vdots & & & & & \vdots \\ \vdots & & & & & \vdots \\ 0 & \cdots & \cdots & \cdots & \cdots & 0 \end{pmatrix} \qquad J_4^{(5)} = \frac{9\sqrt{70}}{4}\begin{pmatrix} 0 & \cdots & \cdots & 0 & \sqrt{5} & 0 \\ \vdots & & & & \ddots & -\sqrt{5} \\ \vdots & & & & & 0 \\ \vdots & & & & & \vdots \\ \vdots & & & & & \vdots \\ 0 & \cdots & \cdots & \cdots & \cdots & 0 \end{pmatrix}$$

$$J_3^{(5)} = \frac{-3\sqrt{35}}{2}\begin{pmatrix} 0 & \cdots & 0 & \sqrt{10} & 0 & 0 \\ \vdots & & & \ddots & -5 & 0 \\ \vdots & & & & \ddots & \sqrt{10} \\ \vdots & & & & & 0 \\ \vdots & & & & & \vdots \\ 0 & \cdots & \cdots & \cdots & \cdots & 0 \end{pmatrix} \qquad J_2^{(5)} = \frac{3\sqrt{210}}{8}\begin{pmatrix} 0 & 0 & \sqrt{10} & 0 & \cdots & 0 \\ \vdots & & \ddots & -5\sqrt{2} & \ddots & \vdots \\ \vdots & & & \ddots & 5\sqrt{2} & 0 \\ \vdots & & & & \ddots & -\sqrt{10} \\ \vdots & & & & & 0 \\ 0 & \cdots & \cdots & \cdots & \cdots & 0 \end{pmatrix}$$

$$J_1^{(5)} = \frac{-3\sqrt{30}}{4}\begin{pmatrix} 0 & \sqrt{5} & 0 & \cdots & \cdots & 0 \\ \vdots & \ddots & -5\sqrt{2} & \ddots & & \vdots \\ \vdots & & \ddots & 10 & \ddots & \vdots \\ \vdots & & & \ddots & -5\sqrt{2} & 0 \\ \vdots & & & & \ddots & \sqrt{5} \\ 0 & \cdots & \cdots & \cdots & \cdots & 0 \end{pmatrix} \qquad J_0^{(5)} = \frac{15}{4}\begin{pmatrix} 1 & 0 & \cdots & \cdots & \cdots & 0 \\ 0 & -5 & \ddots & & & \vdots \\ \vdots & \ddots & 10 & \ddots & & \vdots \\ \vdots & & \ddots & -10 & \ddots & \vdots \\ \vdots & & & \ddots & 5 & 0 \\ 0 & \cdots & \cdots & \cdots & 0 & -1 \end{pmatrix}$$

- Tensor operators based on $J = 4$

$$J_1^{(1)} = \frac{-1}{\sqrt{2}} \begin{pmatrix} 0 & 2\sqrt{2} & 0 & \cdots & \cdots & \cdots & \cdots & \cdots & 0 \\ \vdots & \ddots & \sqrt{14} & \ddots & & & & & \vdots \\ \vdots & & \ddots & 3\sqrt{2} & \ddots & & & & \vdots \\ \vdots & & & \ddots & 2\sqrt{5} & \ddots & & & \vdots \\ \vdots & & & & \ddots & 2\sqrt{5} & \ddots & & \vdots \\ \vdots & & & & & \ddots & 3\sqrt{2} & \ddots & \vdots \\ \vdots & & & & & & \ddots & \sqrt{14} & 0 \\ \vdots & & & & & & & \ddots & 2\sqrt{2} \\ 0 & \cdots & \cdots & \cdots & \cdots & \cdots & \cdots & \cdots & 0 \end{pmatrix}$$

$$J_0^{(1)} = \frac{-1}{\sqrt{2}} \begin{pmatrix} 4 & 0 & \cdots & \cdots & \cdots & \cdots & \cdots & \cdots & 0 \\ 0 & 3 & \ddots & & & & & & \vdots \\ \vdots & \ddots & 2 & \ddots & & & & & \vdots \\ \vdots & & \ddots & 1 & \ddots & & & & \vdots \\ \vdots & & & \ddots & 0 & \ddots & & & \vdots \\ \vdots & & & & \ddots & -1 & \ddots & & \vdots \\ \vdots & & & & & \ddots & -2 & & \vdots \\ \vdots & & & & & & \ddots & -3 & 0 \\ 0 & \cdots & \cdots & \cdots & \cdots & \cdots & \cdots & \cdots & -4 \end{pmatrix}$$

$$J_2^{(2)} = \frac{\sqrt{6}}{2} \begin{pmatrix} 0 & 0 & 2\sqrt{7} & 0 & \cdots & \cdots & \cdots & \cdots & 0 \\ \vdots & & \ddots & 3\sqrt{7} & \ddots & & & & \vdots \\ \vdots & & & \ddots & 3\sqrt{10} & \ddots & & & \vdots \\ \vdots & & & & \ddots & 10 & \ddots & & \vdots \\ \vdots & & & & & \ddots & 3\sqrt{10} & \ddots & \vdots \\ \vdots & & & & & & \ddots & 3\sqrt{7} & 0 \\ \vdots & & & & & & & \ddots & 2\sqrt{7} \\ \vdots & & & & & & & & 0 \\ 0 & \cdots & \cdots & \cdots & \cdots & \cdots & \cdots & \cdots & 0 \end{pmatrix}$$

$$J_1^{(2)} = \frac{-\sqrt{6}}{4} \begin{pmatrix} 0 & 14\sqrt{2} & 0 & \cdots & \cdots & \cdots & \cdots & \cdots & 0 \\ \vdots & \ddots & 5\sqrt{14} & \ddots & & & & & \vdots \\ \vdots & & \ddots & 9\sqrt{2} & \ddots & & & & \vdots \\ \vdots & & & \ddots & 2\sqrt{5} & \ddots & & & \vdots \\ \vdots & & & & \ddots & -2\sqrt{5} & \ddots & & \vdots \\ \vdots & & & & & \ddots & -9\sqrt{2} & \ddots & \vdots \\ \vdots & & & & & & \ddots & -5\sqrt{14} & 0 \\ \vdots & & & & & & & \ddots & -14\sqrt{2} \\ 0 & \cdots & \cdots & \cdots & \cdots & \cdots & \cdots & \cdots & 0 \end{pmatrix}$$

$$J_0^{(2)} = \frac{1}{2} \begin{pmatrix} 28 & 0 & \cdots & \cdots & \cdots & \cdots & \cdots & \cdots & 0 \\ 0 & 7 & \ddots & & & & & & \vdots \\ \vdots & \ddots & -8 & \ddots & & & & & \vdots \\ \vdots & & \ddots & -17 & \ddots & & & & \vdots \\ \vdots & & & \ddots & -20 & \ddots & & & \vdots \\ \vdots & & & & \ddots & -17 & \ddots & & \vdots \\ \vdots & & & & & \ddots & -8 & & \vdots \\ \vdots & & & & & & \ddots & 7 & 0 \\ 0 & \cdots & \cdots & \cdots & \cdots & \cdots & \cdots & \cdots & 28 \end{pmatrix}$$

$$J_3^{(3)} = -3\sqrt{5} \begin{pmatrix} 0 & \cdots & 0 & \sqrt{14} & 0 & \cdots & \cdots & \cdots & 0 \\ \vdots & & & \ddots & \sqrt{35} & \ddots & & & \vdots \\ \vdots & & & & \ddots & 5\sqrt{2} & \ddots & & \vdots \\ \vdots & & & & & \ddots & 5\sqrt{2} & \ddots & \vdots \\ \vdots & & & & & & \ddots & \sqrt{35} & 0 \\ \vdots & & & & & & & \ddots & \sqrt{14} \\ \vdots & & & & & & & & 0 \\ \vdots & & & & & & & & \vdots \\ 0 & \cdots & \cdots & \cdots & \cdots & \cdots & \cdots & \cdots & 0 \end{pmatrix}$$

$$J_2^{(3)} = \frac{3\sqrt{30}}{2}\begin{pmatrix} 0 & 0 & 2\sqrt{7} & 0 & \cdots & \cdots & \cdots & \cdots & 0 \\ \vdots & & \ddots & 2\sqrt{7} & \ddots & & & & \vdots \\ \vdots & & & \ddots & \sqrt{10} & \ddots & & & \vdots \\ \vdots & & & & \ddots & 0 & \ddots & & \vdots \\ \vdots & & & & & \ddots & -\sqrt{10} & \ddots & \vdots \\ \vdots & & & & & & \ddots & -2\sqrt{7} & 0 \\ \vdots & & & & & & & \ddots & -2\sqrt{7} \\ \vdots & & & & & & & & 0 \\ 0 & \cdots & \cdots & \cdots & \cdots & \cdots & \cdots & \cdots & 0 \end{pmatrix}$$

$$J_1^{(3)} = -3\sqrt{3}\begin{pmatrix} 0 & 7\sqrt{2} & 0 & \cdots & \cdots & \cdots & \cdots & \cdots & 0 \\ \vdots & \ddots & \sqrt{14} & \ddots & & & & & \vdots \\ \vdots & & \ddots & -2\sqrt{2} & \ddots & & & & \vdots \\ \vdots & & & \ddots & -3\sqrt{5} & \ddots & & & \vdots \\ \vdots & & & & \ddots & -3\sqrt{5} & \ddots & & \vdots \\ \vdots & & & & & \ddots & -2\sqrt{2} & \ddots & \vdots \\ \vdots & & & & & & \ddots & \sqrt{14} & 0 \\ \vdots & & & & & & & \ddots & 7\sqrt{2} \\ 0 & \cdots & \cdots & \cdots & \cdots & \cdots & \cdots & \cdots & 0 \end{pmatrix}$$

$$J_0^{(3)} = 3\begin{pmatrix} 14 & 0 & \cdots & \cdots & \cdots & \cdots & \cdots & \cdots & 0 \\ 0 & -7 & \ddots & & & & & & \vdots \\ \vdots & \ddots & -13 & \ddots & & & & & \vdots \\ \vdots & & \ddots & -9 & \ddots & & & & \vdots \\ \vdots & & & \ddots & 0 & \ddots & & & \vdots \\ \vdots & & & & \ddots & 9 & \ddots & & \vdots \\ \vdots & & & & & \ddots & 13 & & \vdots \\ \vdots & & & & & & \ddots & 7 & 0 \\ 0 & \cdots & \cdots & \cdots & \cdots & \cdots & \cdots & \cdots & -14 \end{pmatrix}$$

$$J_4^{(4)} = \frac{3\sqrt{70}}{2}\begin{pmatrix} 0 & \cdots & \cdots & 0 & \sqrt{70} & 0 & \cdots & \cdots & 0 \\ \vdots & & & & \ddots & 5\sqrt{7} & \ddots & & \vdots \\ \vdots & & & & & \ddots & 15 & \ddots & \vdots \\ \vdots & & & & & & \ddots & 5\sqrt{7} & 0 \\ \vdots & & & & & & & \ddots & \sqrt{70} \\ \vdots & & & & & & & & 0 \\ \vdots & & & & & & & & \vdots \\ 0 & \cdots & \cdots & \cdots & \cdots & \cdots & \cdots & \cdots & 0 \end{pmatrix}$$

$$J_3^{(4)} = \frac{-3\sqrt{35}}{2}\begin{pmatrix} 0 & \cdots & 0 & 5\sqrt{14} & 0 & \cdots & \cdots & \cdots & 0 \\ \vdots & & & \ddots & 3\sqrt{35} & \ddots & & & \vdots \\ \vdots & & & & \ddots & 5\sqrt{2} & \ddots & & \vdots \\ \vdots & & & & & \ddots & -5\sqrt{2} & \ddots & \vdots \\ \vdots & & & & & & \ddots & -3\sqrt{35} & 0 \\ \vdots & & & & & & & \ddots & -5\sqrt{14} \\ \vdots & & & & & & & & 0 \\ \vdots & & & & & & & & \vdots \\ 0 & \cdots & \cdots & \cdots & \cdots & \cdots & \cdots & \cdots & 0 \end{pmatrix}$$

$$J_2^{(4)} = \frac{3\sqrt{10}}{4}\begin{pmatrix} 0 & 0 & 30\sqrt{7} & 0 & \cdots & \cdots & \cdots & \cdots & 0 \\ \vdots & & \ddots & 10\sqrt{7} & \ddots & & & & \vdots \\ \vdots & & & \ddots & -11\sqrt{10} & \ddots & & & \vdots \\ \vdots & & & & \ddots & -60 & \ddots & & \vdots \\ \vdots & & & & & \ddots & -11\sqrt{10} & \ddots & \vdots \\ \vdots & & & & & & \ddots & 10\sqrt{7} & 0 \\ \vdots & & & & & & & \ddots & 30\sqrt{7} \\ \vdots & & & & & & & & 0 \\ 0 & \cdots & \cdots & \cdots & \cdots & \cdots & \cdots & \cdots & 0 \end{pmatrix}$$

$$J_1^{(4)} = \frac{-3\sqrt{5}}{2}\begin{pmatrix} 0 & 35\sqrt{2} & 0 & \cdots & \cdots & \cdots & \cdots & \cdots & 0 \\ \vdots & \ddots & -5\sqrt{14} & \ddots & & & & & \vdots \\ \vdots & & \ddots & -30\sqrt{2} & \ddots & & & & \vdots \\ \vdots & & & \ddots & -9\sqrt{5} & \ddots & & & \vdots \\ \vdots & & & & \ddots & 9\sqrt{5} & \ddots & & \vdots \\ \vdots & & & & & \ddots & 30\sqrt{2} & \ddots & \vdots \\ \vdots & & & & & & \ddots & 5\sqrt{14} & 0 \\ \vdots & & & & & & & \ddots & -35\sqrt{2} \\ 0 & \cdots & \cdots & \cdots & \cdots & \cdots & \cdots & \cdots & 0 \end{pmatrix}$$

$$J_0^{(4)} = \frac{15}{2}\begin{pmatrix} 14 & 0 & \cdots & \cdots & \cdots & \cdots & \cdots & \cdots & 0 \\ 0 & -21 & \ddots & & & & & & \vdots \\ \vdots & \ddots & -11 & \ddots & & & & & \vdots \\ \vdots & & \ddots & 9 & \ddots & & & & \vdots \\ \vdots & & & \ddots & 18 & \ddots & & & \vdots \\ \vdots & & & & \ddots & 9 & \ddots & & \vdots \\ \vdots & & & & & \ddots & -11 & & \vdots \\ \vdots & & & & & & \ddots & -21 & 0 \\ 0 & \cdots & \cdots & \cdots & \cdots & \cdots & \cdots & \cdots & 14 \end{pmatrix}$$

$$J_5^{(5)} = \frac{-45\sqrt{7}}{2}\begin{pmatrix} 0 & \cdots & \cdots & \cdots & 0 & 2\sqrt{14} & 0 & \cdots & 0 \\ \vdots & & & & & \ddots & 3\sqrt{14} & \ddots & \vdots \\ \vdots & & & & & & \ddots & 3\sqrt{14} & 0 \\ \vdots & & & & & & & \ddots & 2\sqrt{14} \\ \vdots & & & & & & & & 0 \\ \vdots & & & & & & & & \vdots \\ \vdots & & & & & & & & \vdots \\ \vdots & & & & & & & & \vdots \\ 0 & \cdots & \cdots & \cdots & \cdots & \cdots & \cdots & \cdots & 0 \end{pmatrix}$$

$$J_4^{(5)} = \frac{9\sqrt{70}}{2}\begin{pmatrix} 0 & \cdots & \cdots & 0 & 2\sqrt{70} & 0 & \cdots & \cdots & 0 \\ \vdots & & & & \ddots & 5\sqrt{7} & \ddots & & \vdots \\ \vdots & & & & & \ddots & 0 & \ddots & \vdots \\ \vdots & & & & & & \ddots & -5\sqrt{7} & 0 \\ \vdots & & & & & & & \ddots & -2\sqrt{70} \\ \vdots & & & & & & & & 0 \\ \vdots & & & & & & & & \vdots \\ 0 & \cdots & \cdots & \cdots & \cdots & \cdots & \cdots & \cdots & 0 \end{pmatrix}$$

$$J_3^{(5)} = \frac{-3\sqrt{35}}{2}\begin{pmatrix} 0 & \cdots & 0 & 20\sqrt{14} & 0 & \cdots & \cdots & \cdots & 0 \\ \vdots & & & \ddots & 2\sqrt{35} & \ddots & & & \vdots \\ \vdots & & & & \ddots & -35\sqrt{2} & \ddots & & \vdots \\ \vdots & & & & & \ddots & -35\sqrt{2} & \ddots & \vdots \\ \vdots & & & & & & \ddots & 2\sqrt{35} & 0 \\ \vdots & & & & & & & \ddots & 20\sqrt{14} \\ \vdots & & & & & & & & 0 \\ \vdots & & & & & & & & \vdots \\ 0 & \cdots & \cdots & \cdots & \cdots & \cdots & \cdots & \cdots & 0 \end{pmatrix}$$

$$J_2^{(5)} = \frac{3\sqrt{210}}{2}\begin{pmatrix} 0 & 0 & 10\sqrt{7} & 0 & \cdots & \cdots & \cdots & \cdots & 0 \\ \vdots & & \ddots & -5\sqrt{7} & \ddots & & & & \vdots \\ \vdots & & & \ddots & -7\sqrt{10} & \ddots & & & \vdots \\ \vdots & & & & \ddots & 0 & \ddots & & \vdots \\ \vdots & & & & & \ddots & 7\sqrt{10} & \ddots & \vdots \\ \vdots & & & & & & \ddots & 5\sqrt{7} & 0 \\ \vdots & & & & & & & \ddots & -10\sqrt{7} \\ \vdots & & & & & & & & 0 \\ 0 & \cdots & \cdots & \cdots & \cdots & \cdots & \cdots & \cdots & 0 \end{pmatrix}$$

$$J_1^{(5)} = \frac{-21\sqrt{30}}{4}\begin{pmatrix} 0 & 10\sqrt{2} & 0 & \cdots & \cdots & \cdots & \cdots & \cdots & 0 \\ \vdots & \ddots & -5\sqrt{14} & \ddots & & & & & \vdots \\ \vdots & & \ddots & -5\sqrt{2} & \ddots & & & & \vdots \\ \vdots & & & \ddots & 6\sqrt{5} & \ddots & & & \vdots \\ \vdots & & & & \ddots & 6\sqrt{5} & \ddots & & \vdots \\ \vdots & & & & & \ddots & -5\sqrt{2} & \ddots & \vdots \\ \vdots & & & & & & \ddots & -5\sqrt{14} & 0 \\ \vdots & & & & & & & \ddots & 10\sqrt{2} \\ 0 & \cdots & \cdots & \cdots & \cdots & \cdots & \cdots & \cdots & 0 \end{pmatrix}$$

$$J_0^{(5)} = \frac{105}{2}\begin{pmatrix} 4 & 0 & \cdots & \cdots & \cdots & \cdots & \cdots & \cdots & 0 \\ 0 & -11 & \ddots & & & & & & \vdots \\ \vdots & \ddots & 4 & \ddots & & & & & \vdots \\ \vdots & & \ddots & 9 & \ddots & & & & \vdots \\ \vdots & & & \ddots & 0 & \ddots & & & \vdots \\ \vdots & & & & \ddots & -9 & \ddots & & \vdots \\ \vdots & & & & & \ddots & -4 & & \vdots \\ \vdots & & & & & & \ddots & 11 & 0 \\ 0 & \cdots & \cdots & \cdots & \cdots & \cdots & \cdots & \cdots & -4 \end{pmatrix}$$

- Tensor operators based on $J = 9/2$

$$J_1^{(1)} = \frac{-1}{\sqrt{2}} \begin{pmatrix} 0 & 3 & 0 & \cdots & \cdots & \cdots & \cdots & \cdots & \cdots & 0 \\ \vdots & \ddots & 4 & \ddots & & & & & & \vdots \\ \vdots & & \ddots & \sqrt{21} & \ddots & & & & & \vdots \\ \vdots & & & \ddots & 2\sqrt{6} & \ddots & & & & \vdots \\ \vdots & & & & \ddots & 5 & \ddots & & & \vdots \\ \vdots & & & & & \ddots & 2\sqrt{6} & \ddots & & \vdots \\ \vdots & & & & & & \ddots & \sqrt{21} & \ddots & \vdots \\ \vdots & & & & & & & \ddots & 4 & 0 \\ \vdots & & & & & & & & & 3 \\ 0 & \cdots & \cdots & \cdots & \cdots & \cdots & \cdots & \cdots & \cdots & 0 \end{pmatrix} \qquad J_0^{(1)} = \frac{1}{2} \begin{pmatrix} 9 & 0 & \cdots & \cdots & \cdots & \cdots & \cdots & \cdots & \cdots & 0 \\ 0 & 7 & \ddots & & & & & & & \vdots \\ \vdots & \ddots & 5 & \ddots & & & & & & \vdots \\ \vdots & & \ddots & 3 & \ddots & & & & & \vdots \\ \vdots & & & \ddots & 1 & \ddots & & & & \vdots \\ \vdots & & & & \ddots & -1 & \ddots & & & \vdots \\ \vdots & & & & & \ddots & -3 & \ddots & & \vdots \\ \vdots & & & & & & \ddots & -5 & \ddots & \vdots \\ \vdots & & & & & & & \ddots & -7 & 0 \\ 0 & \cdots & \cdots & \cdots & \cdots & \cdots & \cdots & \cdots & 0 & -9 \end{pmatrix}$$

$$J_2^{(2)} = \frac{\sqrt{6}}{2} \begin{pmatrix} 0 & 0 & 6 & 0 & \cdots & \cdots & \cdots & \cdots & \cdots & 0 \\ \vdots & & \ddots & 2\sqrt{21} & \ddots & & & & & \vdots \\ \vdots & & & \ddots & 3\sqrt{14} & \ddots & & & & \vdots \\ \vdots & & & & \ddots & 5\sqrt{6} & \ddots & & & \vdots \\ \vdots & & & & & \ddots & 5\sqrt{6} & \ddots & & \vdots \\ \vdots & & & & & & \ddots & 3\sqrt{14} & \ddots & \vdots \\ \vdots & & & & & & & \ddots & 2\sqrt{21} & 0 \\ \vdots & & & & & & & & \ddots & 6 \\ \vdots & & & & & & & & & 0 \\ 0 & \cdots & \cdots & \cdots & \cdots & \cdots & \cdots & \cdots & \cdots & 0 \end{pmatrix}$$

$$J_1^{(2)} = -\sqrt{6} \begin{pmatrix} 0 & 6 & 0 & \cdots & \cdots & \cdots & \cdots & \cdots & \cdots & 0 \\ \vdots & \ddots & 6 & \ddots & & & & & & \vdots \\ \vdots & & \ddots & \sqrt{21} & \ddots & & & & & \vdots \\ \vdots & & & \ddots & \sqrt{6} & \ddots & & & & \vdots \\ \vdots & & & & \ddots & 0 & \ddots & & & \vdots \\ \vdots & & & & & \ddots & -\sqrt{6} & \ddots & & \vdots \\ \vdots & & & & & & \ddots & -\sqrt{21} & \ddots & \vdots \\ \vdots & & & & & & & \ddots & -6 & 0 \\ \vdots & & & & & & & & & -6 \\ 0 & \cdots & \cdots & \cdots & \cdots & \cdots & \cdots & \cdots & \cdots & 0 \end{pmatrix} \qquad J_0^{(2)} = 3 \begin{pmatrix} 6 & 0 & \cdots & \cdots & \cdots & \cdots & \cdots & \cdots & \cdots & 0 \\ 0 & 2 & \ddots & & & & & & & \vdots \\ \vdots & \ddots & -1 & \ddots & & & & & & \vdots \\ \vdots & & \ddots & -3 & \ddots & & & & & \vdots \\ \vdots & & & \ddots & -4 & \ddots & & & & \vdots \\ \vdots & & & & \ddots & -4 & \ddots & & & \vdots \\ \vdots & & & & & \ddots & -3 & \ddots & & \vdots \\ \vdots & & & & & & \ddots & -1 & \ddots & \vdots \\ \vdots & & & & & & & \ddots & 2 & 0 \\ 0 & \cdots & \cdots & \cdots & \cdots & \cdots & \cdots & \cdots & 0 & 6 \end{pmatrix}$$

$$J_3^{(3)} = \frac{-3\sqrt{5}}{2} \begin{pmatrix} 0 & \cdots & 0 & 2\sqrt{21} & 0 & \cdots & \cdots & \cdots & \cdots & 0 \\ \vdots & & & \ddots & 4\sqrt{14} & \ddots & & & & \vdots \\ \vdots & & & & \ddots & 5\sqrt{14} & \ddots & & & \vdots \\ \vdots & & & & & \ddots & 20 & \ddots & & \vdots \\ \vdots & & & & & & \ddots & 5\sqrt{14} & \ddots & \vdots \\ \vdots & & & & & & & \ddots & 4\sqrt{14} & 0 \\ \vdots & & & & & & & & \ddots & 2\sqrt{21} \\ \vdots & & & & & & & & & 0 \\ \vdots & & & & & & & & & 0 \\ 0 & \cdots & \cdots & \cdots & \cdots & \cdots & \cdots & \cdots & \cdots & 0 \end{pmatrix}$$

$$J_2^{(3)} = \frac{\sqrt{30}}{4}\begin{pmatrix} 0 & 0 & 42 & 0 & \cdots & \cdots & \cdots & \cdots & \cdots & 0 \\ \vdots & \ddots & 10\sqrt{21} & \ddots & & & & & & \vdots \\ \vdots & & \ddots & 9\sqrt{14} & \ddots & & & & & \vdots \\ \vdots & & & \ddots & 5\sqrt{6} & \ddots & & & & \vdots \\ \vdots & & & & \ddots & -5\sqrt{6} & \ddots & & & \vdots \\ \vdots & & & & & \ddots & -9\sqrt{14} & \ddots & & \vdots \\ \vdots & & & & & & \ddots & -10\sqrt{21} & 0 & \\ \vdots & & & & & & & \ddots & -42 & \\ \vdots & & & & & & & & 0 & \\ 0 & \cdots & \cdots & \cdots & \cdots & \cdots & \cdots & \cdots & \cdots & 0 \end{pmatrix}$$

$$J_1^{(3)} = \frac{-\sqrt{3}}{2}\begin{pmatrix} 0 & 84 & 0 & \cdots & \cdots & \cdots & \cdots & \cdots & \cdots & 0 \\ \vdots & \ddots & 42 & \ddots & & & & & & \vdots \\ \vdots & & \ddots & -2\sqrt{21} & \ddots & & & & & \vdots \\ \vdots & & & \ddots & -19\sqrt{6} & \ddots & & & & \vdots \\ \vdots & & & & \ddots & -60 & \ddots & & & \vdots \\ \vdots & & & & & \ddots & -19\sqrt{6} & \ddots & & \vdots \\ \vdots & & & & & & \ddots & -2\sqrt{21} & \ddots & \vdots \\ \vdots & & & & & & & \ddots & 42 & 0 \\ \vdots & & & & & & & & & 84 \\ 0 & \cdots & \cdots & \cdots & \cdots & \cdots & \cdots & \cdots & \cdots & 0 \end{pmatrix}$$

$$J_0^{(3)} = \frac{3}{2}\begin{pmatrix} 42 & 0 & \cdots & \cdots & \cdots & \cdots & \cdots & \cdots & \cdots & 0 \\ 0 & -14 & \ddots & & & & & & & \vdots \\ \vdots & \ddots & -35 & \ddots & & & & & & \vdots \\ \vdots & & \ddots & -31 & \ddots & & & & & \vdots \\ \vdots & & & \ddots & -12 & \ddots & & & & \vdots \\ \vdots & & & & \ddots & 12 & \ddots & & & \vdots \\ \vdots & & & & & \ddots & 31 & \ddots & & \vdots \\ \vdots & & & & & & \ddots & 35 & \ddots & \vdots \\ \vdots & & & & & & & \ddots & 14 & 0 \\ 0 & \cdots & \cdots & \cdots & \cdots & \cdots & \cdots & \cdots & 0 & -42 \end{pmatrix}$$

$$J_4^{(4)} = \frac{3\sqrt{70}}{2}\begin{pmatrix} 0 & \cdots & \cdots & 0 & 3\sqrt{14} & 0 & \cdots & \cdots & \cdots & 0 \\ \vdots & & & & \ddots & 5\sqrt{14} & \ddots & & & \vdots \\ \vdots & & & & & \ddots & 5\sqrt{21} & \ddots & & \vdots \\ \vdots & & & & & & \ddots & 5\sqrt{21} & \ddots & \vdots \\ \vdots & & & & & & & \ddots & 5\sqrt{14} & 0 \\ \vdots & & & & & & & & \ddots & 3\sqrt{14} \\ \vdots & & & & & & & & & 0 \\ \vdots & & & & & & & & & \vdots \\ \vdots & & & & & & & & & \vdots \\ 0 & \cdots & \cdots & \cdots & \cdots & \cdots & \cdots & \cdots & \cdots & 0 \end{pmatrix}$$

$$J_3^{(4)} = \frac{-3\sqrt{35}}{2}\begin{pmatrix} 0 & \cdots & 0 & 6\sqrt{21} & 0 & \cdots & \cdots & \cdots & \cdots & 0 \\ \vdots & & & \ddots & 8\sqrt{14} & \ddots & & & & \vdots \\ \vdots & & & & \ddots & 5\sqrt{14} & \ddots & & & \vdots \\ \vdots & & & & & \ddots & 0 & \ddots & & \vdots \\ \vdots & & & & & & \ddots & -5\sqrt{14} & \ddots & \vdots \\ \vdots & & & & & & & \ddots & -8\sqrt{14} & 0 \\ \vdots & & & & & & & & \ddots & -6\sqrt{21} \\ \vdots & & & & & & & & & 0 \\ \vdots & & & & & & & & & 0 \\ 0 & \cdots & \cdots & \cdots & \cdots & \cdots & \cdots & \cdots & \cdots & 0 \end{pmatrix}$$

$$J_2^{(4)} = \frac{21\sqrt{10}}{4}\begin{pmatrix} 0 & 0 & 18 & 0 & \cdots & \cdots & \cdots & \cdots & \cdots & 0 \\ \vdots & \ddots & 2\sqrt{21} & \ddots & & & & & & \vdots \\ \vdots & & \ddots & -\sqrt{14} & \ddots & & & & & \vdots \\ \vdots & & & \ddots & -5\sqrt{6} & \ddots & & & & \vdots \\ \vdots & & & & \ddots & -5\sqrt{6} & \ddots & & & \vdots \\ \vdots & & & & & \ddots & -\sqrt{14} & \ddots & & \vdots \\ \vdots & & & & & & \ddots & 2\sqrt{21} & 0 & \\ \vdots & & & & & & & \ddots & 18 & \\ \vdots & & & & & & & & 0 & \\ 0 & \cdots & \cdots & \cdots & \cdots & \cdots & \cdots & \cdots & \cdots & 0 \end{pmatrix}$$

$$J_1^{(4)} = \frac{-21\sqrt{5}}{2}\begin{pmatrix} 0 & 12 & 0 & \cdots & \cdots & \cdots & \cdots & \cdots & \cdots & 0 \\ \vdots & \ddots & -2 & \ddots & & & & & & \vdots \\ \vdots & & \ddots & -2\sqrt{21} & \ddots & & & & & \vdots \\ \vdots & & & \ddots & -3\sqrt{6} & \ddots & & & & \vdots \\ \vdots & & & & \ddots & 0 & \ddots & & & \vdots \\ \vdots & & & & & \ddots & 3\sqrt{6} & \ddots & & \vdots \\ \vdots & & & & & & \ddots & 2\sqrt{21} & \ddots & \vdots \\ \vdots & & & & & & & \ddots & 2 & 0 \\ \vdots & & & & & & & & & -12 \\ 0 & \cdots & \cdots & \cdots & \cdots & \cdots & \cdots & \cdots & \cdots & 0 \end{pmatrix}$$

$$J_0^{(4)} = \frac{21}{2}\begin{pmatrix} 18 & 0 & \cdots & \cdots & \cdots & \cdots & \cdots & \cdots & \cdots & 0 \\ 0 & -22 & \ddots & & & & & & & \vdots \\ \vdots & \ddots & -17 & \ddots & & & & & & \vdots \\ \vdots & & \ddots & 3 & \ddots & & & & & \vdots \\ \vdots & & & \ddots & 18 & \ddots & & & & \vdots \\ \vdots & & & & \ddots & 18 & \ddots & & & \vdots \\ \vdots & & & & & \ddots & 3 & \ddots & & \vdots \\ \vdots & & & & & & \ddots & -17 & \ddots & \vdots \\ \vdots & & & & & & & \ddots & -22 & 0 \\ 0 & \cdots & \cdots & \cdots & \cdots & \cdots & \cdots & \cdots & 0 & 18 \end{pmatrix}$$

$$J_5^{(5)} = \frac{-45\sqrt{7}}{2}\begin{pmatrix} 0 & \cdots & \cdots & \cdots & 0 & 3\sqrt{14} & 0 & \cdots & \cdots & 0 \\ \vdots & & & & & \ddots & 4\sqrt{21} & \ddots & & \vdots \\ \vdots & & & & & & \ddots & 21 & \ddots & \vdots \\ \vdots & & & & & & & \ddots & 4\sqrt{21} & 0 \\ \vdots & & & & & & & & \ddots & 3\sqrt{14} \\ \vdots & & & & & & & & & 0 \\ \vdots & & & & & & & & & \vdots \\ \vdots & & & & & & & & & \vdots \\ \vdots & & & & & & & & & \vdots \\ 0 & \cdots & \cdots & \cdots & \cdots & \cdots & \cdots & \cdots & \cdots & 0 \end{pmatrix}$$

$$J_4^{(5)} = \frac{45\sqrt{70}}{4}\begin{pmatrix} 0 & \cdots & \cdots & 0 & 3\sqrt{14} & 0 & \cdots & \cdots & \cdots & 0 \\ \vdots & & & & \ddots & 3\sqrt{14} & \ddots & & & \vdots \\ \vdots & & & & & \ddots & \sqrt{21} & \ddots & & \vdots \\ \vdots & & & & & & \ddots & -\sqrt{21} & \ddots & \vdots \\ \vdots & & & & & & & \ddots & -3\sqrt{14} & 0 \\ \vdots & & & & & & & & \ddots & -3\sqrt{14} \\ \vdots & & & & & & & & & 0 \\ \vdots & & & & & & & & & \vdots \\ \vdots & & & & & & & & & \vdots \\ 0 & \cdots & \cdots & \cdots & \cdots & \cdots & \cdots & \cdots & \cdots & 0 \end{pmatrix}$$

$$J_3^{(5)} = \frac{-45\sqrt{35}}{2}\begin{pmatrix} 0 & \cdots & 0 & 2\sqrt{21} & 0 & \cdots & \cdots & \cdots & \cdots & 0 \\ \vdots & & & \ddots & \sqrt{14} & \ddots & & & & \vdots \\ \vdots & & & & \ddots & -\sqrt{14} & \ddots & & & \vdots \\ \vdots & & & & & \ddots & -7 & \ddots & & \vdots \\ \vdots & & & & & & \ddots & -\sqrt{14} & \ddots & \vdots \\ \vdots & & & & & & & \ddots & \sqrt{14} & 0 \\ \vdots & & & & & & & & \ddots & 2\sqrt{21} \\ \vdots & & & & & & & & & 0 \\ \vdots & & & & & & & & & 0 \\ 0 & \cdots & \cdots & \cdots & \cdots & \cdots & \cdots & \cdots & \cdots & 0 \end{pmatrix}$$

$$J_2^{(5)} = \frac{15\sqrt{210}}{8}\begin{pmatrix} 0 & 0 & 42 & 0 & \cdots & \cdots & \cdots & \cdots & \cdots & 0 \\ \vdots & & \ddots & -2\sqrt{21} & \ddots & & & & & \vdots \\ \vdots & & & \ddots & -9\sqrt{14} & \ddots & & & & \vdots \\ \vdots & & & & \ddots & -7\sqrt{6} & \ddots & & & \vdots \\ \vdots & & & & & \ddots & 7\sqrt{6} & \ddots & & \vdots \\ \vdots & & & & & & \ddots & 9\sqrt{14} & \ddots & \vdots \\ \vdots & & & & & & & \ddots & 2\sqrt{21} & 0 \\ \vdots & & & & & & & & \ddots & -42 \\ \vdots & & & & & & & & & 0 \\ 0 & \cdots & \cdots & \cdots & \cdots & \cdots & \cdots & \cdots & \cdots & 0 \end{pmatrix}$$

$$J_1^{(5)} = \frac{-105\sqrt{30}}{4}\begin{pmatrix} 0 & 6 & 0 & \cdots & \cdots & \cdots & \cdots & \cdots & \cdots & 0 \\ \vdots & \ddots & -6 & \ddots & & & & & & \vdots \\ \vdots & & \ddots & -\sqrt{21} & \ddots & & & & & \vdots \\ \vdots & & & \ddots & \sqrt{6} & \ddots & & & & \vdots \\ \vdots & & & & \ddots & 6 & \ddots & & & \vdots \\ \vdots & & & & & \ddots & \sqrt{6} & \ddots & & \vdots \\ \vdots & & & & & & \ddots & -\sqrt{21} & \ddots & \vdots \\ \vdots & & & & & & & \ddots & -6 & 0 \\ \vdots & & & & & & & & & 6 \\ 0 & \cdots & \cdots & \cdots & \cdots & \cdots & \cdots & \cdots & \cdots & 0 \end{pmatrix}$$

$$J_0^{(5)} = \frac{315}{4}\begin{pmatrix} 6 & 0 & \cdots & \cdots & \cdots & \cdots & \cdots & \cdots & \cdots & 0 \\ 0 & -14 & \ddots & & & & & & & \vdots \\ \vdots & \ddots & 1 & \ddots & & & & & & \vdots \\ \vdots & & \ddots & 11 & \ddots & & & & & \vdots \\ \vdots & & & \ddots & 6 & \ddots & & & & \vdots \\ \vdots & & & & \ddots & -6 & \ddots & & & \vdots \\ \vdots & & & & & \ddots & -11 & \ddots & & \vdots \\ \vdots & & & & & & \ddots & -1 & \ddots & \vdots \\ \vdots & & & & & & & \ddots & 14 & 0 \\ 0 & \cdots & \cdots & \cdots & \cdots & \cdots & \cdots & \cdots & 0 & -6 \end{pmatrix}$$

Bibliography

[1] For review, see G. R. Stewart: Rev. Mod. Phys. 56 (1984) 755.

[2] T. Kasuya and T. Saso (ed.): *Theory of Heavy Fermions and Valence Fluctuations* (Springer, 1985).

[3] P. A. Lee, T. M. Rice, J. W. Serene, L. J. Sham and J. W. Wilkins: *Comments on Condensed Matter Physics* (1986) Vol. XII.

[4] A. C. Hewson: *The Kondo Problem to Heavy Fermions* (Cambridge University Press, 1993).

[5] E. Hirahara: *Physical Properties of Heavy Fermion Compounds* (in Japanese, see Tōhoku University, I (1990), II (1990), III (1991); Continuations I (1993), II (1994))

[6] A. Sumiyama, Y. Oda, H. Nagano, Y. Ōnuki, K. Shibutani and T. Komatsubara: J. Phys. Soc. Jpn. **55** (1986) 1294.

[7] H. Amitsuka, T. Hidano, T. Honma, H. Mitamura and T. Sakakibara: Physica B **186-188** (1993) 337.

[8] H. Amitsuka and T. Sakakibara: J. Phys. Soc. Jpn. **63** (1994) 736.

[9] C. L. Seaman, M. B. Maple, B. W. Lee, S. Ghamaty, M. S. Torikachvili, J. -S. Kang, L. Z. Liu, J. W. Allen and D. L. Cox: Phys. Rev. Lett. **67** (1991) 2882.

[10] J. Kondo: Prog. Theor. Phys. **32** (1964) 37.

[11] P. W. Anderson: Phys. Rev. **124** (1961) 41.

[12] K. G. Wilson: Rev. Mod. Phys. **47** (1975) 773.

[13] N. Andrei, K. Furuya and J. H. Lowenstein: Rev. Mod. Phys. 55 (1983) 331.

[14] N. Andrei: Phys. Rev. Lett. **45** (1980) 379.

[15] P. B. Wiegmann: Sov. Phys. JETP Lett. **31** (1980) 392.

[16] N. Kawakami and A. Okiji: Phys. Lett. A **86** (1981) 483.

[17] B. Coqblin and J. R. Schrieffer: Phys. Rev. **185**, 847 (1969).

[18] I. Okada and K. Yosida: Prog. Theor. Phys. **49** (1973) 1483.

[19] P. Nozières and A. Blandin: J. Phys. (Paris) **41** (1980) 193.

[20] P. B. Wiegmann and A. M. Tsvelik: JETP Lett. **38** (1983) 591.

[21] N. Andrei and C. Destri: Phys. Rev. Lett. **52** (1984) 364.

[22] P. D. Sacramento and P. Schlottmann: Phys. Lett. A **142** (1989) 245; Physica B **163** (1990) 231; Phys. Rev. B **43** (1991) 13294.

[23] D. L. Cox: Phys. Rev. Lett. **59** (1987) 1240; Physica C **153-155** (1988) 1642; J. Magn. Magn. Mater. **76** & **77** (1988) 53.

[24] In Japanese, J. Kondo: *Theory of Electrons in Metals* (Shōkabō, 1983); K. Yosida: *Magnetism* (Iwanami Shoten, 1991); K. Yamada: *Electronic Correlations* (Iwanami Shoten, 1993).

[25] J. R. Schrieffer and P. A. Wolff: Phys. Rev. **149** (1966) 491.

[26] O. Sakai, Y. Shimizu and T. Kasuya: Prog. Theor. Phys. Suppl. **108** (1992) 73; Y. Shimizu: Doctor Thesis (Tōhoku University, 1991)

[27] K. Yamada, K. Yosida and K. Hanzawa: Prog. Theor. Phys. **71** (1984) 450.

[28] K. Yamada, K. Yosida and K. Hanzawa: Prog. Theor. Phys. Suppl. **108** (1992) 141.

[29] K. Miyake, H. Kusunose and O. Narikiyo: J. Phys. Soc. Jpn. **62** (1993) 2553;

[30] H. Kusunose, K. Miyake, Y. Shimizu and O. Sakai: preprint.

[31] I. E. Perakis, C. M. Varma and A. E. Ruckenstein: Phys. Rev. Lett. **70** (1993) 3467.

[32] T. Giamarchi, C. M. Varma, A. E. Ruckenstein and P. Nozières: Phys. Rev. Lett. **70** (1993) 3967.

[33] J. W. Rasul, N. Read and A. C. Hewson: J. Phys. C **16** (1983) L1079.

[34] T. M. Rice and K. Ueda: Phys. Rev. Lett. **55** (1985) 995, 2093(E).

[35] H. Shiba: J. Phys. Soc. Jpn. **55** (1986) 2765.

[36] K. Yamada and K. Yosida: Prog. Theor. Phys. **76** (1986) 621.

[37] S. Doniach: Physica **91B** (1977) 231.

[38] C. Lacroix and M. Cyrot: Phys. Rev. B**20**, 1969 (1979).

[39] P. Coleman: Phys. Rev. B**28** (1983) 5225.

[40] N. Read, D. M. Newns and S. Doniach: Phys. Rev. B**30**, 3841 (1984).

[41] H. Tsunetsugu, M. Sigrist and K. Ueda: Phys. Rev. B**43** (1993) 8345; K. Ueda, M. Sigrist and H. Tsunetsugu: Physca B**186-188** (1993) 358

[42] M. Jarrell: Phys. Rev. B**51** (1995) 7429.

[43] O. Sakai: to be published.

[44] M. Koga and H. Shiba: J. Phys. Soc. Jpn. **64** (1995) 4345.

[45] E. U. Condon and G. H. Shortley: *The Theory of Atomic Spectra* (Cambrige University Press, New York, 1953).

[46] J. C. Slater: *Quantum Theory of Atomic Structure* (McGraw-Hill Book Co., New York, 1960).

[47] S. Sugano, Y. Tanabe and H. Kamimura: *Multiplets of Transition-Metal Ions in Crystal* (Academic Press, 1970); *Ligand Field Theory and Its Applications* (In Japanese, Shōkabō, 1969).

[48] T. Inui, Y. Tanabe and Y. Onodera: *Group Theory and Its Applications in Physics* (In Japanese, Shōkabō, 1976).

[49] K. M. H. Stevens: Proc. Phys. Soc. (London) A**65** (1952) 209.

[50] M. T. Hutchings: Solid State Physics **16** (Academic Press, 1964), p.227.

[51] K. K. Lea, M. J. M. Leask and W. P. Wolf: J. Phys. Chem. Solids **23** (1962) 1381.

[52] D. M. Cragg, P. Lloyd and P. Nozières: J. Phys. C **13** (1980) 803.

[53] H. B. Pang and D. L. Cox: Phys. Rev. B **44** (1991) 9454.

[54] D. L. Cox: Physica B **186-188** (1993) 312.

[55] Y. Kuramoto: *Transport and Thermal Properties of f-Electron Systems*, ed. G. Oomi *et al.* (Plenum, 1993), p.237.

[56] Y. Shimizu, O. Sakai and Y. Kuramoto: Physica B **206 & 207** (1995) 135.

[57] I. Affleck, A. W. W. Ludwig, H.-B. Pang and D. L. Cox: Phys. Rev. B **45** (1992) 7918.